IFT - UNESP
INSTITUTO DE FÍSICA TEÓRICA

Master´s Dissertation IFT-D.13/2022

The muon g-2 discrepancy and hints about new physics

Rodrigo Teixeira Aguiar

Advisor

Prof. Dr. Juan Carlos Montero Garcia

October/ 2022

A283m

Aguiar, Rodrigo Teixeira

The muon g-2 discrepancy and hints about new physics / Rodrigo Teixeira Aguiar. – São Paulo, 2022

96 f.

Dissertação (mestrado) – Universidade Estadual Paulista (Unesp), Instituto de Física Teórica (IFT), São Paulo

Orientador: Juan Carlos Montero Garcia

1. Modelo padrão (Física nuclear). 2. Muons. 3. Partículas (Física nuclear). I. Título

Sistema de geração automática de fichas catalográficas da Unesp. Biblioteca do Instituto de Física Teórica (IFT), São Paulo. Dados fornecidos pelo autor(a).

I dedicate this thesis to the memory of my grandmother, Giselda Vieira de Aguiar, mathematics and logic teacher.

…

Acknowledgements

To my wife and best friend, for always being by my side and supporting me in my trajectory. To my parents and brothers that also always supported me.

To my advisor, Juan Carlos Montero, by the help and incentive in all difficulties that arose at performing this work.

To IFT, all teachers and fellow employees, by giving me an adequate and enabling environment for my studies.

To all the great teachers I've had throughout my life.

And lastly, to CAPES for the financial support that made this work possible.

*"I went to a bookstore and asked the saleswoman,
'Where's the self-help section?'
She said if she told me, it would defeat the purpose."*

George Carlin

Abstract

In this work, the structuring of the standard model was presented and some issues that this model currently faces were analyzed, selecting for discussion the question of the muon $g-2$. A detailed evaluation of this factor was made, including all the necessary tools to obtain the result, the computations up to one loop, and the proof of the gauge invariance for the same. After that, it was shown what is the issue with the muon $g-2$ and provided a detailed explanation of the experiment that confronts the theoretical prediction.

In the second part, a possible solution to the problem was tested: the inclusion of a flavor-violating vertex and two new heavy particles fields, a fermion, and a scalar. Using at first a toy model it was observed that models that contain this type of vertex and particles could include, in the predictions, values at the right order of magnitude as the SM discrepancy, even if the mass scale of these particles is above the experimental exclusion. The ratio between the masses of the new fermion over the new scalar being above 0.1 could result in values for the muon $g-2$ at the order of the current discrepancy between theory and experiment for scalar masses in the *TeV* scale.

Having that in mind, a more concrete example (a 3-3-1 type model, taken from the literature) was analysed, but the same effect was not observed. Due to the chiral interactions of the scalar fields in this theory the contributions to the muon $g-2$ are lowered by around $10^{-3}\left(\frac{m}{M_H}\right)$. Overall, this result seem to be more reliable than the toy model, since the know interactions are chiral, and additions of scalars with SM-like interactions seems to be, in general, unnatural ways of fixing the $g-2$ discrepancy.

Keywords: Standard Model; Muon; Muon g-2; Magnetic Moment; 3-3-1 Model.

Areas of Knowledge: Physics; Muon physics; Beyond the Standard Model.

Resumo

Neste trabalho foi apresentado a estruturação do modelo padrão e analisados alguns problemas que este modelo enfrenta atualmente, selecionando para discussão a questão do muon $g-2$. Uma detalhada avaliação do muon $g-2$ é feita, incluindo todas ferramentas necessárias para se obter os resultados numéricos, a conta a um loop e a prova da invariancia de gauge feitas explicitamente. Feito isso, foi mostrado qual o problema com o muon $g-2$ e foi dada uma explicação detalhada do experimento que confronta a previsão teórica.

Na segunda parte uma possível solução do problema foi testada: a inclusão de um vertice com violação de sabor e duas partículas pesadas novas, um fermion e um escalar. Usando um modelo hipotético foi observado que modelos que contém este tipo de vértice e partículas poderia incluir nas previsões valores da ordem de magnitude necessária, mesmo que a escala de energia destas particulas esteja fora dos limites experimentais. A relação entre as massas do novo fermion sobre a do novo escalar sendo acima de 0.1 poderiam resultar em valores para o muon $g-2$ da ordem da discrepancia entre teoria e experimento atuais para escalares com massa na escala de TeV.

Tendo isso em mente, um modelo concreto como exemplo (um modelo do tipo 3-3-1, retirado da literatura) foi analisado, mas o mesmo efeito não foi observado. Por causa das interações quirais dos escalares dessa teoria, as contribuições para o $g-2$ são reduzidas por volta de $10^{-3}\left(\frac{m}{M_H}\right)$. De modo geral, este resultado parece mais viável, devido as interações conhecidas serem normalmente quirais, e portanto adições de escalares com interações do tipo do modelo padrão parecem ser, em geral, maneiras não naturais de resolver a discrepância do $g-2$.

Palavras-chave: Modelo Padrão; Muon; Muon g-2; Momento Magnético; Modelo 3-3-1.

Áreas de conhecimento: Física; Física de muons; Além do Modelo Padrão.

Contents

Chapter 1

Introduction

The idea of field theory is described by the Lagrangian formalism in the form of Lagrangian densities, a function of the fields, and its covariant derivatives, as:

$$\mathcal{L} = \mathcal{L}\left(\phi^i(x), \partial_\mu \phi^i(x)\right), \tag{1.1}$$

where ϕ^i can represent all relevant fields. The junction of field theory, quantum physics and the theory of relativity created what is called the Quantum Field Theory (QFT), and the Standard Model of particle physics is the QFT that models the current understanding of particle physics. It is one of the most successful theories ever made since it was able to predict many experimental results at incredible precision. For the completeness of the model different types of fields are included, like scalars, fermionic, and vector fields. This work, at the very end, centers around new fermionic and scalar degrees o freedom.

Scalar fields are the simplest fields possible to add to models. The only such field at the fundamental level in our current theory is the Higgs field [1], experimentally observed in 2012 [2]. Besides that, scalar fields are an active area of research, since it is commonly used in effective field theories. For example, the use of a pion pseudoscalar effective field that can represent interactions of the strong forces at large scales (above 1 fermi according to R. Penco [3]). Having that in mind, the addition of scalar fields is valuable since it can probe for new models in simple forms.

Besides the tremendous success of the Standard Model, there are still some questions waiting to be answered, like neutrinos oscillation, quantum gravity, and dark matter for instance. This work focus on one of such issues, the very present topic of the muon anomalous magnetic dipole moment, usually referred to as the *muon* $g-2$.

The muon was discovered in the 1930 decade and although it is not present in everyday life interactions, muons do appear frequently in experiments and observations. The cosmic rays observation of this particle was one of the first confirmations for the time dilatation from relativistic theory, for example. It was also the first particle to show that nature repeated itself, by having the same characteristics and interactions as the electron, being the mass the only difference [4]. Nowadays we know that there exists a threefold replica with each lepton and quark having three families differing only in mass.

Around a decade before the recognition of the muon as a heavy electron, a somewhat strange quantum phenomenon was being discovered, the anomalous magnetic dipole moment of the electron. Such a phenomenon was predicted by Schwinger due to radiative corrections in the electron interaction and became a strong confirmation of the success of the quantum field theory. The implementation of the same idea to the muon case was immediate and came with an advantage: heavy-particles contributions were much more significant for the muon. Since all the heavy particle contributions at one loop is proportional to

$$F_2 \propto \frac{m_f^2}{M_h^2}, \tag{1.2}$$

where m_f is the mass of the fermion that we want to measure the $g-2$ factor, M_{heavy} is the mass of the heavy particle that we are calculating the $g-2$ contribution, and $F_2 = \frac{g-2}{2}$ is the anomalous part of the magnetic dipole moment. For the muon specifically, this factor is often referred to as a_μ. Then, using a fermion with higher mass and the same interactions results in higher precision on the measurement. The relation from Eq. 1.2 will be justified later in this work,

Having that in mind, many experiments, including three major ones made by CERN, confirmed the value of the muon $g-2$ predicted by the theory up to 6 orders of magnitude. In 1984 a collaboration of scientists at Brookhaven began to increase the precision of the measure of the muon $g-2$, to test even further the theory, and so the experiment BNL E-821 began.

It would be the first to present values up to 2.7 standard deviations (σ) above the theoretical value when the final result was released in 2004 [5]. In the following years, experimental improvement of the measure of other parameters and better techniques of computation improved the accuracy of the theoretical prediction for the muon $g-2$, obtaining the current theoretical value of:

$$a_\mu^{SM} = (116591810 \pm 43) \cdot 10^{-11}. \tag{1.3}$$

This higher precision theoretical value made the result of BNL experiment to go up to 3.7 σ.

Although significant, this value of deviation is not decisive to assert the presence of a problem with the SM. The commonly used threshold is $5\,\sigma$ which is approximately 1 chance in 3.5 million of having the discrepancy being a statistical fluctuation. More experimental data was needed, therefore. Hence, a new collaboration began at Fermilab to make a more meticulous measure. In 2021 the release by Fermilab [6] of the first result for the new experiment E-989 agreed with the previous result by BNL E-821 and improved slightly its confidence in the value. The combined result of both experiments is:

$$a_\mu^{EXP} = (116592061 \pm 41) \cdot 10^{-11}. \tag{1.4}$$

Taking the difference between this value and the theoretical one (Eq. 1.3), we obtain:

$$a_\mu^{EXP} - a_\mu^{SM} = (251 \pm 59) \cdot 10^{-11}, \tag{1.5}$$

which gives a divergence of $4.2\,\sigma$, which boosts the discussion about new physics.

Thus we have the motivation for this work: the divergence of results from experiments and theory for the muon $g-2$. With Fermilab E-989 experiment still running and some other experiments with different techniques of measurement (e.g. J-PARC [7] experiment, projected to release the first result in 2023), the muon $g-2$ is a promising area of research.

The main goal of this work is to try to explain this deviation using elements of new physics that add at least one new scalar in the theory which couples to the muon in a non-standard way. We will start by reviewing the construction and other aspects of the Standard Model. Then we will show how to calculate and measure the value of the muon $g-2$. Finally, discuss about hints of beyond the Standard Model physics.

Chapter 2

The Standard Model of Particle Physics

The Standard Model of particle physics (SM) is the name given to one of the most sophisticated physics theories, which models almost all phenomena involving elementary particles. It is the pinnacle of years of study by many scientists, mostly made in the second half of the last century, and became experimentally complete in 2012 with the discovery of the last piece of the model, the Higgs boson [2]. This model became standard because of the extraordinary experimental validation. Some authors consider this theory the one with the best experimental precision among all physical theories [8].

The mathematical tool used for the construction of the SM is Quantum Field Theory, and with it, we can redefine elementary particles as elementary fields. We should emphasize that the concept of elementary is believed to be an effective concept rather than actual elementary. The author C. Quigg [9] (2013, page 2) explains briefly this idea:

> *"An elementary particle, in the time-honored sense of the term, is structureless and indivisible. Although history cautions that the physicist's list of elementary particles is dependent upon experimental resolution — and thus subject to revision with the passage of time - ... . We thus have no experimental reason but tradition to suspect that they are not the ultimate elementary particles."*

In the next sections, we will set forth some definitions and conventions used in this work, and focus on the Electroweak part of the SM (ESM). We will start by reviewing the composition, gauge symmetries, and symmetry breaking of the ESM. Then we will take a look at the generation of mass for the particles, and some interactions among them. Finally, we will explore anomalies cancellation and some of the current issues of the SM.

2.1 Conventions and definitions

Since many different conventions can be found in the literature, this section will lay out the conventions used in this work as well as some useful definitions. Most of them are the same as in M. D. Schwartz [10], and the Feynman rules were taken from J. Romão and J. Silva [11].

2.1.1 Conventions

- All calculations are done in natural units $c = \hbar = 1$;
- In this work it is used the Einstein summation convention, where multiplications with repeated indices are summed over as shown in the example below:

$$A_\mu \cdot B^\mu = A_0 B^0 + A_1 B^1 + A_2 B^2 + A_3 B^3;$$

- Greek letter indexes (μ, ν, σ, ρ...) are used for 4-dimension Minkowski space, and regular letter indexes (i, j, k...) are used for 3-dimension Euclidean space. Exceptions for this rule will be explicitly written in the text;
- The metric of spacetime used is the mostly negative metric:

$$g^{\mu\nu} = \begin{pmatrix} 1 & 0 & 0 & 0 \\ 0 & -1 & 0 & 0 \\ 0 & 0 & -1 & 0 \\ 0 & 0 & 0 & -1 \end{pmatrix}; \tag{2.1}$$

- The Pauli matrices are defined as:

$$\begin{aligned} \sigma^1 &= \begin{pmatrix} 0 & 1 \\ 1 & 0 \end{pmatrix}; \\ \sigma^2 &= \begin{pmatrix} 0 & -i \\ i & 0 \end{pmatrix}; \\ \sigma^3 &= \begin{pmatrix} 1 & 0 \\ 0 & -1 \end{pmatrix}; \end{aligned} \tag{2.2}$$

With which we define a Pauli vector as:

$$\vec{\sigma} = \sigma^i = \left(\sigma^1, \sigma^2, \sigma^3\right); \tag{2.3}$$

And also the Pauli 4-vectors as:

$$\sigma^\mu = (\mathbb{1}, \sigma^i) \quad ; \quad \bar{\sigma}^\mu = (\mathbb{1}, -\sigma^i); \tag{2.4}$$

- The Dirac matrices are defined as:

$$\begin{aligned} \gamma^0 &= \begin{pmatrix} 0 & \mathbb{1} \\ \mathbb{1} & 0 \end{pmatrix}; \\ \gamma^i &= \begin{pmatrix} 0 & \sigma^i \\ -\sigma^i & 0 \end{pmatrix}; \\ \gamma^5 &= i\gamma^0\gamma^1\gamma^2\gamma^3, \end{aligned} \tag{2.5}$$

  where each entry is a 2x2 matrix and σ^i are the Pauli matrices. This definition is called Weyl representation;

- The left and right projectors are defined as:

$$P_L = \frac{1-\gamma^5}{2} \quad ; \quad P_R = \frac{1+\gamma^5}{2}; \tag{2.6}$$

- The Levi-Civita symbol is defined as:

$$\epsilon^{ijk} = \begin{cases} +1 & \text{for even permutations of } i, j \text{ and } k; \\ -1 & \text{for odd permutations of } i, j \text{ and } k; \\ 0 & \text{if } i = j, \text{ or } j = k, \text{ or } k = i. \end{cases} \tag{2.7}$$

2.1.2 Feynman rules

This subsection is devoted to showing explicitly the Feynman rules used in this work. The formulas have the following conventions:

· p and k are always used for the momentum and, unless explicitly shown, always have direction from left to right;

· ξ is the gauge choice;

- m_i and M_i are used for masses of the 'i' particle;
- ε is an infinitesimal increment;
- Q_f is the electrical charge quantum number of the particle in question, for example, +1 for positrons and -1 for electrons;
- I_3 is the third component of the left isospin doublet and can be $\pm 1/2$ as shown in Table 2.1;
- The slashed terms are 4-vectors contracted with gamma matrices, for example:

$$\not{A} = A_\mu \cdot \gamma^\mu.$$

- g' and g are the coupling constants of $U(1)_Y$ and $SU(2)_L$, respectively.

The Feynman rules that were used are:

- Propagators

Photon:

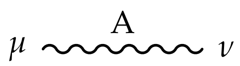

$$= -i \left[\frac{g_{\mu\nu}}{k^2 + i\varepsilon} - (1-\xi) \frac{k_\mu k_\nu}{(k^2)^2} \right]; \tag{2.8}$$

Fermion:

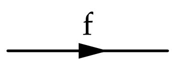

$$= i \frac{\not{p} + m_f}{p^2 - m_f^2 + i\varepsilon}; \tag{2.9}$$

W-boson:

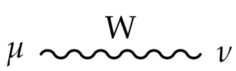

$$= -i \frac{1}{k^2 - M_W^2 + i\varepsilon} \left[g_{\mu\nu} - (1-\xi) \frac{k_\mu k_\nu}{k^2 - \xi M_W^2} \right]; \tag{2.10}$$

Z-boson:

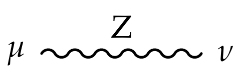

$$= -i \frac{1}{k^2 - M_Z^2 + i\varepsilon} \left[g_{\mu\nu} - (1-\xi) \frac{k_\mu k_\nu}{k^2 - \xi M_Z^2} \right]; \tag{2.11}$$

Higgs-boson:

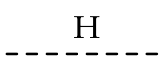

$$= \frac{i}{p^2 - M_H^2 + i\varepsilon}; \tag{2.12}$$

Neutral Golstone-boson:

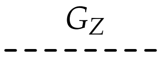

$$= \frac{i}{p^2 - \xi M_Z^2 + i\varepsilon}; \tag{2.13}$$

Charged Golstone-boson:

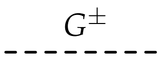

$$= \frac{i}{p^2 - \xi M_W^2 + i\varepsilon}. \tag{2.14}$$

- Vertices:

Fermion - photon vertex

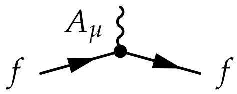

$$= ie\mathrm{Q}_f \gamma_\mu; \tag{2.15}$$

Fermion - Z-boson vertex

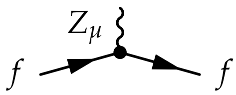

$$= -i\frac{g}{cos\theta_W}\gamma_\mu(\frac{1}{2}I_3 - \mathrm{Q}_f sin^2\theta_W - \frac{1}{2}I_3\gamma^5); \tag{2.16}$$

Fermion - W-boson vertex

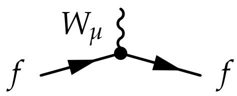

$$= -i\frac{g}{\sqrt{2}}\gamma_\mu P_L; \tag{2.17}$$

Fermion - Higgs-boson vertex

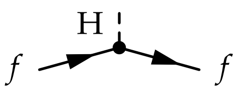

$$= -i\frac{g}{2}\frac{m_f}{M_W}; \tag{2.18}$$

Fermion - neutral Goldstone-boson vertex

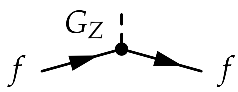

$$= -gI_3\frac{m_f}{M_W}\gamma^5; \tag{2.19}$$

Fermion - charged Goldstone-boson vertex

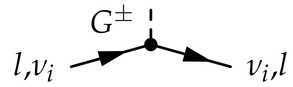

$$= -i\frac{g}{\sqrt{2}}\frac{m_l}{M_W}P_{R,L}; \tag{2.20}$$

Charged Goldstone-boson - photon vertex

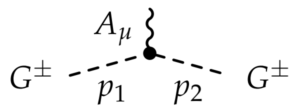

$$= \mp ie(p_1 + p_2)_\mu; \tag{2.21}$$

Charged Goldstone-boson - W-boson - photon vertex

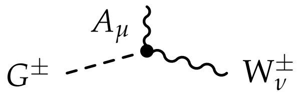

$$= -ieM_W g_{\mu\nu}; \tag{2.22}$$

W-boson - W-boson -photon vertex

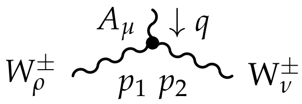

$$= \begin{aligned} -ie\,[g_{\rho\nu}(p_1+p_2)_\mu + \\ g_{\mu\nu}(-p_2-q)_\rho + g_{\mu\rho}(q-p_1)_\nu]\,. \end{aligned} \tag{2.23}$$

2.1.3 Other useful definitions

Some other useful definitions that facilitate to visualise the formulas are shown below:

- The Weinberg angle (θ_W) is defined as the rotation angle between the neutral gauge boson of the $SU(2)_L$ and the $U(1)_Y$ gauge boson:

$$\begin{pmatrix} Z_\mu \\ A_\mu \end{pmatrix} = \begin{pmatrix} cos\theta_W & -sin\theta_W \\ sin\theta_W & cos\theta_W \end{pmatrix} \begin{pmatrix} b^3_\mu \\ A'_\mu \end{pmatrix}; \tag{2.24}$$

$$cos\theta_W = \frac{g}{\sqrt{g^2+g'^2}} \quad ; \quad sin\theta_W = \frac{g'}{\sqrt{g^2+g'^2}}.$$

This angle also relates the masses of the Z and W bosons as:

$$M_W = cos\theta_W M_Z. \tag{2.25}$$

- The electric charge, which is the constant multiplying the photon field interactions, is defined as:

$$e = gsin\theta_W = g'cos\theta_W$$

.

- The fine-structure constant is defined as:

$$\alpha = \frac{e^2}{4\pi}.$$

2.2 Composition and symmetry groups of the SM

The SM has two types of fermions: leptons and quarks. The leptons are composed of three families (the families of the electron (e), muon (μ), and tau(τ), each with its respective neutrino ($\nu_{\{e,\mu,\tau\}}$)). The quarks also have three families, (divided as the family of the up (u) and down (d), of the charm (c) and strange (s), and of the top (t) and bottom (b)) but they have, additionally, three different colours: red, green, and blue. In total, the SM describes the behaviour of 12 fermions: three doublets of leptons and three doublets of quarks [12].

Quarks are not observed free in nature but always coupled to other quarks in a singlet of colour. These composite particles are called hadrons, and we observe mostly two types of them: mesons (composed of a quark and an anti-quark) and baryons (composed of three quarks or three anti-quarks). There are hundreds of such composite particles, including the well-known protons and neutrons, as one can find in [13].

Besides the elementary fermions, there are vector bosons that mediate the interactions among them and which are related to the forces of nature. Leaving aside gravity (it plays no role in the scale of particle physics because of its small magnitude) there is one boson mediating the electromagnetic force (photon), three bosons mediating the weak force (W^+, W^- and Z) and eight gluons mediating the strong force (G_a, a={1 to 8}).

The last particle that composes the SM is the Higgs boson, the particle that generates the masses of all the other particles through the implementation of symmetry breaking, Higgs mechanism, and Yukawa couplings, which will be explained shortly in this chapter. Figure 2.1 shows a summary of the classification of particles of the SM.

Figure 2.1: Summary of the Standard Model particles. Source: The Symmetry Magazine, n. d. (https://www.symmetrymagazine.org/standard-model/)

The symmetry group of the SM particles is

$$SU(3)_C \otimes SU(2)_L \otimes U(1)_Y \,,$$

where C, L, and Y represents the colour, the left chiral symmetry of the fermions, and the hypercharge, respectively. Using this symmetry group and some mathematical tools we are able to compile the final form of the SM, with all interactions, mass terms, and kinetic terms.

2.2.1 SM field description

The fields for the leptons and quarks are very similar. Both contain a doublet of $SU(2)_L$ for each family and singlets for the right component of every particle with the exception of the neutrinos, which only have the left chiral component. This description is exemplified below, for the case of the electron, electron´s neutrino, quark up and quark down.

$$\begin{aligned} P_L\psi_e = \psi_L = \begin{pmatrix} \nu_{e,L} \\ e_L \end{pmatrix} \quad &; \quad P_R\psi_e = \psi_R = e_R; \\ P_L Q = Q_L = \begin{pmatrix} u_L \\ d_L \end{pmatrix} \quad &; \quad P_R Q = Q_R = \{u_R\ ,\ d_R\}\,. \end{aligned} \tag{2.26}$$

The gauge bosons are vector fields, therefore each of them is a 4-components Lorentz vector (T^{μ}). There is also a complex scalar doublet of $SU(2)_L$, described as:

$$\varphi = \begin{pmatrix} \phi^{+} \\ \phi^{0} \end{pmatrix}. \tag{2.27}$$

The Gell-Mann-Nishijima relation [14] defines the charge operator as:

$$\mathrm{Q} = I_3 + \frac{1}{2}Y, \tag{2.28}$$

where I_3 is the third component of the $SU(2)_L$ isospin, Y is the value of the $U(1)_Y$ hypercharge, and Q is the quantized electric charge. And with it, we can find the quantum numbers for each particle field of the theory. The results are shown in Table 2.1. Also included in this table is the Higgs boson field (H) quantum numbers, which will be used in the next sections.

Particle	I	I_3	Y	Q
$\nu_{\{e,\mu,\tau\}L}$	$\frac{1}{2}$	$+\frac{1}{2}$	-1	0
$\{e,\mu,\tau\}_L$	$\frac{1}{2}$	$-\frac{1}{2}$	-1	-1
$\{e,\mu,\tau\}_R$	0	0	-2	-1
$\{u,c,t\}_L$	$\frac{1}{2}$	$+\frac{1}{2}$	$\frac{1}{3}$	$\frac{2}{3}$
$\{d,s,b\}_L$	$\frac{1}{2}$	$-\frac{1}{2}$	$\frac{1}{3}$	$-\frac{1}{3}$
$\{u,c,t\}_R$	0	0	$\frac{4}{3}$	$\frac{2}{3}$
$\{d,s,b\}_R$	0	0	$-\frac{2}{3}$	$-\frac{1}{3}$
H	$\frac{1}{2}$	$-\frac{1}{2}$	$+1$	0

Table 2.1: Quantum numbers for the fermion fields

2.2.2 Spontaneous Symmetry Breaking

Considering the Lagrangian for a complex scalar field:

$$\mathcal{L} = \frac{1}{2}\partial_\mu \phi^* \partial^\mu \phi - V(\phi), \tag{2.29}$$

with the potential:

$$V(\phi) = -\mu^2 \phi^* \phi + \lambda (\phi^* \phi)^2, \tag{2.30}$$

where μ^2 and λ are arbitrary positive real constants.

It is manifest that if $\phi \to e^{i\theta}\phi$ the Lagrangian is invariant, configuring a $U(1)$ symmetry. Such potential (Eq. 2.30) has a minimum where the field is different from zero. Therefore the field ϕ acquires a Vacuum expected Value (VeV) in the lowest energy state, represented by $\frac{v}{\sqrt{2}}$ as in:

$$\langle \phi \rangle_{\text{vacuum}} = \frac{v}{\sqrt{2}} = \sqrt{\frac{\mu^2}{2\lambda}}. \tag{2.31}$$

There is a liberty to choose the direction of the VeV, so it is convenient to choose it in the real positive axis, as shown below:

$$\phi(x) = \frac{1}{\sqrt{2}}\left[v + \phi_1'(x) + i\phi_2'(x)\right], \tag{2.32}$$

where ϕ_1' and ϕ_2' are real scalar fields.

Rewriting the potential in terms of ϕ_1' and ϕ_2' gives:

$$V = -\frac{\mu^4}{4\lambda} + \mu^2 \phi_1'^2 + \mu\sqrt{\lambda}\,\phi_1'^3 + \mu\sqrt{\lambda}\,\phi_1'\phi_2'^2 + \frac{\lambda}{4}\left(\phi_1'^2 + \phi_2'^2\right)^2. \tag{2.33}$$

This potential doesn't have a U(1) symmetry like the original Lagrangian from Eq. 2.29 (if $\phi_i' \to e^{i\theta}\phi_i'$ the extra phase in the terms with $\phi_1'^3$ and with $\phi_1'\phi_2'^2$ doesn't cancel). Thus the symmetry is said to be broken or hidden [10]. Other consequence is that the field ϕ_1' has a mass term, while ϕ_2' is massless. The appearance of massless fields in theories with spontaneously broken continuous symmetry is called *Goldstone theorem*. It states that for every spontaneously broken linearly independent generator of a continuous symmetry there is a massless boson, usually called Goldstone-boson.

For the case of the SM scalar doublet field (Eq. 2.27) with Eq. 2.30 representing the potential (trading ϕ by φ and ϕ^* by $\varphi^\dagger$), the broken symmetry is the $SU(2)_L$ that has three generators. Consequently, it will have three Goldstone-bosons. We can choose a parametrization for this scalar in a clever form as in:

$$\varphi = \frac{e^{-i\frac{\sigma_i}{2}\frac{\varphi^i(x)}{v}}}{\sqrt{2}} \begin{pmatrix} 0 \\ v+H \end{pmatrix}, \tag{2.34}$$

where σ_i are the Pauli matrices, $\varphi^i(x)$ are the Goldstone-bosons fields and H is the physical scalar field of the SM, the Higgs-boson field. This formula is simply another way to write Eq. 2.27, but with the VeV and the physical Higgs field explicit. Remarking that the VeV choice in the second component of this doublet is due to it being neutral. This always has to be the case, since we cannot have a charged vacuum.

2.2.3 Higgs mechanism

After analysing the symmetry breaking, we can include local (gauge) symmetries for the SM and the gauge invariance concept. For that, we have to use the concept of covariant derivatives, defined as:

$$\partial_\mu \to D_\mu = \partial_\mu + \frac{i}{2} Y g' A'_\mu + \frac{i}{2} g \sigma_i b^i_\mu, \tag{2.35}$$

for $SU(2) \otimes U(1)$. And the gauge transformations are defined as:

$$\begin{aligned} \varphi &\to e^{i\alpha(x) + i\sigma_i\beta^i(x)}\varphi; \\ \left\{A'_\mu, b_\mu\right\} &\to \left\{A'_\mu - \frac{i}{g'}\partial_\mu\alpha(x), e^{i\sigma_i\beta^i(x)}\left[b_\mu - \frac{i}{g}\partial_\mu\right] e^{-i\sigma_i\beta^i(x)}\right\}. \end{aligned} \tag{2.36}$$

It is evident that with the right choice of the gauge in the equation above we can correctly cancel the phase term from Eq. 2.34, leaving the scalar of the SM with the standard form of:

$$\phi = \frac{1}{\sqrt{2}} \begin{pmatrix} 0 \\ v+H \end{pmatrix}. \tag{2.37}$$

The consequence of this choice of gauge is that the kinetic term of the scalar field ($D_\mu \phi^\dagger D^\mu \phi$) will present a product of the gauge bosons with the VeV. The result after calculating this kinetic term is:

$$D_\mu\phi^\dagger D^\mu\phi = \frac{(\partial_\mu H)^2}{2} + \frac{1}{8}g^2v^2\left(b_\mu^1 + ib_\mu^2\right)\left(b_\mu^1 - ib_\mu^2\right) + \frac{1}{8}v^2(g'A'_\mu - gb_\mu^3)^2 + \text{interactions}. \tag{2.38}$$

It is practical to make a rotation of the fields to the mass eigenstates using the definitions of Eq. 2.24, rewritten below for the substitution of fields:

$$\begin{aligned} A'_\mu &= \frac{1}{\sqrt{g^2+g'^2}}\left(gA_\mu - g'Z_\mu\right); \\ b_\mu^3 &= \frac{1}{\sqrt{g^2+g'^2}}\left(g'A_\mu + gZ_\mu\right); \\ \left(b_\mu^1 \mp ib_\mu^2\right) &= \sqrt{2}\,W_\mu^\pm, \end{aligned} \tag{2.39}$$

to get the final result for the masses of the physical fields, including the Higgs (from Eq. 2.33), written as:

$$\mathcal{L}_{SSB,mass} = \frac{(\partial_\mu H)^2}{2} + M_W^2 W_\mu^+ W^{\mu-} + \frac{1}{2}M_Z^2(Z_\mu)^2 + \frac{1}{2}M_H^2H^2 + \text{interactions}, \tag{2.40}$$

where $M_W^2 = \frac{1}{4}g^2v^2$, $M_Z^2 = \frac{M_W^2}{cos^2\theta_W} = \frac{1}{4}\left(g^2+g'^2\right)v^2$ and $M_H^2 = \lambda v^2$. The gauge fields have acquired mass from the disappearance of the Goldstone-bosons in the theory. This mechanism of acquisition of mass by the gauge field caused by a spontaneous symmetry breaking in a gauge invariant theory is called the *Higgs Mechanism* [15].

We should emphasize that the degrees of freedom of the theory remain the same since the acquisition of mass by the gauge bosons increases its degree of freedom by one, and the Goldstone-bosons have one degree of freedom each. We can also point out that the field A_μ has not acquired mass, as expected. Therefore it is interpreted as the $U(1)_{EM}$ gauge field of the electromagnetic theory - the photon field.

2.3 Particle mass and interactions

The leptons and quarks cannot have direct mass terms in the Lagrangian, because it would not respect the imposed symmetries. We can see this by trying to manually introduce mass to the electron using:

$$m_e\bar{\psi}_e\psi_e = m_e\bar{\psi}_e(\frac{1+\gamma^5}{2})\psi_e + m_e\bar{\psi}_e(\frac{1-\gamma^5}{2})\psi_e = m_e(\bar{\psi}_L\psi_R + \bar{\psi}_R\psi_L). \tag{2.41}$$

This result does not respect the invariance under $SU(2)_L$, therefore cannot be inserted in the Lagrangian. This idea can be generalized to all families of quarks and leptons.

Hence we will have to look for allowed terms of interactions that respect the symmetries. In the next sections, a careful look at the interactions of leptons and quarks will be exhibited together with the gauge boson kinetic terms.

2.3.1 Lepton interactions

We start by looking at the kinetic term for the leptons. Using the Dirac equation the Lagrangian without mass is simply:

$$\bar{\psi}i\gamma^\mu\partial_\mu\psi \rightarrow \bar{\psi}i\gamma^\mu D_\mu\psi = \bar{\psi}_L i\gamma^\mu D_\mu\psi_L + \bar{\psi}_R i\gamma^\mu D_\mu\psi_R. \tag{2.42}$$

Then, using Eq. 2.36, the values from Table 2.1, and the physical gauge fields from Eq. 2.39 and Eq. 2.26 it is possible to compute the interaction between leptons and gauge bosons. After some algebra, the resultant Lagrangian is shown in Eq. 2.43, divided in the following way: the first line is the charged lepton neutral current, the second is the neutrino neutral current and the third is the lepton charged current.

$$\begin{gathered}\bar{\psi}_e i\gamma^\mu\partial_\mu\psi_e + e\bar{\psi}_e\gamma^\mu A_\mu\psi_e + \frac{g}{4cos\theta_W}\bar{\psi}_e\gamma^\mu\left(1-4sen^2\theta_W-\gamma^5\right)Z_\mu\psi_e;\\ \bar{\psi}_\nu i\gamma^\mu\partial_\mu\psi_\nu - \frac{g}{4cos\theta_W}\bar{\psi}_\nu\gamma^\mu\left(1-\gamma^5\right)Z_\mu\psi_\nu;\\ -\frac{g}{2\sqrt{2}}\left(\bar{\psi}_\nu\gamma^\mu\left(1-\gamma^5\right)W^+_\mu\psi_e + \bar{\psi}_e\gamma^\mu\left(1-\gamma^5\right)W^-_\mu\psi_\nu\right),\end{gathered} \tag{2.43}$$

where $\psi_e = \{e,\mu,\tau\}$ and $\psi_\nu = \{\nu_e,\nu_\mu,\nu_\tau\}$.

Next, the interaction terms. The simplest allowed terms that preserve the symmetries are the Yukawa interactions between the Higgs and two lepton fields, as shown below:

$$G_{\mathcal{Y},ij}\bar{\psi}_i\phi\psi_j + H.c.. = G_{\mathcal{Y},ij}\left(\bar{\psi}_{L,i}\phi\psi_{R,j} + \bar{\psi}_{R,i}\phi^{\dagger}\psi_{L,j}\right) + H.c.., \tag{2.44}$$

where $G_{Y,ij}$ is the Yukawa coupling of the Higgs field with each pair of fermion $''i,j''$. This coupling is a free parameter for the theory that can be any complex number.

After the spontaneous symmetry breaking, the Higgs VeV (Eq. 2.31) will appear as a constant factor multiplying the left-right components, which should be interpreted as a mass term. And because of the chosen parametrization of the Higgs doublet (Eq. 2.37), it will only multiply the isospin $(-\frac{1}{2})$ of the left lepton doublet, giving mass terms only for the electron, muon, and tau. We should also note that in Eq. 2.44 the $''i''$ and $''j''$ can belong to any family of leptons, hence mixing of mass terms will appear in the most general form of this Yukawa Lagrangian as can be seen in:

$$\begin{aligned}\mathcal{L}_{\mathcal{Y},\text{lepton}} =& G_{\mathcal{Y},ee}\frac{v}{\sqrt{2}}\bar{e}e + G_{\mathcal{Y},\mu\mu}\frac{v}{\sqrt{2}}\bar{\mu}\mu + G_{\mathcal{Y},\tau\tau}\frac{v}{\sqrt{2}}\bar{\tau}\tau + G_{\mathcal{Y},e\mu}\frac{v}{\sqrt{2}}\bar{e}\mu \\ &+ G_{\mathcal{Y},e\tau}\frac{v}{\sqrt{2}}\bar{e}\tau + G_{\mathcal{Y},\mu\tau}\frac{v}{\sqrt{2}}\bar{\mu}\tau + \text{interactions} + H.c..\end{aligned} \tag{2.45}$$

The next step is to diagonalize the mass matrix of this Lagrangian, eliminating crossed terms, and finding the actual physical mass for the fields. Since one of the suppositions of the SM is that the neutrinos have no mass, we can freely rotate the neutrino fields to match the mass eigenstates of the charged lepton and eliminate the complex phase resultant with a chiral rotation. The final Lagrangian with lepton mass terms and Higgs interaction is:

$$\mathcal{L}_{\mathcal{Y},\text{lepton}} = m_e\bar{e}e + m_\mu\bar{\mu}\mu + m_\tau\bar{\tau}\tau + \frac{m_e}{v}\bar{e}eH + \frac{m_\mu}{v}\bar{\mu}\mu H + \frac{m_\tau}{v}\bar{\tau}\tau H, \tag{2.46}$$

where $m_i = G'_{\mathcal{Y},i}\frac{v}{\sqrt{2}}$, being $G'_{\mathcal{Y}}$ the eigenvalues of the mass matrix of the Lagrangian from Eq. 2.45, therefore are reals.

With the results Eq. 2.46 and Eq. 2.43, we can generate all Feynman diagrams and propagators for the leptons in the SM.

2.3.2 Quark interactions

Ignoring at first the $SU(3)_C$, because it will not change throughout the calculations, the quark interactions follow the same logic as the lepton one. We commence with a massless Dirac equation term (Eq. 2.42) to derive the interactions between quarks and gauge bosons. Again we use Eq. 2.36, Table 2.1, Eq. 2.39, and Eq. 2.26 to derive the resulting Eq. 2.47. The first and second lines show the neutral currents and the third one shows the charged current.

$$\bar{\psi_u} i\gamma^\mu \partial_\mu \psi_u - \frac{2}{3} e\bar{\psi_u}\gamma^\mu A_\mu \psi_u + \frac{g}{\cos\theta_W}\bar{\psi_u}\gamma^\mu \left(\frac{4\sin^2\theta_W - 1}{2} - \frac{1-\sin^2\theta_W}{2}\gamma^5\right) Z_\mu \psi_u;$$

$$\bar{\psi_d} i\gamma^\mu \partial_\mu \psi_d + \frac{1}{3} e\bar{\psi_d}\gamma^\mu A_\mu \psi_d + \frac{g}{\cos\theta_W}\bar{\psi_d}\gamma^\mu \left(\frac{1}{2} + \frac{2}{3}\sin^2\theta_W - \frac{1}{2}\gamma^5\right) Z_\mu \psi_d; \quad (2.47)$$
$$-\frac{g}{\sqrt{2}}\left(\bar{\psi_u}\gamma^\mu\left(1-\gamma^5\right) W_\mu^+ \psi_d + \bar{\psi_d}\gamma^\mu\left(1-\gamma^5\right) W_\mu^- \psi_u\right),$$

where $\psi_u = \{u, s, t\}$ and $\psi_d = \{d, c, b\}$.

Then we take into account the Yukawa interactions, and this is where a difference from the leptons appears. The right-handed field for the isospin $(+\frac{1}{2})$ has to be considered as well since both quarks need to have mass terms due to experimental evidence. Fortunately, for the $SU(2)$ the conjugate representation is identical to the original one and we can have both written for the scalar field in the Lagrangian, as shown below:

$$\phi = \frac{1}{\sqrt{2}}\begin{pmatrix} 0 \\ v+H \end{pmatrix} \quad ; \quad \tilde{\phi} = i\sigma^2\phi = \frac{1}{\sqrt{2}}\begin{pmatrix} v+H \\ 0 \end{pmatrix}.$$

With that we can write the Yukawa interactions as follows:

$$\mathcal{L}_{\mathcal{Y},\text{quark}} = G_{\mathcal{Y},d}\bar{Q}_L\phi Q_R + G_{\mathcal{Y},u}\bar{Q}_L\tilde{\phi}Q_R. \quad (2.48)$$

Remarking again that Q_L and Q_R can represent any of the families of the quarks so we will need to make the correct rotation to the mass eigenstates. In this case, since we do not have the liberty to freely rotate the fields like with the leptons, it will result in a mixed state for the masses. Realizing this effect, the authors M.Kobayashi and T.Maskawa [16] deduced the mixing matrix that is now called the Cabibbo–Kobayashi–Maskawa (CKM) matrix, commonly written as:

$$V_{CKM} = \begin{pmatrix} c_{12}c_{13} & s_{12}c_{13} & s_{13}e^{-i\delta} \\ -s_{12}c_{23} - c_{12}s_{23}s_{13}e^{i\delta} & c_{12}c_{23} - s_{12}s_{23}s_{13}e^{i\delta} & s_{23}c_{13} \\ s_{12}s_{23} - c_{12}c_{23}s_{13}e^{i\delta} & -c_{12}s_{23} - s_{12}c_{23}s_{13}e^{i\delta} & c_{23}c_{13} \end{pmatrix}, \tag{2.49}$$

where c_{ij} and s_{ij} are the cosine and sine of the mixing angle between the i^{th} and j^{th} particle, respectively.

The final Yukawa Lagrangian is shown below:

$$\mathcal{L}_{\mathcal{Y},\mathrm{quark}} = m_q\bar{q}q + \frac{m_q}{v}\bar{q}qH, \tag{2.50}$$

where again, $m_q = G'_{\mathcal{Y},q}\frac{v}{\sqrt{2}}$, being $G'_{\mathcal{Y}}$ the eigenvalues of the mass matrix and $q = \{u, d, s, c, t, b\}$.

One consequence of the mixed states will appear in the charged current, which is not written in the physical basis in Eq. 2.47. So, we need to fix that term rotating to the mass eigenstates (multiplying by V_{CKM}) which gives:

$$-\frac{g}{\sqrt{2}}\begin{pmatrix}\bar{u} & \bar{c} & \bar{t}\end{pmatrix}\gamma^{\mu}W^{+}_{\mu}V_{CKM}\begin{pmatrix}d \\ s \\ b\end{pmatrix} - \frac{g}{\sqrt{2}}\begin{pmatrix}\bar{d} & \bar{s} & \bar{b}\end{pmatrix}\gamma^{\mu}W^{-}_{\mu}V^{\mathrm{T}}_{CKM}\begin{pmatrix}u \\ c \\ t\end{pmatrix}. \tag{2.51}$$

Another consequence that we will just remark on here is that the phase angle δ is responsible for the CP-violation phenomena in the SM. This can be seen in Eq. 2.51 since the terms in this equation are not CP invariant. This will be important when discussing some issues with the SM in section 2.5.

2.3.3 Gauge bosons kinetic terms

The ending piece of the SM is the kinetic terms for the gauge sector. It is known [15] that the kinetic terms for gauge fields can be written using the antisymmetric tensor $T^{\mu\nu}$ as:

$$-\frac{1}{4}T_{\mu\nu}T^{\mu\nu} = -\frac{1}{4}\sum_{a}\left(\partial_{\mu}T^{a}_{\nu} - \partial_{\nu}T^{a}_{\mu} + gf^{abc}T^{b}_{\mu}T^{c}_{\nu}\right)^{2}, \tag{2.52}$$

where f^{abc} is the structure constant of the group and the summation is over all gauge fields.

With Eq. 2.52 we can directly write the kinetic terms for the SM in the following way:

$$\mathcal{L}_{\text{gauge}} = -\frac{1}{4}A'_{\mu\nu}A'^{\mu\nu} - \frac{1}{4}B_{\mu\nu}B^{\mu\nu} - \frac{1}{4}G_{\mu\nu}G^{\mu\nu}, \tag{2.53}$$

where we keep the notations that A', B, and G are representative of $U(1)_Y$, $SU(2)_L$ and $SU(3)_C$ gauge fields, respectively.

Since we want to write the Lagrangian in terms of the physical fields there is a few computation steps to do that are omitted here. Using Eq. 2.39 to modify Eq. 2.53 and some algebra, we get:

$$\mathcal{L}_{\text{gauge}} = -\frac{1}{4}F_{\mu\nu}F^{\mu\nu} - \frac{1}{4}Z_{\mu\nu}Z^{\mu\nu} - \frac{1}{4}W^{+}_{\mu\nu}W^{-\mu\nu} - \frac{1}{4}G_{\mu\nu}G^{\mu\nu} + \text{interactions}, \tag{2.54}$$

where $F_{\mu\nu} = \left(\partial_\mu A_\nu - \partial_\nu A_\mu\right)$, $Z_{\mu\nu} = \left(\partial_\mu Z_\nu - \partial_\nu Z_\mu\right)$ and $W^{\pm}_{\mu\nu} = \left(\partial_\mu W^{\pm}_\nu - \partial_\nu W^{\pm}_\mu\right)$. The gluons (gauge bosons of $SU(3)_C$) kinetic term remains intact.

2.4 Anomalies in the SM

Anomalies in quantum field theory refer to having symmetries of the classical theory that is somehow not present in the quantum theory. Another way to say it is that the Slavnov-Taylor or the Ward identity is violated [17], like:

$$D_\mu J^\mu = 0 \quad ; \quad \left\langle D_\mu J^\mu \right\rangle \neq 0, \tag{2.55}$$

where J^μ is the Noether conserved current.

For the case of global symmetries, anomalies will only imply in the classical rules not to be obeyed, but for gauge symmetries, anomalies have to be canceled otherwise unitarity and renormalizability would be violated. In the following subsections, we will look at an example of gauge anomaly and then connect it with the SM.

2.4.1 An example of gauge anomaly

A common example of a gauge anomaly is for massless fermions with chiral interactions in a $U(1)$ gauge: supposing a theory with the following Lagrangian:

$$\mathcal{L} = \bar{\psi}_R \left(i\partial\!\!\!/ + Q_f e A\!\!\!/\right)\psi_R + \bar{\psi}_L \left(i\partial\!\!\!/ + Q_f e A\!\!\!/\right)\psi_L. \tag{2.56}$$

This Lagrangian is invariant under the transformation:

$$\psi \rightarrow e^{i\alpha}\psi, \tag{2.57}$$

where the parameter alpha can either be local ($\alpha(x)$) or global if we have the proper gauge field transformations, and from that, we derive the relations of Eq. 2.55

In quantum field theory, the path integral is written as:

$$\langle \Theta\left(x_1 \cdots x_n\right) \rangle = \frac{1}{Z\left(0\right)} \int DAD\bar{\psi}D\psi \, e^{i\int d^4 x i\bar{\psi}\not{D}\psi} \Theta\left(x_1 \cdots x_n\right), \tag{2.58}$$

where Z(0) is a renormalization factor and Θ is any operator invariant under the symmetry.

Even though the Lagrangian is invariant under the transformation from Eq. 2.57, the measure of this integral is not always invariant. If this change of variable contains a chiral term ($\alpha = \beta\gamma^5$) the Jacobian for this change of variable is:

$$\jmath = Det[exp(i\alpha)] = exp\left[i\int dx\beta Tr[\gamma^5]\right], \tag{2.59}$$

and the proper transformation for the measure is:

$$D\bar{\psi}D\psi \rightarrow D\bar{\psi}'D\psi' \left|\jmath\right|^{-2} = D\bar{\psi}'D\psi' e^{-i\int 2\beta Tr[\gamma^5]}, \tag{2.60}$$

where $\left|\jmath\right|^{-2}$ is the inverse Jacobian square due to the anticommuting objects in the measure.

The integral in the exponent seems to vanish due to $\gamma^5 = 0$ but if $\beta(x)$ does not vanish at $x \rightarrow \infty$ this may not be true. In that case, the integral in x is divergent and can be regulated using an exponential of a gauge invariant term like $exp[-\frac{\not{D}^2}{\Lambda^2}]$, with Λ being the regulator. For brevity only the result for the anomalous current is shown:

$$\partial_\mu J^{\mu 5} = \frac{e^2}{16\pi^2}\varepsilon^{\mu\nu\rho\sigma}F_{\mu\nu}F_{\rho\sigma} = \mathcal{A}. \tag{2.61}$$

If the quantum effective action is not invariant ($\mathcal{A} \neq 0$), this symmetry is anomalous and one can show that anomalies in 4 dimensions are 1-loop 3-point function effect. Therefore it is proportional to:

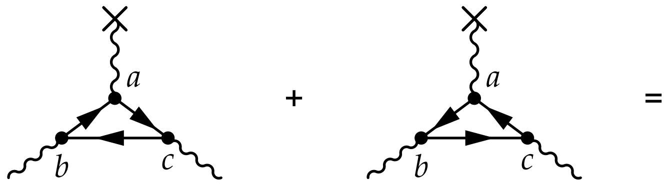

$$\mathbf{A} \propto \quad Tr\left[T^a T^b T^c\right] \quad + \quad Tr\left[T^a T^c T^b\right] \quad , \tag{2.62}$$

where $T^{\{a,b,c\}}$ are the gauge generators being the hypercharge absorbed in this definition.

2.4.2 Anomaly cancellation in the SM

The form of the anomaly in Eq. 2.61 is for an Abelian group but it can also be generalized for non-Abelian groups. The traces from Eq. 2.62 can be divided into a symmetric and an antisymmetric part, but since the antisymmetric part is summed it will vanish. Hence:

$$\mathbf{A} \propto d^{abc} = Tr\left[T^a \left\{T^b, T^c\right\}\right], \tag{2.63}$$

Noting that the symmetric matrix $Tr[T^a \left\{T^b, T^c\right\}]$ may contain mixed representation for the symmetries of the theory, which, for the SM, means mixed representations of $SU(3)_C$, $SU(2)_L$and $U(1)_Y$. Also, observing that in the fermion loops any fermion can be inserted, implies that we have to sum over all of their contributions. With the above and bearing in mind that gauge anomalies are a sign of a flawed theory, the gauge anomalies have to cancel in the SM, as it will be seen. If we are talking about gauge symmetry, then $\beta = \beta(x)$ is a function of the position.

Firstly QCD theory is non-chiral so left and right anomalies will cancel each other in a $SU(3)^3_C$ anomaly. Also for the $SU(2)^3_L$ we can use $\left\{\sigma^\alpha, \sigma^\beta\right\} = \frac{1}{2}\delta^{\alpha\beta}\mathbb{I}$ and $Tr[\sigma^\alpha] = 0$ to verify that there is no anomaly. And the trace of any separated generator of $SU(N)$ for $N \geq 2$ is also zero, therefore any mixed state containing only one $SU(N)$ will also give zero. Thus, the only ones that need to be checked are $U(1)^3_Y$, $U(1)_Y \times SU(2)^2_L$, and $U(1)_Y \times SU(3)^2_C$. Here we will not discuss anomalies due to gravity, but it can also be shown that they are not present in the SM [10,15].

For the $U(1)_Y^3$ we have:

$$d^{abc} = \sum_{Left} Y^3 - \sum_{Right} Y^3, \tag{2.64}$$

where T=Y was used for the Abelian gauge group.

Then using the values from Table 2.1:

$$Y_{eL} = Y_{\nu L} = -1\,;\; Y_{eR} = -2\,;\; Y_{uL} = \frac{1}{3}\,;\; Y_{uR} = \frac{4}{3}\,;\; Y_{dL} = \frac{1}{3}\,;\; Y_{dR} = -\frac{2}{3},$$

and the fact that we have 3 quark colors, we get:

$$\left[2(-1)^3 + 6\left(\frac{1}{3}\right)^3\right] - \left[(-2)^3 + 3\left(\frac{4}{3}\right)^3 + 3\left(-\frac{2}{3}\right)^3\right] = 0. \tag{2.65}$$

For $U(1)_Y \times SU(2)_L^2$ we only get contributions for left-handed fermions. Using again $\{\sigma^\alpha, \sigma^\beta\} = \frac{1}{2}\delta^{\alpha\beta}\mathbb{I}$, we have:

$$tr[T^a\left\{\sigma^b, \sigma^c\right\}] = \frac{1}{2}\delta_{bc}\sum_{Left} Y = \frac{1}{2}\delta_{bc}\left[2(-1) + 6\left(\frac{1}{3}\right)\right] = 0. \tag{2.66}$$

And finally, for $U(1)_Y \times SU(3)_C^2$ we only have the contribution from quarks:

$$tr\left[Y\left\{T^b, T^c\right\}\right] \propto \frac{1}{2}\delta_{bc}\left[\sum_{Left}^{Quarks} Y - \sum_{Right}^{Quarks} Y\right] \propto \left[6\left(\frac{1}{3}\right)\right] - \left[3\left(\frac{4}{3}\right) + 3\left(-\frac{2}{3}\right)\right] = 0, \tag{2.67}$$

where we used $Tr\left\{T^b, T^c\right\} \propto \frac{1}{2}\delta_{bc}$.

Eq. 2.65, Eq. 2.66, and Eq. 2.67 shows that the SM is free of all possible gauge anomalies, showing its robustness. An important remark is that for the consistency of any new model it will have to be anomaly-free as well, implying in a reevaluation of the computations above.

2.5 Issues of the SM

Besides the tremendous success of the SM, it still has some issues or fails to explain some phenomena. In what follows, some of these issues are listed and a brief explanation is provided.

- **Number of free parameters**

The amount of free parameters of the SM is relatively large: 19 according to M. Thomson [18], and when accounting for the additional masses of the neutrinos and the respective mixing angles, it could come up to 26. This might not seem like an issue, but the Bayesian model comparison method [19] states that the theory that best fit the experimental data with the less amount of input is the most complete one.

U. Wiese [20] says that "it is hard to believe that there should not be a more fundamental theory that will be able to explain the values of these parameters", and I. Britto and M. Trott [21] indicate that an excessive number of parameters is a sign of an effective theory, rather than a fundamental one. Since physicists always intend to build the most fundamental theory, the search for a better understanding of where these free parameters come from, especially those coming from the Higgs sector (that accounts for the majority of them), is an ongoing one.

- **Neutrino Oscillation**

  Since 1998, with the strong evidence of neutrinos oscillation from the Super-Kamiokande collaboration [22], this issue has been one of the most studied themes of particle physics. In 2006 the SNO collaboration [23] demonstrated that solar neutrinos indeed oscillate, asserting that this is an issue for the SM.

  The fact that neutrinos oscillate implies directly that they have mass, and, therefore, a right-handed component. This contradicts one of the first assumptions of the SM. Although it is possible to add a non-interacting right-handed neutrino trivially, the addition of a very low-mass particle with the same mass acquisition mechanism (The Higgs Mechanism) as all the other massive particles is not very satisfactory. Hence the search for new physics.

  The search is for a model that provides the low mass for neutrinos without the use of many more free parameters, for the same reasons stated in the first item of this section. The author E. K. Akhmedov [24] presents a more detailed explanation of neutrino physics and the consequences of neutrino oscillation.

- **Strong CP Problem**

  The strong CP problem, as mentioned before, is related to the free phase of the CKM mass matrix (Eq. 2.49). The combination of the CKM phase with an anomalous gauge chiral phase in QCD, if large enough, would cause

QCD not to conserve the CP (or T) symmetry, and would be observable, for example, as an electric dipole in the neutron. The fact that we do not observe such electric dipole nor strong CP violation means that this combination of phases has a small magnitude (less than 10^{-10}, according to E. Kolb and M. Turner [25]).

Since we know that the phase of the CKM matrix is of order 1 by measures in weak CP violation, the exact cancellation of the CKM phase by an anomalous phase without any obvious correlation is not intuitive. Thus the hunt for a mechanism that explains the smallness of the QCD phase in a natural way.

- **Matter-antimatter asymmetry**

  This issue is related to the strong CP problem. The baryon-antibaryon asymmetry in the universe can only be caused by a certain amount of CP violation, that in the SM is not present (the full set of prerequisites for explaining this effect is the same as for the baryogenesis and was laid down by A. Sakharov in 1967 [26]). Even though some CP violation is allowed in the SM, it is not sufficient to amount to the values from cosmological data [27].

- **Lepton Flavour Violation**

  In current experiments, there is no evidence of lepton flavour violation, which agrees with the strong suppression of this phenomenon in the SM. This means that any new physics that one adds to the current model will have very high restrictions on its free parameters, imposed by the present-day observations.

  One of the most relevant flavour violation restrictions for this work is the decay of the muon into an electron and a photon and the branching ratio of this decay is limited to $\Pi(\mu \rightarrow e + \gamma) < 4.2 \cdot 10^{-13}$ (90% CL) [28].

- **Dark Matter**

  One of the main areas of physics research today is a candidate for dark matter: an unknown matter that does not interact with the photon. Evidences for such matter are quite abundant, especially from cosmological and astrophysical data, and date back to even the first half of the 20^{th} century. E. Schmitz [29] makes a reasonable summary of such pieces of evidence.

The only particle in the SM that have the characteristics of dark matter (long-lived, and without interaction with a photon) are neutrinos, but the thermal production of neutrinos gives hints that they are probably not the correct answer to the missing matter. Therefore, the SM does not provide a candidate particle to solve the issue, and the natural way to think is to make an extension to the SM. In the literature, there are many such extensions (e.g. complex scalar dark matter [30], axions [31], among others), but none has been proved experimentally yet.

- **Dark Energy**

  Like Dark Matter, little is known about what composes the dark energy, but cosmological theories predict that it does exist in abundance in our universe (around 70% of the composition of the universe). The SM does not have a natural candidate for it [32]. Also, some models try to solve this issue, but most of them are not in the current experimental range.

- **Gravity**

  For many reasons, gravity has not yet been incorporated in the SM, mainly because there is no theory of quantum gravity broadly accepted. Supersymmetry and String theory are areas that try to solve that issue but have not yet succeeded [8].

- **Higgs hierarchy**

  The Higgs hierarchy problem arrives if we have new physics at a certain scale Λ. Radiative corrections for a scalar boson determine that the mass parameter for the Higgs should be:

$$M_H^2 = M_H'^2 - \Sigma - \delta m \quad ; \quad \Sigma \propto \Lambda^2, \tag{2.68}$$

  where M_H' is the bare mass and δm is the renormalization term containing the infinities. This happens even if the new particle interacts with the Higgs field only through loops.

  Since we know that the Higgs mass is roughly 125 GeV, it is not reasonable for the new scale to be too much above it, since it would require an unnatural cancellation of many decimal places for the Higgs to have the known specified mass. With present experiments, we were able to probe for particles up to a few TeV but none was found. This suggests that we need new ways to explain this phenomenon if we are to find new physics. Some examples of a different explanation are Supersymmetry, which solves the problem by adding a fermion counterpart for the Higgs and cancel the radiative correction by gauge invariance, or composite Higgs models, that can raise the allowance of the new physics scale without the need of fine-tuning the parameters [33].

- **Anomalous mass of the W boson**

  A recent publication by the CDF collaboration [34] exposed a precise measure of the W boson mass to be significantly above the SM prediction (around 7 standard deviations).

  The value predicted by the SM is $M_W^{SM} = 80.357 \pm 0.006\, GeV$ and the measurement by CDF is $M_W^{CDF} = 80.433 \pm 0.009\, GeV$. This result, if confirmed, would require a correction to the SM to explain it and is in clear conflict with some other experiments as well.

- **Muon $g-2$**

  This issue comes from an experimental measure of the muon $g-2$ factor that is in disagreement with the SM prediction. This is the focus of the present study, therefore it will be explained in detail in the next section.

Chapter 3

The Muon $g-2$

The issue with the SM selected for this study is, as mentioned before, the muon $g-2$. It refers to the anomalous magnetic dipole moment of the muon or, more specifically, the divergence of the classical value of this factor. In recent years, after the release by the Fermilab Muon $g-2$ Collaboration [6] of the results for the measure of this factor, it was confirmed that the discrepancy between experiments and theory can be large enough to indicate new physics, which is the motivation for this work.

In this chapter, some of the backgrounds for understanding how to compute, the relevance, as well as a complete leading order (LO) and next to leading order (NLO) calculation of the muon $g-2$ will be shown.

3.1 History of the Anomalous Magnetic Moment

The non-relativistic Hamiltonian of a fermion in the presence of an external magnetic field is:

$$\mathcal{H}_{\vec{\mu}} = \left[\frac{p^2}{2m} + V(x) - \vec{\mu}\cdot\vec{B}\right], \tag{3.1}$$

where $V(x)$ is a potential that depends only on the position, $\vec{B}$ is the magnetic field, and $\vec{\mu}$ is the magnetic moment.

The magnetic moment is known from classical physics to have a relation with the orbital angular moment which can be derived for a classical point charge as:

$$\vec{L} = m\vec{r}\times\vec{v} \quad ; \quad \vec{\mu} = \frac{\mathsf{q}}{2}\vec{r}\times\vec{v} = g_L\frac{\mathsf{q}}{2m}\vec{L}, \tag{3.2}$$

where $\vec{L}$ is the orbital angular momentum, $\vec{r}$ is the radius, m is the mass of the particle, $\vec{\mu}$ is the magnetic moment, $\vec{v}$ is the velocity, and q is the charge. Also included is the g_L which is called the Landé g factor, the same g as in the title of the chapter. For this particular case of a point-like classical particle, the g_L factor is simply 1.

For elementary particles with spin angular momentum ($\vec{S}$), there is no particular reason to assume a value for the Landé g factor. Hence the correct formula for it is to add the spin contribution like:

$$\vec{\mu} = \frac{e}{2m}\left(\vec{L} + g_S\vec{S}\right), \tag{3.3}$$

where e is the electron charge and g_S is, at first, a free parameter of the theory.

Pauli was the first to find out that the actual value for g_S is 2 and using the Dirac equation, published in 1928, it is easy to figure out this number. It can be shown how to extract the magnetic moment as follows:

Starting with the Dirac equation:

$$\left(\not{D} - m\right)\psi = 0, \tag{3.4}$$

we multiply by $(\not{D} + m)$, and using the relation $(\not{D}^2 = D^2 + \frac{e}{2}F_{\mu\nu}\sigma^{\mu\nu})$, with $\sigma^{\mu\nu} = i/2\left[\gamma^\mu, \gamma^\nu\right]$, to obtain:

$$\left(D^2 + m^2 + \frac{e}{2}F_{\mu\nu}\sigma^{\mu\nu}\right)\psi = 0. \tag{3.5}$$

Comparing this equation to the Klein-Gordon equation:

$$\left(D^2 + m^2\right)\phi = 0, \tag{3.6}$$

we can see that there is an extra term for particles with spin half. Expanding this extra term using the Weyl representation we obtain:

$$\frac{e}{2}F_{\mu\nu}\sigma^{\mu\nu} = -e\begin{pmatrix} \left(\vec{B} + i\vec{E}\right)\vec{\sigma} & \\ & \left(\vec{B} - i\vec{E}\right)\vec{\sigma} \end{pmatrix}. \tag{3.7}$$

Then, rewriting Eq. 3.5 as:

$$\left(D^2 + m^2 - 2e\vec{B}\cdot\vec{S} \pm i2e\vec{E}\cdot\vec{S}\right)\psi = 0, \tag{3.8}$$

we can show that the dipole magnetic moment is the term that multiplies the magnetic field ($\vec{B}$) divided by $2m$. The proof of this relation is shown in Appendix A. Comparing Eq. 3.8 with Eq. 3.3, we can see that the value of the g factor is indeed 2.

Although the experiments at the time were consistent with the value for g equal to 2 within 10% accuracy [35], Schwinger [36] realized that there were still some quantum effects unaccounted for. In 1947 he calculated the first radiative correction to the anomalous magnetic moment, the famous $\frac{\alpha}{2\pi}$. Figure 3.1 shows the Dirac magnetic moment factor and the Schwinger one-loop correction diagram.

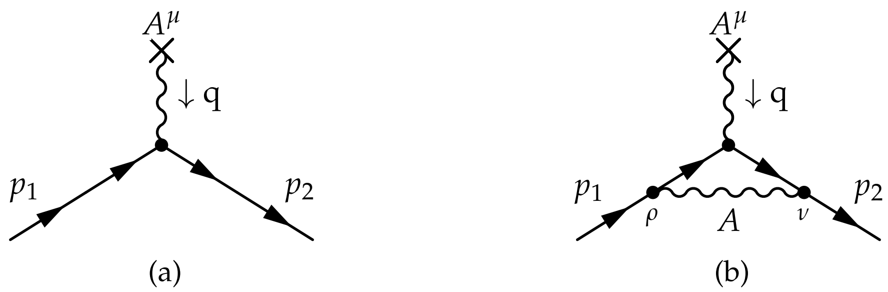

Figure 3.1: Feynman diagram for (a) tree-level contribution and (b) one loop photon contribution to the muon g factor

Schwinger's predictions were then measured with extreme precision in experiments later on and it was one of the greatest confirmations of the validity of quantum field theory. In section 3.2.2 Schwinger's computation will be shown explicitly, and although he calculated it for the electron, the same procedure is valid for the muon and it will be used for the NLO computation of the muon $g-2$ factor.

3.2 Feynman diagram calculation of the g factor

The first step to understanding where the magnetic moment appears is to identify all possible terms that can contribute to it. We want to write all possible terms with just one uncontracted Lorentz index because we know that these are the possible terms that contract with the external magnetic field. Figure 3.2 shows the most general Feynman diagram to be drawn and Eq. 3.9 gives the most general form of the evaluation of this diagram.

$$i\mathcal{M}^\mu = (-ie)\,\bar{u}(p_2)\left(f_1\gamma^\mu + f_3 p_1^\mu + f_4 p_2^\mu\right) u(p_1). \tag{3.9}$$

Terms with γ^5 are ignored because QED is parity invariant. Also, terms with q^μ can be directly rewritten as the other two momenta by momentum conservation ($q^\mu = p_2^\mu - p_1^\mu$) so they are absorbed in the definition of f_3 and f_4. The next step is

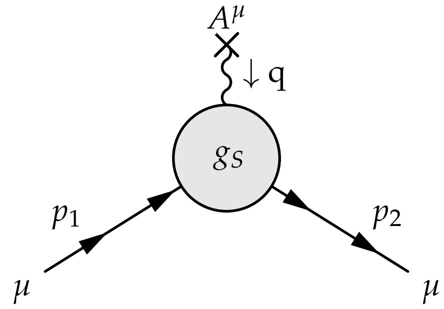

Figure 3.2: General Feynman diagram for g_S factor contribution. The symbol $\times$ at the photon propagator indicates that it is a virtual photon.

to use the ward identity:

$$q_\mu M^\mu = (-e)\,\bar{u}(p_2)\left(f_1 q_\mu \gamma^\mu + f_3 q_\mu p_1^\mu + f_4 q_\mu p_2^\mu\right) u(p_1) = 0, \tag{3.10}$$

and find more relations among the f factors.

In the first term inside the bracket, we can use the relations from the Dirac equation

$$\begin{aligned} \not{p}_1 u(p_1) &= m_1 u(p_1); \\ \bar{u}(p_2)\not{p}_2 &= m_2 \bar{u}(p_2), \end{aligned} \tag{3.11}$$

and momentum conservation again to find the trivial $m_1 = m_2$. So for now on, we will drop the index in the mass term and m will be used exclusively for the muon mass.

For the second term in the brackets, some work needs to be done. Using

$$q_\mu p_i^\mu = (p_2 - p_1)_\mu\, p_i^\mu = \left(m^2 - p_2 p_1\right)(-1)^i \;\; ; \;\; i = 1, 2, \tag{3.12}$$

we write:

$$f_3 q_\mu p_1^\mu + f_4 q_\mu p_2^\mu = \left(p_2 p_1 - m^2\right)(f_3 - f_4) = 0, \tag{3.13}$$

and show that $f_3 = f_4$. Another useful redefinition is to write $f_3 = -\frac{F_2}{2m}$ so that the F_2 factor is dimensionless. The minus sign and the factor $\frac{1}{2}$ are conventions that simplify the notation. After these changes we have:

$$i\mathcal{M}^\mu = (-ie)\,\bar{u}(p_2)\left[f_1\gamma^\mu - \frac{F_2}{2m}\left(p_1^\mu + p_2^\mu\right)\right] u(p_1). \tag{3.14}$$

Using Gordon's identity [10] for on-shell spinors:

$$\bar{u}(p_2)\left(p_1^\mu + p_2^\mu\right) u(p_1) = \bar{u}(p_2)\left[2m\gamma^\mu - i\sigma^{\mu\nu}(p_2 - p_1)_\nu\right] u(p_1), \tag{3.15}$$

we rewrite the second term of Eq. 3.14 and use a last redefinition of $f_1 - F_2 = F_1$ to acquire the final form of this equation:

$$i\mathcal{M}^{\mu} = (-ie)\,\bar{u}(p_2)\left[F_1\gamma^{\mu} + iF_2\frac{\sigma^{\mu\nu}}{2m}q_{\nu}\right]u(p_1). \tag{3.16}$$

The terms F_1 and F_2 are called the form factors and are functions of q^2 and m^2. More precisely, they need to be functions of $\frac{q^2}{m^2}$ since they are dimensionless, but because we will consider the non-relativistic limit ($q^2 \to 0$) they shall be considered as constant.

The final step is to relate the form factors and the Landé g factor. Using:

$$u(p) = \begin{pmatrix}\sqrt{p\cdot\sigma}\\ \sqrt{p\cdot\bar{\sigma}}\end{pmatrix}u(0), \tag{3.17}$$

where u(0) are the 0 momentum solutions of the Dirac equation. Considering the non-relativistic limit:

$$\sqrt{p\sigma} = \frac{p\sigma + m}{\sqrt{2\,(E+m)}} \cong \frac{E + m - \vec{p}\vec{\sigma}}{\sqrt{4m}} \cong \sqrt{m}\left(1 - \frac{\vec{p}\vec{\sigma}}{2m}\right), \tag{3.18}$$

we can show that the first term in the brackets of Eq. 3.16 is:

$$\begin{aligned}
F_1\bar{u}(p_2)\gamma^{\mu}u(p_1) &= F_1\,u^{\dagger}(0)\begin{pmatrix}\sqrt{p_2\sigma} & \sqrt{p_2\bar{\sigma}}\end{pmatrix}\gamma^0\gamma^{\mu}\begin{pmatrix}\sqrt{p_1\sigma}\\ \sqrt{p_1\bar{\sigma}}\end{pmatrix}u(0)\\
&= m\,F_1u^{\dagger}(0)\left[\left(1-\frac{\vec{p}_2\vec{\sigma}}{2m}\right)\sigma^i\left(1-\frac{\vec{p}_1\vec{\sigma}}{2m}\right)\right.\\
&\qquad\left. - \left(1-\frac{\vec{p}_2\vec{\bar{\sigma}}}{2m}\right)\sigma^i\left(1-\frac{\vec{p}_1\vec{\bar{\sigma}}}{2m}\right)\right]u(0)\\
&= m\,F_1u^{\dagger}(0)\left(\frac{\vec{p}_1\vec{\sigma}}{m}\sigma^i + \sigma^i\frac{\vec{p}_2\vec{\sigma}}{m}\right)u(0),
\end{aligned} \tag{3.19}$$

where in the last line we used $\bar{\sigma}^i = -\sigma^i$ from Eq. 2.5 and only the crossed terms remained. Now we can use the Pauli matrices identity $\sigma^i\sigma^j = \delta^{ij} + i\epsilon^{ijk}\sigma^k$ to find:

$$F_1\bar{u}(p_2)\gamma^{\mu}u(p_1) = F_1u^{\dagger}(0)\left(p_1^i + p_2^i + i\epsilon^{ijk}\,(p_2 - p_1)_j\,\sigma_k\right)u(0), \tag{3.20}$$

where we can ignore the terms p_1^i and p_2^i since they are spin-independent, and look only at the magnetic moment term, identifying $i\epsilon^{ijk}q_jA_k = -B^i$, with $q_j = (p_2 - p_1)_j$. Then we have to use the identities $\sigma_i = 2S_i$ and $u^{\dagger}(0)S_iu(0) = \frac{1}{2m}\langle S\rangle_i$

to end up with the known format of the magnetic moment:

$$2F_1 \frac{e}{2m} \left\langle \vec{S} \right\rangle \cdot \vec{B}. \tag{3.21}$$

For the second term of Eq. 3.16, we have to do similar considerations. First, we expand the terms using the non-relativistic approximation (Eq. 3.18) and remembering that $\sigma^{\mu\nu} = \frac{i}{2}\left[\gamma^\mu, \gamma^\nu\right]$, we get:

$$\begin{aligned} \bar{u}(p_2)\left[\sigma^{\mu\nu} q_\nu\right] u(p_1) = \frac{i}{2} m u^\dagger(0) &\left[\left(1 + \frac{\vec{p}_2\vec{\sigma}}{2m}\right) \left[\sigma^j, \sigma^i\right] \left(1 - \frac{\vec{p}_1\vec{\sigma}}{2m}\right) \right. \\ &\left. + \left(1 - \frac{\vec{p}_2\vec{\sigma}}{2m}\right) \left[\sigma^j, \sigma^i\right] \left(1 + \frac{\vec{p}_1\vec{\sigma}}{2m}\right) \right] u(0) q_j \\ = -imu^\dagger(0) &\left[\epsilon^{jik}\sigma_k\right] u(0) q_j + O\left(\frac{1}{m}\right), \end{aligned} \tag{3.22}$$

and again, make the identification of the magnetic moment term using the same identities as before. The final result, obtained after multiplying by the appropriate constants, is:

$$2F_2 \frac{e}{2m} \left\langle \vec{S} \right\rangle \cdot \vec{B}. \tag{3.23}$$

Finally, we combine Eq. 3.21 and Eq. 3.23 to have the relation between the form factors and the Landé g factor, shown below:

$$g_S = 2\left(F_1(0) + F_2(0)\right), \tag{3.24}$$

where the zero shows explicitly that the non-relativistic limit was used.

3.2.1 Leading order calculation of the Form Factors

The tree-level Feynman diagram evaluation from Figure 3.1a gives directly:

$$i\mathcal{M}_0^\mu = -ie\bar{u}(p_2)\gamma^\mu u(p_1), \tag{3.25}$$

which is a term similar to the one found when computing the F_1 form factor in the last section. Comparing this equation with Eq. 3.16 it is straightforward to conclude that $F_1 = 1$ and $F_2 = 0$ for this diagram. This reproduces $g_S = 2$ precisely, as one should expect.

3.2.2 NLO calculation of the Form Factors

The Feynman diagram of the loop with a photon is the most relevant one since it has the strongest coupling. As pointed out before, this calculation was primarily done by Schwinger for the electron but the same computation applies to the muon since it does not depend on the fermion mass. The momentum convention for loop diagrams used in this work is shown in Figure 3.3.

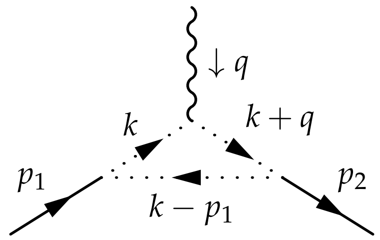

Figure 3.3: Momentum convention for one-loop diagrams. All arrows in this diagram are for the momentum direction used, not to indicate any kind of spin or propagator.

With this convention we can now evaluate the diagram from Figure 3.1b as follows:

$$\begin{aligned} i\mathcal{M}_\gamma^\mu &= (-ie)^3 \int \frac{d^4k}{(2\pi)^4} \frac{-ig^{\nu\rho}}{[(k-p_1)^2+i\varepsilon]} \bar{u}(p_2) \\ &\quad \times \gamma^\nu \frac{i(\not{q}+\not{k}+m)}{[(q+k)^2-m^2+i\varepsilon]} \gamma^\mu \frac{i(\not{k}+m)}{[k^2-m^2+i\varepsilon]} \gamma^\rho u(p_1) \\ &= -e^3 \bar{u}(p_2) \int \frac{d^4k}{(2\pi)^4} \frac{\gamma^\nu(\not{q}+\not{k}+m)\gamma^\mu(\not{k}+m)\gamma_\nu}{[(k-p_1)^2+i\varepsilon]\,[(q+k)^2-m^2+i\varepsilon]\,[k^2-m^2+i\varepsilon]} u(p_1), \end{aligned} \tag{3.26}$$

where m is the mass of the on-shell fermion.

To proceed we need to use the Feynman trick:

$$\frac{1}{ABC} = \int_0^1 \int_0^1 \int_0^1 dxdydz \frac{\Gamma(3)\delta(1-x-y-z)}{[xA+yB+zC]^3}, \tag{3.27}$$

where x, y and z are called the Feynman parameters. Separating the numerator and denominator inside the integral to facilitate the notation of Eq. 3.26 we get:

$$i\mathcal{M}_\gamma^\mu = -e^3 \int \frac{d^4k}{(2\pi)^4} \int_0^1 dx \int_0^{1-x} dy \quad \left(\frac{N_\gamma}{D_\gamma}\right), \tag{3.28}$$

with the denominator being:

$$D_\gamma = [k^2 - 2xkp_1 + 2ykq + xp_1^2 + yq^2 - (y+z)m^2 + i\varepsilon]^3. \tag{3.29}$$

Following the procedure of the Feynman trick, we perform the change of variables:

$$k^\mu \to l^\mu - yq^\mu + xp_1^\mu \quad ; \quad d^4k \to d^4l, \tag{3.30}$$

and using $p_1^2 = p_2^2 = m^2$ and $p_1 \cdot p_2 = m^2 - \frac{q^2}{2}$, we obtain the final form of this denominator, shown below:

$$\begin{aligned} D_\gamma &= (l^2 - \Delta_\gamma + i\varepsilon)^3; \\ \Delta_\gamma &= (y^2 + xy - y)q^2 + (1-x)^2 m^2. \end{aligned} \tag{3.31}$$

This same format of denominator will appear many times, with small changes in the 'Δ' parameter.

For the numerator, some algebra is needed. Leaving aside, for now, the integration and the factor of $-e^3$, we substitute for the new variable from Eq. 3.30 and use the property of Dirac matrices $\gamma^\nu \not{a} \not{b} \not{c} \gamma_\nu = -2\not{c}\not{b}\not{a}$ to get:

$$N_\gamma = (2!)(-2)\bar{u}(p_2)[\not{l} + x\not{p}_1 - y\not{q} + m]\gamma^\mu[\not{l} + x\not{p}_1 + (1-y)\not{q} + m]u(p_1). \tag{3.32}$$

Because of Lorentz invariance we have the following relations:

$$\begin{aligned} \int d^4l\,[l^\mu l^\nu] &= \int d^4l \left[\frac{1}{4} g^{\mu\nu} l^2\right]; \\ \int d^4l \left[l^\mu f(l^2)\right] &= 0, \end{aligned} \tag{3.33}$$

and with that we can eliminate any odd powers of l inside the integral. Then use the relations from Eq. 3.11 and $\gamma^\mu\gamma^\nu = 2g^{\mu\nu} - \gamma^\nu\gamma^\mu$, to obtain:

$$\begin{aligned} N_\gamma = \; & 2l^2\,[\bar{u}(p_2)\gamma^\mu u(p_1)] \\ & + 4\left[x^2 + 2x - 1\right] m^2\,[\bar{u}(p_2)\gamma^\mu u(p_1)] \\ & + 4\,[(x+y)(y-1)]\,q^2\,[\bar{u}(p_2)\gamma^\mu u(p_1)] \\ & - 8\left[x^2 + xy - 2x - 2y + 1\right] m\,[\bar{u}(p_2)p_1^\mu u(p_1)] \\ & - 8\,[-xy + x + 2y - 1]\,m\,[\bar{u}(p_2)p_2^\mu u(p_1)]\,. \end{aligned} \tag{3.34}$$

The objective now is to use the Gordon identity (Eq. 3.15). Then we have to work on the last two lines of Eq. 3.34 to get the terms with $(p_2 - p_1 = q)$ and $(p_2 + p_1)$. For that we use the simple relations:

$$\begin{aligned} Ap_1 + Bp_2 &= C_1(p_1+p_2) + C_2(p_2-p_1); \\ C_1 = \frac{A+B}{2} &\quad ; \quad C_2 = \frac{B-A}{2}, \end{aligned} \tag{3.35}$$

which gives:

$$\begin{aligned} & -8\left[x^2+xy-2x-2y+1\right] m\left[\bar{u}(p_2)p_1^\mu u(p_1)\right] \\ & -8\left[-xy+x+2y-1\right] m\left[\bar{u}(p_2)p_2^\mu u(p_1)\right] \\ = & -4(x^2-x)m\left[\bar{u}(p_2)(p_1+p_2)^\mu u(p_1)\right] \\ & -4(x^2+2xy-3x-4y+2)m\left[\bar{u}(p_2)q^\mu u(p_1)\right]. \end{aligned} \tag{3.36}$$

Then finally we can use the Gordon identity (Eq. 3.15) and find:

$$\begin{aligned} N_\gamma = \quad & 2\left[l^2 - 2m^2(x^2-4x+1) + 2(x+y)(y-1)q^2\right]\left[\bar{u}(p_2)\gamma^\mu u(p_1)\right] \\ & + 4im(x^2-x)q_\nu\left[\bar{u}(p_2)\sigma^{\mu\nu}u(p_1)\right] \\ & - 4m(x^2+2xy-3x-4y+2)q^\mu\left[\bar{u}(p_2)u(p_1)\right]. \end{aligned} \tag{3.37}$$

The last line of the above equation is zero because the Feynman parameters can be rewritten as $(x-2)(z-y)$ when using the Feynman parameters delta $[\delta(1-x-y-z)]$. Since this term is asymmetric in the exchange of y and z and everything else in the integral is symmetric over the same exchange, then it must be zero. Therefore, we have the same structure as Eq. 3.16 from where we can extract the form factors from the expression above as:

$$\begin{aligned} -ieF_{1,\gamma} &= -2e^3\int_0^1 dx\int_0^{1-x} dy\int\frac{d^4l}{(2\pi)^4}\frac{\left[l^2-2m^2(x^2-4x+1)+2(x+y)(y-1)q^2\right]}{D_\gamma}; \\ \frac{eF_{2,\gamma}}{2m} &= -4ie^3m\int_0^1 dx\int_0^{1-x} dy\int\frac{d^4l}{(2\pi)^4}\frac{(x^2-x)}{D_\gamma}, \end{aligned} \tag{3.38}$$

where we can see explicitly the dependence on q^2 and m^2 of the form factors that were stated before.

The first integral will not be evaluated here, because it is a long calculation that leads to zero when we take the limit of $q^2 \to 0$ and renormalize the theory.

This result can be found in Appendix C and is not surprising, since as $q^2 \to 0$ we should reproduce the coulomb potential, consistent with the tree-level result. And since this must be true for all orders in the perturbative expansion, for now on, the terms multiplying γ^μ will simply be ignored in loop diagrams, and $F_1 = 1$ will be maintained, representing the classical part of the g factor.

With that in mind, we can recognize that the full loop effect happens when

$$F_2 = \frac{g-2}{2} \neq 0. \tag{3.39}$$

This factor is called the anomalous magnetic dipole moment, and for the muon is often referred to by a_μ (remarking that this μ is not a Lorentz index). Using the integral identity:

$$\int \frac{d^4l}{(2\pi)^4} \frac{1}{(l^2 - \Delta + i\varepsilon)^3} = \frac{-i}{32\pi^2\Delta}, \tag{3.40}$$

we can compute the second term of Eq. 3.38 to arrive at:

$$F_{2,\gamma} = \frac{\alpha m^2}{\pi} \int_0^1 \int_0^{1-x} \frac{x(1-x)}{(y^2 + xy - y)q^2 + (1-x)^2 m^2}, \tag{3.41}$$

where we used the definition of the fine-structure constant from section 2.1.3. Finally, taking the limit of $q^2 \to 0$, the integration gives simply $\frac{1}{2m^2}$, and we are able to repeat the famous result by Schwinger [36]:

$$F_{2,\gamma} = a_{\mu,\gamma} = \frac{\alpha}{2\pi}. \tag{3.42}$$

3.3 Muon $g-2$ in the SM

So far the calculations done are the same for the muon and the electron since it is independent of the lepton mass. So we can safely say that the NLO correction for the muon is the same as Eq. 3.42. The differences from the electron will appear when we consider the heavy particles inside the loop diagram. Since the muon is approximately 200 times heavier than the electron these loop diagrams will not be as suppressed as for the case of the electron. So we can identify the one-loop diagrams that will contribute to the muon $g-2$ shown in Figure 3.4.

We will analyze each diagram separately in the next subsections, but the momentum convention used will be the same as for the photon loop, from Figure 3.3.

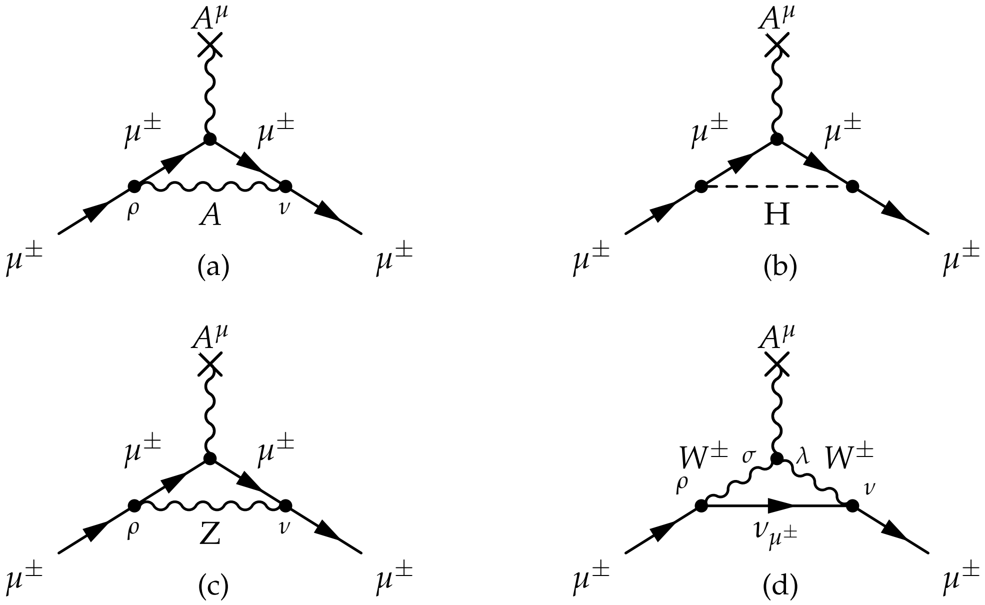

Figure 3.4: One-loop Feynman diagrams for the muon $g-2$ contribution. (a) photon loop, (b) Higgs-boson loop, (c) Z-boson loop , and (d) W-boson loop.

The computations that follow will be done in less detail since we can search directly for the terms that multiply $(\sigma^{\mu\nu}q_\nu)$, knowing that these contain the anomalous part of the magnetic dipole moment.

3.3.1 Higgs-boson contributions

Probably the simpler of the three remaining calculations is the one with the Higgs-boson loop, for it is a scalar field. The evaluation of the Feynman diagram from Figure 3.4b is given by:

$$\begin{aligned}
i\mathcal{M}_H^\mu = (-ie)\left(\frac{-g^2}{4}\right)\left(\frac{m}{M_W}\right)^2 \int \frac{d^4k}{(2\pi)^4}\bar{u}(p_2)\frac{i}{[(k-p_1)^2-M_H^2+i\varepsilon]} \\
\frac{i(\not{k}+\not{q}+m)}{[(k+q)^2-m^2+i\varepsilon]}\gamma^\mu\frac{i(\not{k}+m)}{[k^2-m^2+i\varepsilon]}u(p_1) \\
= (-ie)\left(\frac{ig^2}{4}\right)\left(\frac{m}{M_W}\right)^2 \int \frac{d^4k}{(2\pi)^4}\bar{u}(p_2) \\
\frac{(\not{k}+\not{q}+m)\gamma^\mu(\not{k}+m)}{[(k-p_1)^2-M_H+i\varepsilon]\,[(q+k)^2-m^2+i\varepsilon]\,[k^2-m^2+i\varepsilon]}u(p_1) \\
= (-ie)\left(i\frac{g^2}{4}\right)\left(\frac{m}{M_W}\right)^2 \int \frac{d^4k}{(2\pi)^4}\int_0^1 dx\int_0^{1-x} dy\ \left(\frac{N_H}{D_H}\right).
\end{aligned} \tag{3.43}$$

The denominator is similar to the one for the photon loop, with the only difference being an extra xM_H^2 in the delta term, as shown below:

$$\begin{aligned} D_H &= [l^2 - \Delta_H + i\varepsilon]^3; \\ \Delta_H &= (y^2 + xy - y)q^2 + (1-x)^2 m^2 + xM_H^2. \end{aligned} \tag{3.44}$$

The numerator, however, is simpler. The computation, following the same steps as before, yields:

$$\begin{aligned} N_H &= (2!)\bar{u}(p_2)(\not{k} + \not{q} + m)\gamma^\mu(\not{k} + m)u(p_1) \\ &= 2m(1-x^2)i[\bar{u}(p_2)\sigma^{\mu\nu}q_\nu u(p_1)] + O\left[\bar{u}(p_2)\gamma^\mu u(p_1)\right]. \end{aligned} \tag{3.45}$$

Substituting these values in Eq. 3.43 we can calculate the F_2 factor as:

$$\frac{eF_{2,H}}{2m} = (-ie)\left(\frac{g^2}{4}\right)\left(\frac{m}{M_W}\right)^2 \int \frac{d^4l}{(2\pi)^4} \int_0^1 dx \int_0^{1-x} dy \quad \left[\frac{2m(x^2-1)}{[l^2 - \Delta_H + i\varepsilon]^3}\right], \tag{3.46}$$

that can be computed analytically. The result expanded in powers of $\left(\frac{m}{M_H}\right)$ is shown below:

$$\begin{aligned} F_{2,H} = \frac{g^2}{64\pi^2}\left(\frac{m}{M_W}\right)^2 &\left[\left(\frac{m}{M_H}\right)^2 \frac{1}{6}\left(-7 - 12ln\left(\frac{m}{M_H}\right)\right)\right. \\ &+ \left.\left(\frac{m}{M_H}\right)^4 \frac{1}{4}\left(-13 - 24ln\left(\frac{m}{M_H}\right)\right)\right] + O\left[\left(\frac{m}{M_H}\right)^6\right]. \end{aligned} \tag{3.47}$$

3.3.2 Z-boson contributions

To simplify the calculations everything will be computed using the Feynman gauge ($\xi = 1$), and in appendix B.1 the gauge invariance is proven with more details. Since it is not the unitary gauge there will be an extra diagram, the loop with the Goldstone-boson in the place of the Z-boson. These two diagrams can be seen in Figure 3.5.

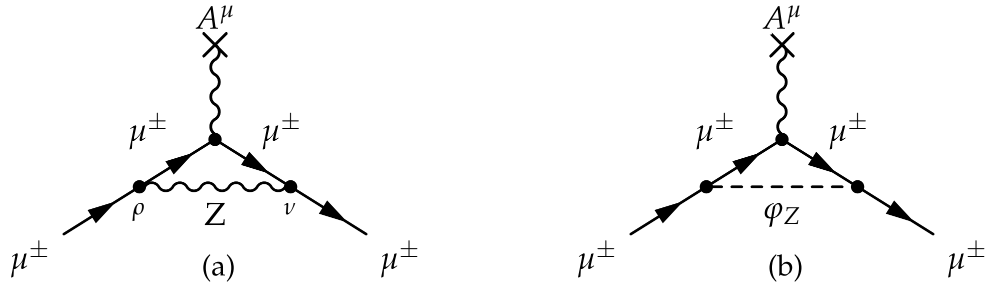

Figure 3.5: Feynman diagrams for the Z-boson contribution in the Feynman gauge. (a) is the Z-boson loop, and (b) the neutral Goldstone-boson loop.

The first diagram (Figure 3.5a) is evaluated as:

$$\begin{aligned} i\mathcal{M}^\mu_{Z_1} &= (-ie)\,(-i)\left(\frac{g}{4cos\theta_w}\right)^2 \int \frac{d^4k}{(2\pi)^4} \\ &\bar{u}(p_2)\frac{\gamma^\nu(A_Z+\gamma^5)(\not{k}+\not{q}+m)\gamma^\mu(\not{k}+m)\gamma_\nu(A_Z+\gamma^5)}{[(k+q)^2-m^2+i\varepsilon][k^2-m^2+i\varepsilon][(k-p_1)^2-M_Z^2+i\varepsilon]}u(p_1) \\ &= (-ie)\,(-i)\left(\frac{g}{4cos\theta_w}\right)^2 \int \frac{d^4k}{(2\pi)^4}\int_0^1 dx\int_0^{1-x} dy \quad \left(\frac{N_{Z_1}}{D_Z}\right), \end{aligned} \tag{3.48}$$

where $A_Z = 4sin^2\theta_w - 1$.

Once again, we divide the numerator and denominator to facilitate the computations. The denominator acquires the familiar form of:

$$\begin{aligned} D_z &= [l^2 - \Delta_Z + i\varepsilon]^3; \\ \Delta_Z &= (y^2+xy-y)q^2 + (1-x)^2m^2 + xM_Z^2, \end{aligned} \tag{3.49}$$

and the numerator, after following the same steps as before, yields:

$$\begin{aligned} N_{Z_1} &= (2!)\gamma^\nu(A_Z+\gamma^5)(\not{k}+\not{q}+m)\gamma^\mu(\not{k}+m)\gamma_\nu(A_Z+\gamma^5) \\ &= 4m[A_Z^2(x^2-x)+x^2+3x)]i[\bar{u}(p_2)\sigma^{\mu\nu}q_\nu u(p_1)] \\ &+ O\left[\ \bar{u}(p_2)\gamma^\mu u(p_1)\ ,\ \bar{u}(p_2)(...)\gamma^5 u(p_1)\ \right]. \end{aligned} \tag{3.50}$$

The second diagram (Figure 3.5b) is a little simpler, evaluated as:

$$\begin{aligned}
i\mathcal{M}^{\mu}_{Z_2} &= (-ie)\,(-i)\left(\frac{g^2}{4}\right)\left(\frac{m}{M_W}\right)^2\int\frac{d^4k}{(2\pi)^4} \\
&\quad \bar{u}(p_2)\frac{\gamma^5(\not{k}+\not{q}+m)\gamma^{\mu}(\not{k}+m)\gamma^5}{[(k+q)^2-m^2+i\varepsilon][k^2-m^2+i\varepsilon][(k-p_1)^2-M_Z^2+i\varepsilon]}u(p_1) \\
&= (-ie)\,(-i)\left(\frac{g}{4cos\theta_W}\right)^2 4\left(\frac{m}{M_Z}\right)^2\int\frac{d^4k}{(2\pi)^4}\int_0^1 dx\int_0^{1-x} dy\;\left(\frac{N_{Z_2}}{D_Z}\right).
\end{aligned} \tag{3.51}$$

The denominator is exactly the as (Eq. 3.49). And the numerator computation is shown below:

$$\begin{aligned}
N_{Z_2} &= (2!)\gamma^5(\not{k}+\not{q}+m)\gamma^{\mu}(\not{k}+m)\gamma^5 \\
&= [2m(1-x)^2]i[\bar{u}(p_2)\sigma^{\mu\nu}q_{\nu}u(p_1)] + O(\bar{u}(p_2)\gamma^{\mu}u(p_1)).
\end{aligned} \tag{3.52}$$

The combination of the results from Eq. 3.50 and Eq. 3.52 give the F_2 factor of:

$$\begin{aligned}
\frac{eF_{2,Z}}{2m} &= (-ie)\left(\frac{g}{2cos\theta_w}\right)^2\int\frac{d^4l}{(2\pi)^4}\int_0^1 dx\int_0^{1-x} dy \\
&\quad \frac{m[A_Z^2(x^2-x)+x^2+3x)]+[2m\left(\frac{m}{M_Z}\right)^2(1-x)^2]}{[l^2-\Delta_Z+i\varepsilon]^3},
\end{aligned} \tag{3.53}$$

which can be integrated analytically. The result after expanding in powers of $\left(\frac{m}{M_Z}\right)$ is:

$$\begin{aligned}
F_{2,Z} &= \frac{1}{64\pi^2}\left(\frac{g}{cos\theta_w}\right)^2\left[\left(\frac{m}{M_Z}\right)^2\frac{1}{3}\left(A_Z^2-5\right)\right. \\
&\quad \left.+\frac{1}{12}\left(\frac{m}{M_Z}\right)^4\left(25A_Z^2+24ln\left(\frac{m}{M_Z}\right)A_Z^2-19-24ln\left(\frac{m}{M_Z}\right)\right)\right] \\
&\quad +O\left[\left(\frac{m}{M_Z}\right)^6\right],
\end{aligned} \tag{3.54}$$

which agrees with R. Jackiw and S. Weinberg [37].

3.3.3 W-boson contributions

The W-boson loop is the most complicated, involving 4 diagrams, shown in Figure 3.6. The muon antineutrino and muon neutrino are represented by ν_{μ^+} and ν_{μ^-}, respectively. Remarking again that here we are using the Feynman gauge, and the gauge invariance is proven in appendix B.2.

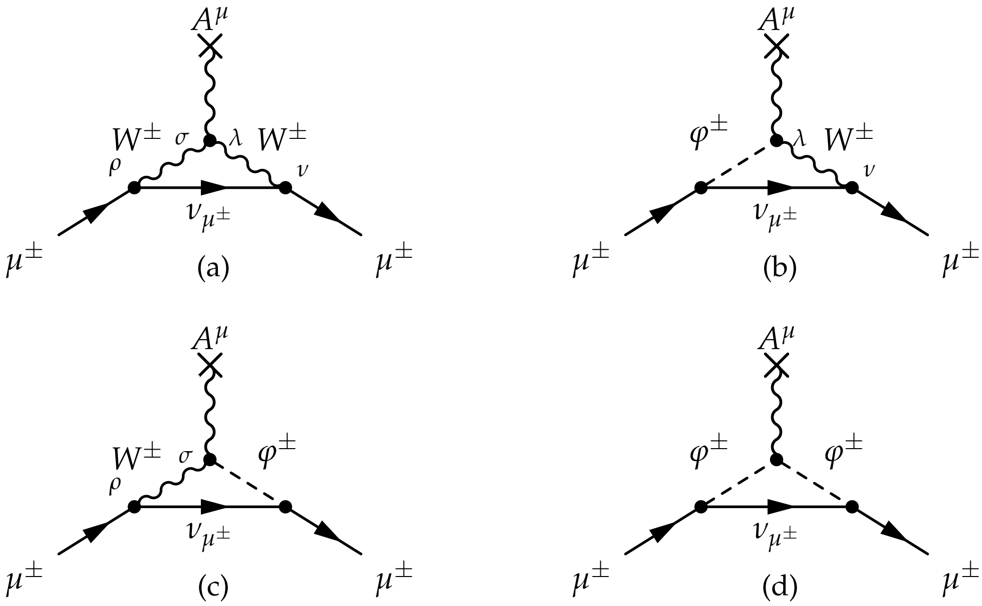

Figure 3.6: Feynman diagram for the calculation of the W-boson contribution in the Feynman gauge. (a) is the pure W-boson loop, (b) and (c) the mixed loop with one W-boson and one charged Goldstone-boson, and (d) the pure charged Goldstone-boson loop.

The evaluation of the first diagram (Figure 3.6a) grants:

$$
\begin{aligned}
i\mathcal{M}^\mu_{W_1} &= (-ie)\left(i\frac{g^2}{2}\right)\int\frac{d^4k}{(2\pi)^4} \\
&\quad \bar{u}(p_2)\frac{\gamma^\nu P_L g_{\nu\lambda}\cdot Int_W^{\lambda\sigma\mu}\cdot g_{\sigma\rho}(\not{k}-\not{p}_1)\gamma^\rho P_L}{[(k+q)^2-M_W^2+i\varepsilon][k^2-M_W^2+i\varepsilon][(k-p_1)^2+i\varepsilon]}u(p_1) \\
&= (-ie)\left(i\frac{g^2}{2}\right)\int\frac{d^4k}{(2\pi)^4}\int_0^1 dx\int_0^{1-x}dy\ \left(\frac{N_{W_1}}{D_W}\right),
\end{aligned}
\tag{3.55}
$$

with

$$
Int_W^{\lambda\sigma\mu} = \left[g^{\lambda\sigma}(2k+q)^\mu + g^{\lambda\mu}(-k-2q)^\sigma + g^{\sigma\mu}(q-k)^\lambda\right]. \tag{3.56}
$$

Once again, we divide the denominator and the numerator. The denominator will be the same for all four diagrams due to the choice of gauge, and is shown in:

$$\begin{aligned} D_W &= [l^2 - \Delta_W + i\varepsilon]^3; \\ \Delta_W &= (y^2 + xy - y)q^2 + (x^2 - x)m^2 + (1-x)M_W^2. \end{aligned} \tag{3.57}$$

The numerator for the diagram evaluation in Eq. 3.55 is:

$$\begin{aligned} N_{W_1} &= (2!)\gamma_\lambda Int_W^{\lambda\sigma\mu}(\not{k} - \not{p}_1)\gamma_\sigma P_L \\ &= m[2x^2 - 5x + 3]i[\bar{u}(p_2)\sigma^{\mu\nu}q_\nu u(p_1)] \\ &+ O\left[\, \bar{u}(p_2)\gamma^\mu u(p_1)\, ,\, \bar{u}(p_2)(...)\gamma^5 u(p_1)\,\right]. \end{aligned} \tag{3.58}$$

The second and third diagrams (Figures 3.6b and 3.6c) are evaluated jointly as:

$$\begin{aligned} i\mathcal{M}^\mu_{W_{2,3}} &= (-ie)\left(i\frac{g^2}{2}\right)\int \frac{d^4k}{(2\pi)^4} \\ &\bar{u}(p_2)\frac{m\left[\gamma^\mu(\not{k} - \not{p}_1)P_R + (\not{k} - \not{p}_1)\gamma^\mu P_L\right]}{[(k+q)^2 - M_W^2 + i\varepsilon][k^2 - M_W^2 + i\varepsilon][(k-p_1)^2 + i\varepsilon]}u(p_1) \\ &= (-ie)\left(-i\frac{g^2}{2}\right)\int \frac{d^4k}{(2\pi)^4}\int_0^1 dx \int_0^{1-x} dy \,\left(\frac{N_{W_{2,3}}}{D_W}\right). \end{aligned} \tag{3.59}$$

Having the same denominator as Eq. 3.57, all we need to do is evaluate the numerator, computed in terms of the Feynman parameters like:

$$\begin{aligned} N_{W_{2,3}} &= (2!)m\gamma^\mu(\not{k} - \not{p}_1)P_R + (\not{k} - \not{p}_1)\gamma^\mu P_L \\ &= m[1-x]i[\bar{u}(p_2)\sigma^{\mu\nu}q_\nu u(p_1)] \\ &+ O\left[\, \bar{u}(p_2)\gamma^\mu u(p_1)\, ,\, \bar{u}(p_2)(...)\gamma^5 u(p_1)\,\right]. \end{aligned} \tag{3.60}$$

The fourth and last diagram (Figure 3.6d) for the W-boson contribution is evaluated as:

$$\begin{aligned} i\mathcal{M}^\mu_{W_4} &= (-ie)\left(-i\frac{g^2}{2}\right)\left(\frac{m^2}{M_W^2}\right)\int \frac{d^4k}{(2\pi)^4} \\ &\bar{u}(p_2)\frac{(2k-q)^\mu(\not{k} - \not{p}_1)P_R}{[(k+q)^2 - M_W^2 + i\varepsilon][k^2 - M_W^2 + i\varepsilon][(k-p_1)^2 + i\varepsilon]}u(p_1) \\ &= (-ie)\left(-i\frac{g^2}{2}\right)\left(\frac{m^2}{M_W^2}\right)\int \frac{d^4k}{(2\pi)^4}\int_0^1 dx \int_0^{1-x} dy \,\left(\frac{N_{W_4}}{D_W}\right), \end{aligned} \tag{3.61}$$

and the numerator computed in terms of the Feynman parameters is:

$$\begin{aligned} N_{W_4} &= (2!)(2k+q)^{\mu}(\not{k} - \not{p}_1)P_R \\ &= m[x-x^2]i[\bar{u}(p_2)\sigma^{\mu\nu}q_{\nu}u(p_1)] \\ &+ O\left[\, \bar{u}(p_2)\gamma^{\mu}u(p_1)\,,\ \bar{u}(p_2)(...)\gamma^5 u(p_1)\,\right]. \end{aligned} \tag{3.62}$$

To compute the F_2 factor for the W-boson, we combine Eq. 3.55, Eq. 3.59, and Eq. 3.61 obtaining:

$$\begin{aligned} \frac{eF_{2,W}}{2m} = (-ie)\left(\frac{g^2}{2}\right)\int \frac{d^4 l}{(2\pi)^4}\int_0^1 dx \int_0^{1-x} dy \\ \frac{\left[-m(2x^2-5x+3)\right] - \left[m(1-x)\right] + \left[m[x-x^2]\left(\frac{m^2}{M_W^2}\right)\right]}{[l^2-\Delta_W+i\varepsilon]^3}. \end{aligned} \tag{3.63}$$

Following the previous computations, we perform the integral and then expand in terms of $\left(\frac{m}{M_W}\right)$ to get:

$$F_{2,W} = \frac{g^2}{64\pi^2}\left[\frac{10}{3}\left(\frac{m}{M_W}\right)^2 + \frac{2}{3}\left(\frac{m}{M_W}\right)^4\right] + O\left[\left(\frac{m}{M_W}\right)^6\right]. \tag{3.64}$$

One final comment on this result is that the mass of the W boson appears squared in the denominator, so corrections to the mass due to the measures shown in section 2.5 would be $1-\left(\frac{M_W^{CDF}}{M_W^{SM}}\right)^2 \cong 0.19\%$ which is currently outside of the experimental resolution, as will be shown in the next chapter.

3.4 Theoretical value for the muon $g-2$ in the SM

The computations shown explicitly so far are only for the one-loop contributions for the $g-2$ factor, but one can go further and calculate more loop diagrams to increase the theoretical precision of the result. This was done by a collaboration of many researchers and they are all shown in very detail by the White Paper report [38]. A brief explanation of the results will be provided in this section.

The diagram contribution for the muon $g-2$ factor can be divided into electromagnetic (QED), weak (EW), and hadronic (QCD). The full SM theoretical result for the muon $g-2$ is the sum of all these contributions:

$$a_\mu^{SM} = a_\mu^{QED} + a_\mu^{EW} + a_\mu^{QCD}. \tag{3.65}$$

The QED and EW multiple loops computations have features similar to the one-loop calculations shown in earlier sections. The largest contribution by far is the electromagnetic one. It has been calculated up to five loops (corrections up to $\left(\frac{\alpha}{2\pi}\right)^5$) which gives the target precision of around 10^{-11} of the current experiments. Six loops or more would range around values of 10^{-12}, therefore are ignored. The leading order for this QED computation is exemplified in Figure 3.4a, as stated before.

To precisely compute the value of the anomaly for the QED contribution a very precise measure of the fine structure constant (α) is needed. There are two major techniques to obtain it: atom interferometry and electron $g-2$ experiments. The result shown here [39] was obtained by using atom interferometry and has the value of:

$$\alpha = [137.035999046(27)]^{-1}, \tag{3.66}$$

but we remark that the value found using the other technique is within the same range of precision and agrees with this result. It can be found in [40]. The result of the muon $g-2$ for the QED contribution considering this value of α is given by:

$$a_\mu^{QED} = (116584718.931 \pm 0.104) \cdot 10^{-11}. \tag{3.67}$$

The EW contributions go up to NLO only (the leading order contribution is already around $\sim 10^{-9}$). The leading order contribution is exemplified by Figures 3.4c and 3.4d, as stated before, and the result for this contribution is:

$$a_\mu^{EW} = (153.6 \pm 1.0) \cdot 10^{-11}. \tag{3.68}$$

Lastly the hadronic computation. This is the one that gives the most uncertainties and discussion. We cannot calculate directly this contribution due to non-perturbative computations in Quantum-Chromo Dynamics (QCD). Therefore it requires some data-driven or lattice QCD simulation results.

There are two main diagrams to evaluate the QCD contribution. They are called Hadronic Vacuum Polarization (HVP) and Hadronic Light-by-Light contribution (HLbL). These diagrams are exemplified at leading order in Figure 3.7.

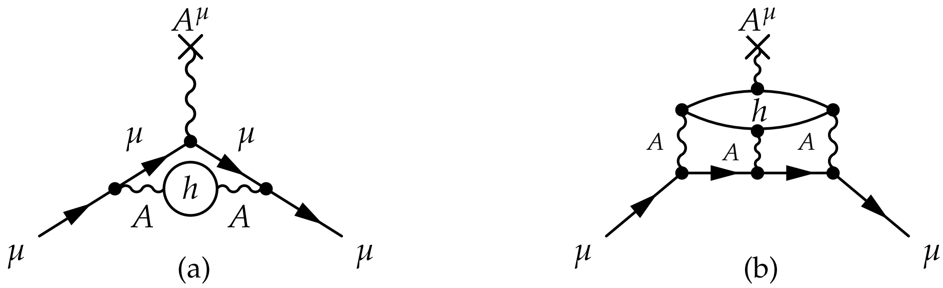

Figure 3.7: Feynman diagrams of the leading order hadronic (h) contribution to the muon $g-2$. (a) is the HVP contribution and (b) the HLbL contribution.

The HVP muon $g-2$ value was calculated up to 3 orders using only the data-driven methods, since lattice QCD results still have a higher order uncertainty ($\pm 184 \cdot 10^{-11}$). The resulting computed value is:

$$\begin{aligned} a_\mu^{HVP} =& a_\mu^{HVP,LO} + a_\mu^{HVP,NLO} + a_\mu^{HVP,NNLO} \\ &= (6931 \pm 40) \cdot 10^{-11} + (-98.3 \pm 7) \cdot 10^{-11} + (12.4 \pm 1) \cdot 10^{-11} \\ &= (6845 \pm 40) \cdot 10^{-11}. \end{aligned} \tag{3.69}$$

The HLbL result is a combination of data-driven and lattice QCD for the leading order result, summed with the next leading order for the data-driven result. The resulting contribution is:

$$\begin{aligned} a_\mu^{HLbL} =& a_\mu^{HLbL,LO} + a_\mu^{HLbL,NLO} \\ &= (90 \pm 17) \cdot 10^{-11} + (2 \pm 1) \cdot 10^{-11} = (92 \pm 18) \cdot 10^{-11}. \end{aligned} \tag{3.70}$$

Combining the results from Eq. 3.67, Eq. 3.68, Eq. 3.69, and Eq. 3.70 considering their uncertainties uncorrelated, we find that the most recent theoretical value for the muon $g-2$ is:

$$a_\mu^{SM} = a_\mu^{QED} + a_\mu^{EW} + a_\mu^{HVP} + a_\mu^{HLbL} = (116591810 \pm 43) \cdot 10^{-11}. \tag{3.71}$$

This result is a combination of values found in [40–59] which should be cited in any work that uses or cites the result above.

For completeness, we should mention that there is one lattice result, from the BMW collaboration [60] that calculated the LO of the HVP diagrams to be:

$$a_\mu^{HVP_{BMW},LO} = (7075 \pm 55) \cdot 10^{-11}, \tag{3.72}$$

which is in a greater agreement with the current experiments, giving:

$$a_\mu^{BMW} = (116591954 \pm 58) \cdot 10^{-11}, \tag{3.73}$$

a $1.5\,\sigma$ discrepancy when considered alone. When combined with the previously mentioned SM result (Eq. 3.71) it gives:

$$a_\mu^{SM+BMW} = (116591881.5 \pm 38) \cdot 10^{-11}, \tag{3.74}$$

which, in turn, is a $3.2\,\sigma$ discrepancy. Lattice results are usually laborious to check and take time, so for this work we will assume the result published by the White Paper [38] to be correct (result from Eq.3.71), but keeping in mind that there is a conflict among the current theoretical results that need further evaluation.

Chapter 4

Muon $g-2$ experiments

We discussed how the anomalous magnetic moment of the muon appears in the theory, but we have not yet justified the use of the muon for the experiments to test the SM. If there exists new physics at a scale of Λ, then the sensibility of a lepton anomalous magnetic moment to this new physics is of order

$$\left(\frac{m_l}{\Lambda}\right)^2, \tag{4.1}$$

according to A. Pich [61], where m_l is the lepton mass. This is in agreement with the results obtained in the last chapter. Therefore the heavier the lepton, the greater the sensibility to heavier particles in the $g-2$ factor. In the SM we have three massive leptons to use. The electron, the muon and the tau, in ascending order of mass. The tau particle is very unstable and decays in around $2.9 \cdot 10^{-13}s$, which makes it very hard to use in experiments. In turn, electrons are very light, implying that very high precision is needed to find a heavy unknown particle. Consequently, the use of muons becomes the most reasonable choice.

The objective of this chapter is to give an overview of the more than 60 years of historical experiments searching for the muon $g-2$. Some characteristics of their evolution will be laid out, and a more detailed explanation of the latest experiment to release results, the Fermilab (E-989), will be provided, clarifying how the measure was done.

4.1 History of the muon $g-2$ experiments

The first observation of a muon-related phenomenon was made by Paul Kunze in 1933 [62], [63] but was only recognized as an elementary particle in 1936 by C. D. Anderson and S. H. Neddermeyer [64]. And the recognition of the muon as heavy lepton is attributed to the 1957 experiment by R. L. Garwin, L. M. Lederman, and M. Weinrich [65], which observed the muon spin and its precession under a Magnetic field. Since then, many other experiments were done to measure, each time more precisely, the $g-2$ for the muon in the never-ending search for new physics.

The first measurement of the muon g factor was done by R. L. Garwin in 1957 using the decay of $\pi^+ \to \mu^+ + \nu_{\mu^+}$, yielding a rough measure of $g_{S,\mu} = 2 \pm 0.2$, but in the same year Cassels and Garwin again would, separately, improve this measure to $g_{S,\mu} = 2\left(1.00113^{+0.00016}_{-0.00012}\right)$ that confirmed the calculations by Schwinger and the behaviour of the muon as a heavy lepton.

After these early measures, CERN made 3 important experiments, each improving methods and techniques, and consequently the precision of the measure. The first experiment was done with a rectangular magnet with a small gradient that caused the circular orbit of the muon to go to the edge of the magnet. Then another magnet would eject the muon to a target that would stop it without destroying its polarization. The subsequent decay of the muon contained information about the amount it precessed, hence a measure of the a_μ factor. Some technical issues, that would be solved later, crippled the accuracy, and the final result of this experiment, attained in 1962, was

$$a_\mu^{C1} = (1\,162 \pm 5) \cdot 10^{-6}.$$

So far all measures included stopping the muon at a target, which meant that only μ^+ could be used. Low energy μ^- would be captured into atomic orbits resulting in a lower effective lifetime for the muon, which made it very hard to use in experiments.

The second CERN experiment was the first to use a storage ring, and the future ones would all repeat this kind of storage for the muons that allows for much higher energy beams of particles. Other improvements were also made, like the use of kickers to stabilize the orbits, incident beam of particles, etc... [35]. Some technical issues hindered the accuracy of this result as well, like the use of a magnetic gradient to trap the muons, and large noise in the detectors. The result obtained in 1968 was:

$$a_\mu^{C2} = (11\,661 \pm 3.1) \cdot 10^{-7}.$$

The third and last CERN experiment made some considerable advances in precision. It was the first to use an electrostatic focusing of the particles, the so-called Penning trap, and the use of the "magic" energy of $3.09\,GeV$ for the muon, which importance will be discussed later in this work. The use of the Penning trap allowed for a uniform magnetic field, which is important to guarantee that all muons precess at the same rate. Another important innovation was the use of a tool to cancel the magnetic field at the pion entrance (called pulsed magnetic inflector), diminishing the noise in the detectors and allowing a more uniform beam to enter the storage ring. The improved result obtained in 1979 was:

$$a_\mu^{C3} = (1\,165\,924\ \pm 8.5) \cdot 10^{-9}.$$

So far all the results were still in accordance with the SM up to three orders of radiative correction. The experiment that changed this was the Brookhaven BNL E-821 experiment, located in New York, USA. BNL experiment was a collaboration that took around 20 years, and more than 100 scientists to obtain a more accurate measure of the muon $g-2$. The technical advances made by CERN experiments were added, including the storage ring, the penning trap, the "magic" energy, and others. To improve the precision some other advances were made, including a more uniform magnetic field and incident beam energy, a higher density incident beam, a faster muon kicker, and more small advances in technique. The accuracy of this experiment was the first to include four orders of radiative correction, including weak and hadronic loops, and the last measure released in 2004 [5] was:

$$a_\mu^{BNL} = (116\,592\,080\ \pm 63) \cdot 10^{-11}.$$

This result was the first to deviate from the theoretical result by between 2.2 and 2.7 standard deviations (σ). Thus, there is a glimpse of new physics and a more precise experiment started to be elaborated at Fermilab to test to a higher accuracy this phenomenon. This experiment will be described in detail in the next section.

4.2 The Fermilab experiment

The Fermilab experiment (E-989) is an ongoing experiment to the date this work is written which is taking place in Illinois, USA. It is a collaboration of many scientists with measurements up to $0.46 \cdot 10^{-9}$ precision and with still some data to be released. To understand how this measure is made a brief description of the experiment and its technicalities will be provided.

To measure the magnetic moment it is used the fact that a particle with a magnetic moment inside a magnetic field precesses with a certain frequency. In the case of polarized particles perpendicular to the magnetic field, this frequency is proportional to its magnetic moment times the magnetic field, as shown in:

$$\vec{w}_L = \vec{\mu} \times \vec{B} \overset{\perp}{=} g \left(\frac{Q_f e}{2m} \right) \vec{B}, \tag{4.2}$$

where Q_f is again ± 1 depending on the charge of the fermion, and w_L is called the Larmor frequency. Looking at this formula, it becomes clear the importance of a very uniform magnetic field for measurement accuracy: maintaining a uniform magnetic field keeps the frequency of precession constant. The magnet used in the Fermilab experiment is the same as the earlier experiment BNL E-821 since it has an extremely uniform magnetic field.

This precession frequency (Larmor frequency) can be measured either by observing electromagnetic radiation emitted or absorbed at the Larmor frequency, or by directly observing through a characteristic of the parity violation decay of the muon that will be discussed in section 4.2.1. This latest is the technique used in the Fermilab experiment.

To create a perpendicular polarized beam of muons there are lots of steps. First high energy positrons are created and collided with a target in the particle accelerator at Fermilab, producing many different elementary particles. Among them the charged pions ($\pi^{\pm}$) are selected, using their specific mass and charge, to enter in the pion decay chamber, a tunnel that allows pions to decay during its course.

Pions decay into muon and neutrinos with a 99.99% branching ratio [13], and this is a 100% parity violation weak decay (illustrated in Eq. 4.3). Therefore the forward and backward direction of this decay can be selected to create an extremely polarized beam of muons.

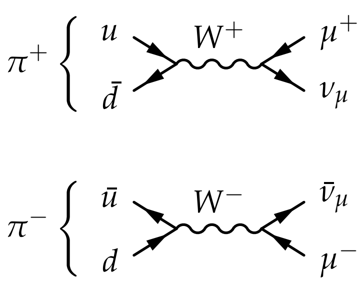

$$\Rightarrow \quad \pi^+ \rightarrow \mu^+ + \bar{\nu}_\mu;$$

$$\Rightarrow \quad \pi^- \rightarrow \mu^- + \nu_\mu. \tag{4.3}$$

This polarized beam of muons is then inserted into the storage ring. To enter the ring it passes through what is called a superconducting inflector magnet [66] that cancels the magnetic field of the ring at the entering point to facilitate the adjustment of the beam inside the ring. To make sure that the inflector does not intervene in the trajectory of the muon inside the ring, it is positioned slightly to the external side.

Then, since the muon does not have the energy necessary to maintain its trajectory inside the ring, it spirals inwards. After about a quarter of a turn a very quick magnetic pulse, called kicker [67], is used to boost the muon to the exact energy necessary to be kept inside the ring. This process is done with extreme precision equipment, and all uncertainties are measured in detail, which were thoroughly analysed by the Fermilab Muon $g-2$ Collaboration [68].

Finally, with the muon stored inside the ring, it is possible to measure the precession frequency. Since the muons of the experiment are highly energetic, the actual precession frequency needs to be corrected due to relativistic effects by:

$$\begin{aligned}\vec{w}_S = -\frac{Q_f e}{m}\Bigg[&\left(\frac{g}{2}-1+\frac{1}{\gamma}\right)\vec{B}-\left(\frac{g}{2}-1\right)\frac{\gamma}{\gamma+1}\left(\vec{\beta}\cdot\vec{B}\right)\vec{\beta}\\&-\left(\frac{g}{2}-\frac{\gamma}{\gamma+1}\right)\vec{\beta}\times\vec{E}\Bigg].\end{aligned} \tag{4.4}$$

where β is the velocity of the particle in natural units, $\gamma = \frac{1}{\sqrt{1-\beta^2}}$ is the Lorentz factor, and $\vec{E}$ is the electric field. The inclusion of the correction relative to the electric field is due to the Penning trap, technique implemented in the Fermilab experiment as well.

We can disregard the term $\vec{\beta}\cdot\vec{B}$ because of the perpendicular polarization of the muon beam. Now we need to subtract the rotation frequency (w_C) due to the movement of the charged particle in the magnetic field, which is

$$\vec{w}_C = -\frac{Q_f e}{m}\left[\frac{\vec{B}}{\gamma}-\frac{\gamma}{\gamma^2-1}\vec{\beta}\times\vec{E}\right], \tag{4.5}$$

resulting in the frequency called w_{a_μ} written as:

$$\vec{w}_{a_\mu} = \vec{w}_S - \vec{w}_C = -\frac{Q_f e}{m}\left[a_\mu\vec{B}-\left(a_\mu-\frac{1}{\gamma^2-1}\right)\vec{\beta}\times\vec{E}\right], \tag{4.6}$$

where we used the substitution $a_\mu = g/2-1$.

Looking at the term that multiplies $\vec{\beta}\times\vec{E}$ we can see that there will be a value of γ that will make it vanish, as shown below:

$$a_\mu - \frac{1}{\gamma_m^2 - 1} = 0\ ;\ \gamma_m \simeq 29.3\ ;\ E_m \simeq 3.09GeV. \tag{4.7}$$

These values are the so-called "magic" Lorentz factor and energy mentioned in the last section, represented by γ_m and E_m. We should note that some iterations are needed to obtain this value since a_μ is the factor that we want to measure with precision.

Another advantage of using this "magic" gamma is the time dilation of the muon lifetime. It goes from 2.2 μs in the muon reference frame, to the extended 64.4 μs in the laboratory reference frame. And since one full precession takes around 4.4 μs to occur, this elongated lifetime gives enough duration for the muon frequency to be calculated.

After these simplifications the final form of this frequency is simply:

$$\vec{w}_{a_\mu} = -a_\mu \frac{q\vec{B}}{m}, \tag{4.8}$$

and this result is very useful since it gives directly the anomalous part of the magnetic moment, after a simple division, justifying the choice of the convention for the name ($\vec{w}_{a_\mu}$).

The final step is to detect this frequency, and this was done in Fermilab with the use of 24 calorimeters evenly disposed along the internal part of the ring that can sense the energy of the decay electron or positron above $50MeV$. To understand this step a more detailed look at the muon decay distribution will be shown in the following subsection.

4.2.1 Muon decay

To better comprehend the muon $g-2$ experiments it is important to understand the decay modes of the muon. Primordially there is only one decay channel, the weak decay, shown in Figure 4.1. This mode corresponds experimentally to more than 99.99% of the muon decays [13]. The diagram exchanging the $W^\pm$ with the Goldstone-boson ($\varphi^\pm$) can be ignored since it will have a factor of $\frac{m_e m_\mu}{M_W^2} \sim 10^{-8}$ to its contribution, hence we have only one diagram to evaluate.

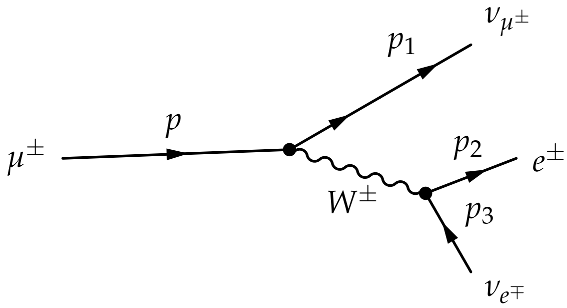

Figure 4.1: Main decay mode for the muon

Again, we will use the Feynman gauge ($\xi = 1$). The evaluation of this diagram using the Feynman rules from section 2.1.2 grants:

$$i\mathcal{M}_{\mu\to e\nu\bar{\nu}} = \bar{u}(p_1)\left[-i\frac{g}{\sqrt{2}}\gamma^\mu P_L\right]u(p)\left[\frac{-ig_{\mu\nu}}{k^2 - M_W^2 + i\varepsilon}\right]\bar{u}(p_2)\left[-i\frac{g}{\sqrt{2}}\gamma^\mu P_L\right]u(p_3). \tag{4.9}$$

The first simplification is $k^2 << M_W^2$ (since $k^2 < m_\mu^2 << M_W^2$) and we can ignore it. Knowing that we need to calculate the modulus square of this element for the decay width, we can also use for the neutrinos and electrons the relations:

$$\sum_s u^s(p)\bar{u}^s(p) = \not{p} + m; \quad \sum_s v^s(p)\bar{v}^s(p) = \not{p} - m, \tag{4.10}$$

since we are not interested in their spin configuration. For the muon, we want to keep the information about the direction of the spin, so it is useful to use the projection operators for spin and energy [69]:

$$u^s(p)\bar{u}^s(p) = (\not{p} + m)\frac{1+\gamma^5\not{s}}{2}, \tag{4.11}$$

where $s^\mu = (0, \vec{s})$ and $\vec{s}$ is the spin direction is space. Ignoring the electron and neutrino masses, we obtain:

$$\begin{aligned} |\mathcal{M}|^2 =& \frac{g^4}{4M_W^4} Tr\left[(\not{p}+m)\frac{1+\gamma^5\not{s}}{2}\gamma^\nu \not{p}_1\gamma_\mu P_L\right] Tr\left[\not{p}_3\gamma_\nu\not{p}_2\gamma^\mu P_L\right] \\ =& 2\frac{g^4}{M_W^4}[(p-ms)\cdot p_3][p_1\cdot p_2]. \end{aligned} \tag{4.12}$$

In order to calculate the decay width, according to D. Bailin and A. Love [70], we use:

$$d\Gamma(\mu \to e\nu\bar{\nu}) = \frac{1}{(2\pi)^5}|\mathcal{M}|^2\delta^4(p-p_1-p_2-p_3)\frac{d^3p_1 d^3p_2 d^3p_3}{2m2E_1 2E_2 2E_3}. \tag{4.13}$$

Since we are interested in the energy distribution of the electron, we can integrate over the momentum of the neutrinos, using:

$$\int \frac{d^3p_1}{2E_1}\frac{d^3p_3}{2E_3}\delta(p-p_1-p_2-p_3)p_{1,\mu}p_{3,\nu} = \frac{\pi}{24}[(p-p_2)^2 g_{\mu\nu} + 2(p-p_2)_\mu (p-p_2)_\nu], \tag{4.14}$$

and writing the integral over the electron momentum in terms of the energy $d^3p_2 = E_2^2 dE_2 d\Omega$, we have:

$$\begin{aligned} d\Gamma(\mu \to e\nu\bar{\nu}) = \left(\frac{g}{M_W}\right)^4 \frac{E_2 dE_2 d\Omega}{96(2\pi)^4 m} \Big\{ &[(p\cdot p_2) - m(s\cdot p_2)]\left[p^2 - 2(p\cdot p_2) + p_2^2\right] \\ &+ \left[p^2 - (p\cdot p_2) - m(s\cdot p) + m(s\cdot p_2)\right]\left[(p\cdot p_2) - p_2^2\right]\Big\}. \end{aligned} \tag{4.15}$$

Then, we can use θ to be the angle between the electron and the spin direction, $p_2 \cdot s = -E_2 \cos\theta$ (since $|s| = 1$), $p_2^2 = p\cdot s = 0$ and $p^\mu = (m, 0, 0, 0)$ to obtain:

$$d\Gamma(\mu \to e\nu\bar{\nu}) = \left(\frac{g}{M_W}\right)^4 \frac{m^2 E_2^2 dE_2 d\Omega}{96(2\pi)^4}\left[3 - 4\frac{E_2}{m} + (1 - 4\frac{E_2}{m})\cos\theta\right]. \tag{4.16}$$

To continue, we look at the Mandelstam variable [71] $s_2 = (p-p_2)^2$ and we can see that we can choose a frame where $p = p_2$ so that $s_2 = 0 = p^2 - 2pp_2\cos\kappa + p_2^2 = m^2 - mE_2$ and the highest possible energy is:

$$E_{2(max)} = \frac{m_\mu^2 + m_e^2}{2m_\mu} \approx \frac{m_\mu}{2}. \tag{4.17}$$

So we can define $x = \frac{2E_2}{m_\mu}$ which is the proportion of the maximum energy, use $d\Omega = 2\pi d\cos\theta$ and rewrite Eq. 4.16 as:

$$\frac{d\Gamma(\mu \to e\nu\bar{\nu})}{dx\, d\cos\theta} = \left(\frac{g}{M_W}\right)^4 \frac{m^5}{768(2\pi)^3}x^2\left[3 - 2x + (1-2x)\cos\theta\right]. \tag{4.18}$$

Since we know that the energy threshold for the calorimeters used in the experiment is around $50MeV$, which is approximately the maximum energy, we can fix $x \rightarrow 1$ and plot the distribution, obtaining Figure 4.2, where it is clear that most of the high energy electrons will be found in the direction directly opposite to the muon spin. Figure 4.3 shows this relation simplified for the case of the positron and the electron.

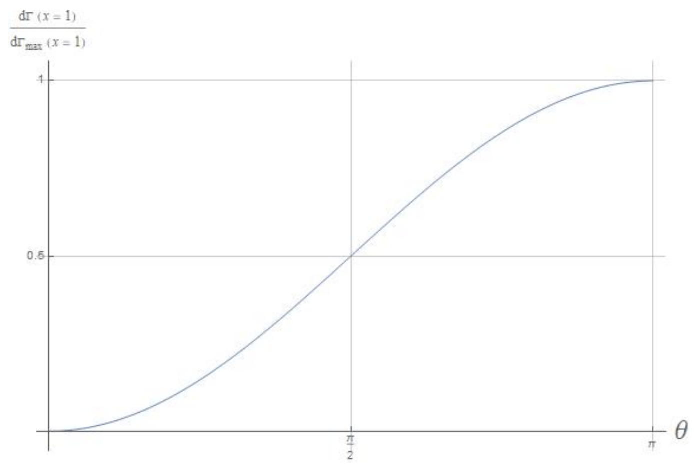

Figure 4.2: Angular distribution of the resulting electron with maximum possible energy ($E_2 = \frac{m_\mu}{2}$) at a muon decay

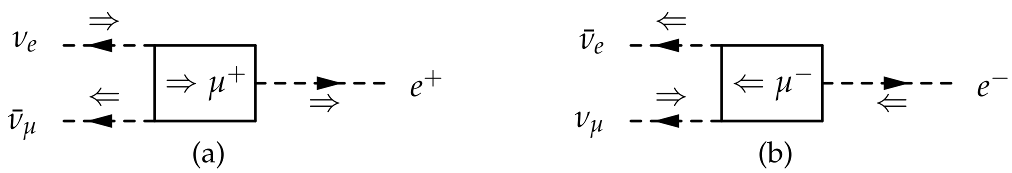

Figure 4.3: Relation between the muon polarization and the maximum distribution probability of the maximum energy decayed positron [electron] (a), [(b)], respectively. The double arrow represents the spin direction, and the dashed arrow the momentum direction.

4.2.2 Fermilab Results

As a summary of the topics discussed, Figure 4.4 shows the schematics of the storage ring used in the experiment and illustrates many of the features exposed in this section.

Now that all the tools to calculate the muon $g-2$ have been laid the results can be understood deeply. One of the graphical results obtained is shown in Figure 4.5 that demonstrates the behaviour of the oscillation of the number of electrons (or positrons) absorbed in the calorimeters above the threshold energy (50 MeV).

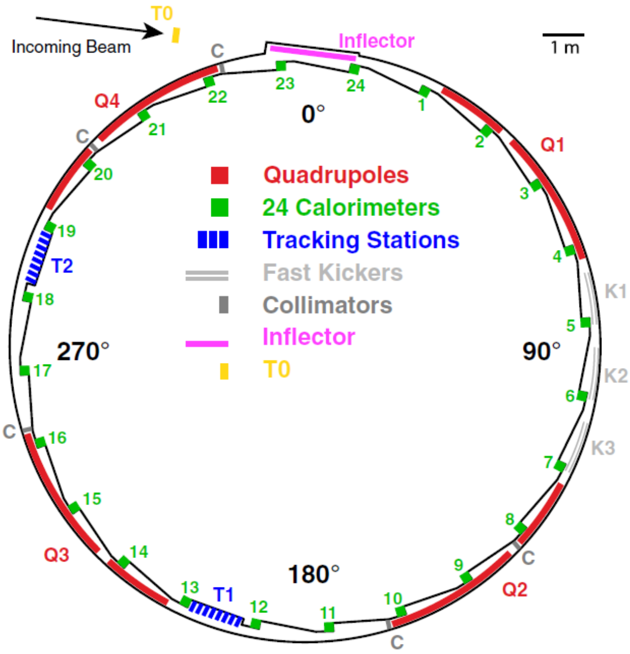

Figure 4.4: Fermilab's muon $g-2$ experiment schematics. In the image can be seen the location of quadrupoles for the Penning Trap, the calorimeters (detectors), the fast muon kickers, and the inflector. Also shown are the Tracking stations that track where the bean is located relative to the center of the ring optimal trajectory and the collimators that help correct this beam trajectory. Source: Fermilab Muon $g-2$ Collaboration [68].

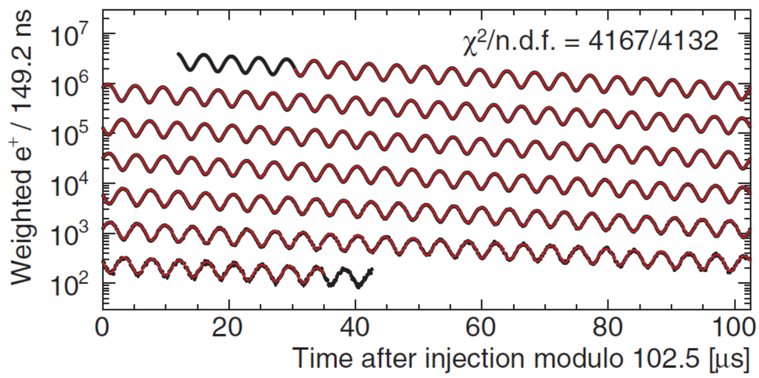

Figure 4.5: Electron decay energy 102.5 μs after injection of muon beam into the storage ring in Fermilab's muon $g-2$ experiment. Source: Fermilab Muon $g-2$ Collaboration [6]

Using only this figure we can estimate the value of the muon $g-2$: there are approximately 645.0μs of data and 148 oscillations which results in a period of $T_\mu = 4.36\mu s$ for each precession. The frequency is then $\omega_\mu = \frac{2\pi}{T_\mu} = 1.44 \cdot 10^6 s^{-1}$.

Using this result in formula 4.8 with the Magnetic field used in Fermilab of $\vec{B} = 1.45T$ ($T = Kg \cdot C^{-1} \cdot s{-}1$), a charge of $-1.6 \cdot 10^{-19}C$ and a muon mass of $105.7 MeV \cong 188 \cdot 10^{-30} Kg$, we obtain:

$$a_\mu^{estimate} = \frac{(1.44 \cdot 10^6\, s^{-1})(188 \cdot 10^{-30}\, kg)}{(1.6 \cdot 10^{-19}\, C)(1.45\, Kg \cdot C^{-1} \cdot s{-}1)} \approx 1.16 \cdot 10^{-3}, \tag{4.19}$$

which gives the expected Schwinger computation. A more detailed and accurate measurement of these factors mentioned was done, giving the final result of:

$$a_\mu^{FNAL} = (116\,592\,040\, \pm 54) \cdot 10^{-11}, \tag{4.20}$$

which agreed with the previous BNL E-821 experiment, differing from the theoretical result by $3.3\,\sigma$. The combined results from both of them give a value of:

$$a_\mu^{EXP} = (116\,592\,061\, \pm 41) \cdot 10^{-11}, \tag{4.21}$$

which gives a deviation of:

$$\Delta(a_\mu) = a_\mu^{EXP} - a_\mu^{SM} = (251 \pm 59) \cdot 10^{-11}. \tag{4.22}$$

These values can be found in the Fermilab Muon $g-2$ Collaboration result report [6].

Such a result is very significant because it deviates from the theoretical calculation by $4.2\,\sigma$, as can be seen in Figure 4.6. There is a consensus that around $5\,\sigma$ deviation is enough statistical confirmation to mark the result as an issue, or as a real indication of new physics.

The experiment E-989 at Fermilab is still running. So far it only used around 6% of its full statistical data [72]. Therefore a more complete result from the following runs of the experiment will give a more precise measurement and could increase the confidence that new physics is needed.

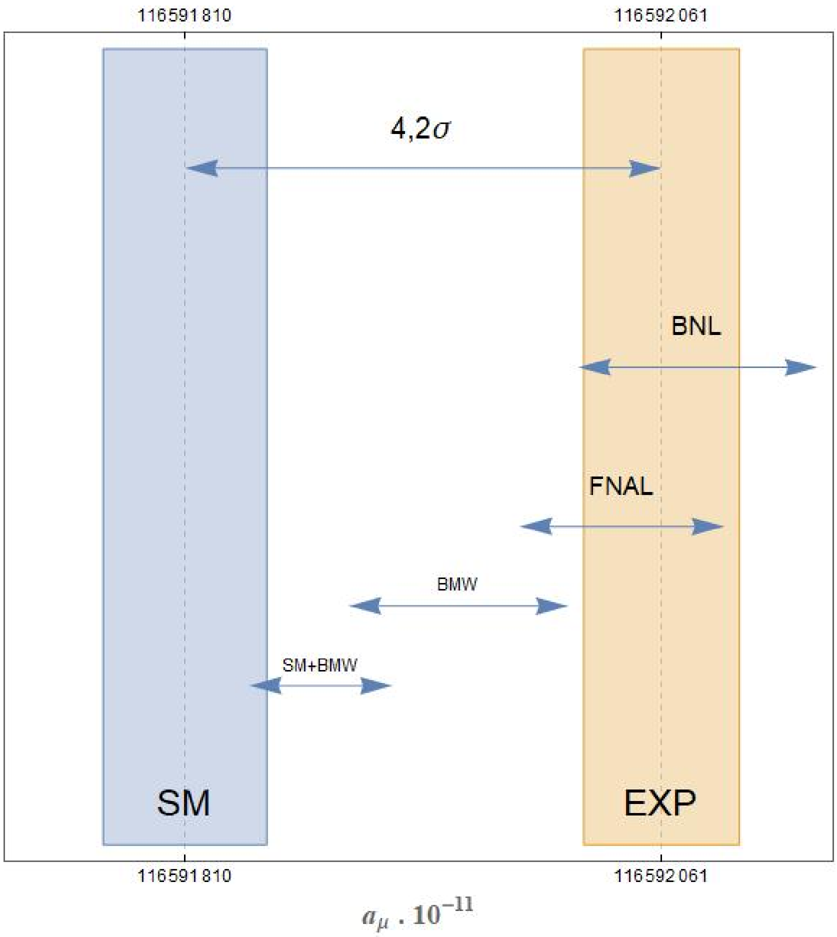

Figure 4.6: Comparison between experimental and theoretical value of a_μ. In the image, the results from the last two experiments (BNL E-821 and FNAL E-989) are shown, along with the combined result of both, the standard model prediction and the discrepancy between them. The results from the BMW collaboration and its combination with the white paper result are also shown for the demonstration of the theoretical tension.

Chapter 5

Beyond the SM

The SM is a very successful theory with, as stated before, many precise predictions. Presently, many physicists focus on discovering what lies beyond the SM. In Section 2.4 we explored a few issues with the SM that indicates the need for new physics in order to explain them.

New physics can be "bottom-up", meaning we add the new physics to explain an issue and then see the implication of them, or "top-down", meaning we departure from a more fundamental theory or postulates, like supersymmetry or grand unification theories, and attempt to find the correct values for the free parameters when comparing with the experiment. There are many possibilities when making extensions to the SM. For example, the addition of new types of particles, the extension of the gauge group to higher scales, among others. Mostly used is the addition or extension of gauge groups. This also means new free parameters and new particles that have to obey the known experimental limits.

As explained along with the issues with the SM, additions to the theory can cause a conflict favouring high scales to solve some of them (e.g. baryogenesis, dark energy) and low scales to not to cause others (e.g. Higgs hierarchy, flavour changing). This shows that whatever the new theory is, if we do not want one more fine-tuning problem, it will have constraints coming from different angles.

One thing many of the new physic theories have in common is the extension of the number of particles of the SM with new interactions and masses. In the literature many such cases can be found, for example, axions [73] that add only one particle in a singular manner, or Supersymmetric models like the MSSM (Minimal Supersymmetric Standard Model) [74] that add many particles. From extensions like these, we can extract some of the new types of Feynman diagrams that could contribute to the muon $g-2$.

To probe for new physics some techniques can be used. One of them is direct observation, which is directly producing the new particle or bound states. This method needs to achieve the scale of energy of the new physics, which translates directly to limitations of both economical and technological types. Another way to search for new physics is through indirect measures, for example, flavour violations, CP violation, or exotic decay modes. All of these will include loop evaluations, for the reason that at the tree level they would not be allowed.

One such indirect measure is the muon $g-2$. As stated before the deviations in the muon $g-2$ value can be evidence of new particles through loop contributions, and, as we have seen in the previous chapter, this evidence is becoming strong. So we can look for the $g-2$ contributions of a new model to try to correct the prediction discrepancy or at least impose boundary conditions on the new model in question.

For the reasons displayed in the introduction, the idea is to try to solve the issue with the addition of at least one new scalar field. In the beginning of chapter 4, it was affirmed that the contribution to the muon $g-2$ depends on the mass of the lepton squared divided by the new physics scale squared (Eq. 4.1), which means that simply adding one new heavy scalar is probably not enough, at least not in a natural way. But that affirmation comes from flavour diagonal theories ("SM-like interactions").

One possibility we may test is what happens if the lepton running in the loop is heavy. Following the same logic as before, there will always be at least one factor of the muon mass in the numerator, but maybe the sensibility can be reduced to:

$$\left(\frac{m_\mu}{\Lambda}\right). \tag{5.1}$$

For this to happen, we need a model with at least one new heavy fermion, one heavy scalar, and non-diagonal interactions.

This hypothesis will be tested in the next sections, first by introducing a new interaction and new particles without any care for the practicality of the theory. Then, a more concrete example taken from the literature, the 3-3-1 model [75], will be analysed in the same manner. This model will be explained briefly and, in the end, the muon $g-2$ for a specific diagram in this model will be evaluated using its rules. The objective is to test if a flavour-violating theory with new heavy fermions and scalar fields could solve the muon $g-2$ issue.

5.1 Scalar-like and heavy lepton-like particles in a flavour violation muon $g-2$ loop

To test if the prediction from Eq. 5.1 is correct, we can make a toy model with a heavy scalar and a heavy lepton running in the loop as shown in Figure 5.1.

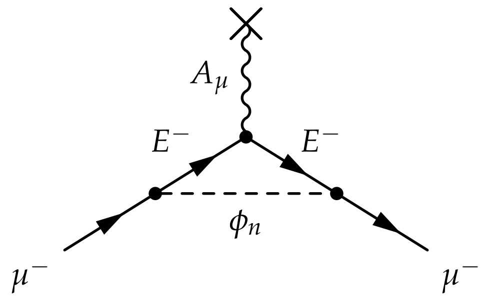

Figure 5.1: Diagram for the simple new scalar with a heavy lepton running in the loop

For simplicity we will add an interaction like:

$$\mathcal{L}_{\phi_n} = -g_{\phi_n}\bar{\psi}_\mu \phi_n \psi_E + H.c. \quad , \tag{5.2}$$

where ϕ_n is the new neutral scalar field, ψ_e is the known muon field and ψ_E the charged heavy fermion, hypothesized. It is known that these Yukawa-like interactions are usually proportional to a linear combination of the masses of the leptons divided by the VeV of the scalar, but we will keep this omitted in the definition of the coupling constant g_{ϕ_n} for now.

It is important to remark that for this analysis we are not considering flavour-violation among the usual fermions, so an interaction with the electron field instead of the muon field is not added for simplification.

The evaluation of this diagram gives:

$$\begin{aligned} i\mathcal{M}^\mu_{\phi,n} &= (-ie)\left(ig^2_{\phi_n}\right)\int \frac{d^4k}{(2\pi)^4}\bar{u}(p_2) \\ &\times \frac{(\not{k}+\not{q}+M_E)\gamma^\mu(\not{k}+M_E)}{[(k+q)^2-M_E^2+i\varepsilon][k^2-M_E^2+i\varepsilon][(k-p_1)^2-M^2_{\phi_n}+i\varepsilon]}u(p_1) \\ &= (-ie)\int\frac{d^4l}{(2\pi)^4}\int_0^1 dx\int_0^{1-x} dy \quad \left(\frac{N_{\phi_n}}{D_{\phi n}}\right), \end{aligned} \tag{5.3}$$

with:

$$
\begin{aligned}
D_{\phi_n} &= (l^2 - \Delta_{\phi_n} + i\varepsilon)^3; \\
\Delta_{\phi_n} &= (x+y)\left[(x+y-1)m^2 + M_E^2\right] - (x+y-1)M_{\phi_n}^2,
\end{aligned}
\tag{5.4}
$$

where the limit of $q \to 0$ was already taken. And the numerator is:

$$
\begin{aligned}
N_{\phi_n} &= (2!)\bar{u}(p_2)(\not{k} + \not{q} + M_E)\gamma^\mu(\not{k} + M_E)u(p_1) \\
&= -2(x+y)\left[(x+y-1)m - M_E\right] i\left[\bar{u}(p_2)\sigma^{\mu\nu}q_\nu u(p_1)\right] \\
&+ O\left[\bar{u}(p_2)\gamma^\mu u(p_1)\right].
\end{aligned}
\tag{5.5}
$$

With this we compute the form factor:

$$
\frac{eF_{2,\phi_n}}{2m} = (-ie)\, g_{\phi_n}^2 \int \frac{d^4 l}{(2\pi)^4} \int_0^1 dx \int_0^{1-x} dy \frac{2(x+y)\left[(x+y-1)m - M_E\right]}{(l^2 - \Delta_{\phi_n} + i\varepsilon)^3}; \tag{5.6}
$$

$$
F_{2,\phi_n} = g_{\phi_n}^2 \int_0^1 dz \frac{(1-z)^2 m(zm + M_E)}{8\pi^2\left[(z-1)zm^2 - (z-1)M_E^2 + zM_{\phi_n}^2\right]}, \tag{5.7}
$$

where in the last equation we used $\delta(1-x-y-z)$ to simplify the notation, and the integral in y becomes trivial, adding the factor of $(1-z)$.

To compute the integral we ignore the factor of m^2 in the denominator since the other masses are expected to be way heavier (above the 100 GeV scale, as will be explained in the next section). Then the integration gives the extensive result:

$$
\begin{aligned}
F_{2,\phi_n} &= \frac{g_{\phi_n}^2 m^2 \left[3M_E^2 M_{\phi_n}^4 \left(ln\left(\frac{M_E^4}{M_{\phi_n}^4}\right) + 1\right) - 6M_E^4 M_{\phi_n}^2 + M_E^6 + 2M_{\phi_n}^6\right]}{48\pi^2(M_E^2 - M_{\phi_n}^2)^4} \\
&+ \frac{3g_{\phi_n}^2 m M_E(M_E^2 - M_{\phi_n}^2)\left[M_{\phi_n}^4 ln\left(\left(\frac{M_E^4}{M_{\phi_n}^4}\right) + 3\right) - 4M_E^2 M_{\phi_n}^2 + M_E^4\right]}{48\pi^2(M_E^2 - M_{\phi_n}^2)^4}.
\end{aligned}
\tag{5.8}
$$

To analyse this result we can introduce the factor κ, which is the ratio of the new particle masses:

$$
\kappa = \frac{M_E}{M_{\phi_n}}, \tag{5.9}
$$

and then expand in terms of $\left(\frac{m}{M_{\phi n}}\right)$, to obtain:

$$\begin{aligned} F_{2,\phi_n} = \frac{g_{\phi_n}^2}{16\pi^2} \Bigg[\left(\frac{m}{M_{\phi_n}}\right) \kappa \frac{\kappa^4 - 4\kappa^2 + 4ln(\kappa) + 3}{(\kappa^2-1)^3} \\ + \left(\frac{m}{M_{\phi_n}}\right)^2 \frac{\kappa^6 - 6\kappa^4 + 3\kappa^2 + 12\kappa^2 ln(\kappa) + 2}{(\kappa^2-1)^3} \Bigg] + O\left[\left(\frac{m}{M_{\phi_n}}\right)^3\right], \end{aligned} \tag{5.10}$$

and we see that indeed, there is a contribution of the type of Eq. 5.1. This means that we can continue the analysis because such contribution can be larger than the usual diagonal interactions.

5.1.1 Numerical analysis

With the computations done in this section, we can estimate values for the free parameters of the theory and compute the contribution that they will give to the muon $g-2$. For that, we first need to check the current experimental limit for such particles.

The PDG group [13] gives limits for a neutral scalar to be:

- Extended Higgs model: $M > 110.3\,GeV$ (95% Confidence Level(CL));
- Minimal Supersymmetric Model [76]: $M > 1496\,GeV$ (95% CL);
- Other Supersymmetric Models: $M > 88.56\,GeV$ (95% CL);

And for a heavy charged lepton to be [77]:

- Sequential charged heavy lepton: $M > 100.8\,GeV$ (95% CL);
- Stable charged heavy lepton: $M > 102.6\,GeV$ (95% CL);

For this analysis, the higher of limits will be assumed.

To evaluate the ratio of the new particle masses (κ) we can take the SM as reference: the scalar VeV is proportional to its mass ($\mathbf{u} = \frac{M_{\phi n}}{\sqrt{\lambda}}$, see Eq. 2.31) and the Yukawa interaction of the scalar and the fermions is proportional to $G_{\mathcal{Y}} = \frac{M_E}{\mathbf{u}} = \frac{M_E\sqrt{\lambda}}{M_{\phi n}}$ (see Eq. 2.46). If we have a theory with $M_E >> M_{\phi_n}$ (or $\kappa >> 1$) we would need a fine-tuning of the parameter λ to avoid problems with perturbative expansion of this interaction, which we want to avoid.

Despite that, we can think about the mass of the fermion being slightly above the mass of the new scalar, following the physical example of the top quark being slightly heavier than the Higgs-boson. The important thing to remember is that the fermion and the scalar mass should be smaller than the new VeV. That being the case we will only look for values of this κ at most of order 1.

For the Yukawa coupling, we can again take the SM as a guide. Since $M_H \cong 125\,GeV$ and $v \cong 246\,GeV$, this gives $g_{Y,SM} \cong \frac{\kappa_{SM}}{2}$. We can make a guess of:

$$g_{\phi_n} = \frac{\kappa}{2}, \tag{5.11}$$

to continue the analysis.

Then we can choose some specific values for the mass of the new scalar and plot the F_2 contribution in relation to κ. Figure 5.2 shows the value of F_{2,ϕ_n}, in terms of κ for choices of the scalar mass of 1, 2, 3, and 4 TeV. With this example, a scalar with a mass above the TeV scale would need a charged fermion with a mass above 100 GeV which fits the experimental preclusion disclosed above, and they are shown by the dashed curves in the figure.

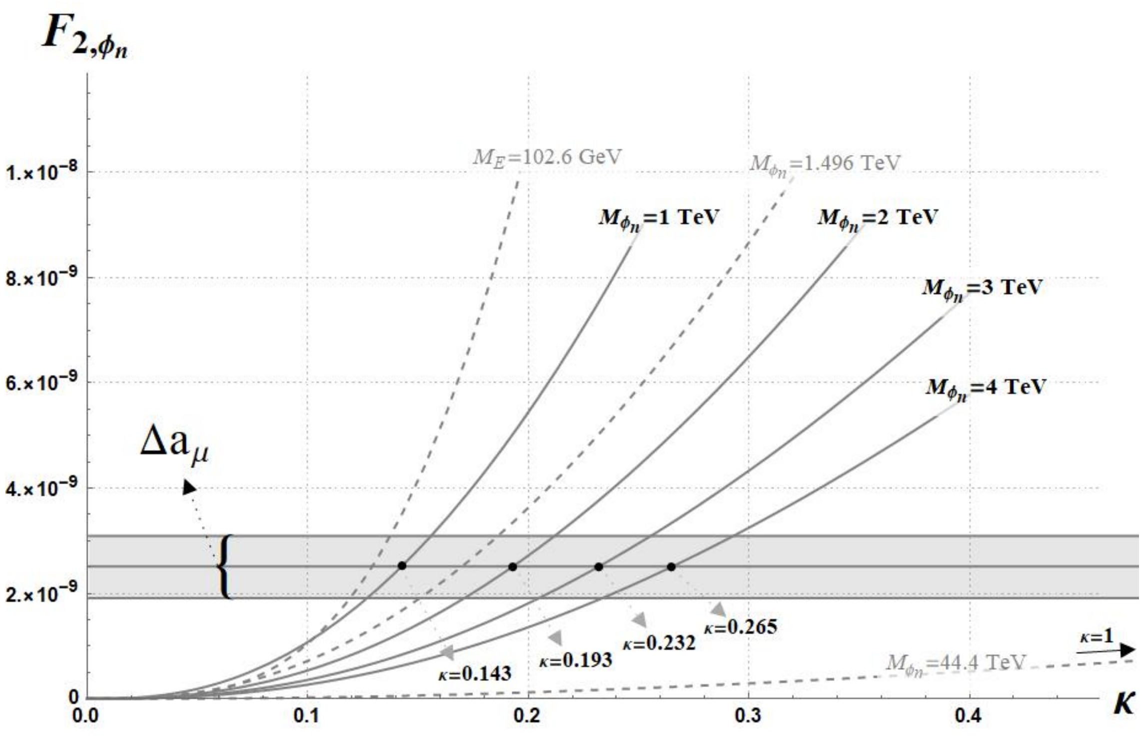

Figure 5.2: Visualization of the value o F_{2,ϕ_n} when varying κ for the values of M_{ϕ_n} of 1, 2, 3, and 4 TeV. The horizontal gray bar is the value of Δa_μ, shown in Eq. 4.22.

This Figure also shows that the value of κ needed to correct the SM deviation of the muon $g-2$ always increases with increasing values of the scalar mass. Since

κ should not be much greater than 1, there is a limit value for the scalar mass, related to the value of:

$$M_{\phi_n}\left(\kappa = 1\,,\, F_{2,\phi_n} = \Delta a_\mu\right) = 44.4\,TeV. \tag{5.12}$$

The same computation can be done with hypothetical neutral heavy fermion and new charged scalars, but the result is of the same order. That being the case, we can skip it and proceed to a more solid example taken from the literature.

5.2 The 3-3-1 Model

The 3-3-1 model is a kind of "top-down" new physics, that departs from a symmetry group of a higher order than the SM, that at some scale breaks to the SM physics. It consists of an expansion of the $SU(2)_L$ symmetry to a $SU(3)_L$. The motivations for such model can be found in [78] and it implies in the transformation of the doublet from Eq. 2.26 to a triplet. The matrix representation for leptons is:

$$\psi_{a,L} = \begin{pmatrix} \nu_{a,L} \\ e_{a,L} \end{pmatrix} \xrightarrow{SU(2)_L \to SU(3)_L} \psi_{a,L} = \begin{pmatrix} \nu_{a,L} \\ e_{a,L} \\ E_{a,L} \end{pmatrix} \sim (\mathbf{3}, 1), \tag{5.13}$$

where this last parenthesis represents the transformation under the symmetry $(SU(3)_L, U(1)_N)$, $E_{a,L}$ can be a new fermion or a known one and the a index is 1, 2 or 3, the family index, meaning that there will be three of such fermions. For the example that is used in this work, from [79], it is a new heavy fermion with a positive electric charge. This model does not introduce new families of fermions, but it needs new scalar fields to break the symmetry consistently to the SM one at a certain energy scale, as:

$$SU(3)_C \otimes SU(3)_L \otimes U(1)_N \xrightarrow[\mathbf{w}]{scale} SU(3)_C \otimes SU(2)_L \otimes U(1)_Y. \tag{5.14}$$

The charge operator is defined as:

$$\frac{Q}{e} = \frac{1}{2}\left(\lambda_3 - \sqrt{3}\lambda_8\right) + N, \tag{5.15}$$

where:

$$\lambda_3 = \begin{pmatrix} 1 & 0 & 0 \\ 0 & -1 & 0 \\ 0 & 0 & 0 \end{pmatrix} \quad ; \quad \lambda_8 = \frac{1}{\sqrt{3}} \begin{pmatrix} 1 & 0 & 0 \\ 0 & 1 & 0 \\ 0 & 0 & -2 \end{pmatrix}, \tag{5.16}$$

is the usual definition of the Gell-Mann matrices of $SU(3)$, but using a abuse of notation, since only the diagonal values are used, and N is the $U(1)_N$ hypercharge for this model.

The new scalar sector is composed of three scalar triplets, and they are represented as:

$$\eta' = \begin{pmatrix} \eta'^0 \\ \eta'^- \\ \eta'^+ \end{pmatrix} \sim (\mathbf{3}, 0) \quad ; \quad \rho' = \begin{pmatrix} \rho'^+ \\ \rho'^0 \\ \rho'^{++} \end{pmatrix} \sim (\mathbf{3}, 1) \quad ; \quad \chi' = \begin{pmatrix} \chi'^- \\ \chi'^{--} \\ \chi'^0 \end{pmatrix} \sim (\mathbf{3}, -1), \tag{5.17}$$

The potential with all terms allowed can be written as:

$$\begin{aligned} V(\eta', \rho', \chi') = {} & \mu_\eta^2(\eta'^\dagger \eta') + \mu_\rho^2(\rho'^\dagger \rho') + \mu_\chi'^2(\chi'^\dagger \chi') + \lambda_1(\eta'^\dagger \eta')^2 + \lambda_2(\rho'^\dagger \rho')^2 \\ & + \lambda_3(\chi'^\dagger \chi')^2 + \lambda_4(\eta'^\dagger \eta')(\rho'^\dagger \rho') + \lambda_5(\eta'^\dagger \eta')(\chi'^\dagger \chi') \\ & + \lambda_6(\rho'^\dagger \rho')(\chi'^\dagger \chi') + \lambda_7(\eta'^\dagger \rho')(\rho'^\dagger \eta') + \lambda_8(\eta'^\dagger \chi')(\chi'^\dagger \eta') \\ & + \lambda_9(\rho'^\dagger \chi')(\chi'^\dagger \rho') + \lambda_{10}(\chi'^\dagger \eta')(\rho'^\dagger \eta') + \alpha \epsilon^{ijk} \eta'_i \rho'_j \chi'_k + H.c. \end{aligned} \tag{5.18}$$

The VeV of the η field is represented by $\frac{\mathbf{v}}{\sqrt{2}}$, of the ρ field is represented by $\frac{\mathbf{u}}{\sqrt{2}}$ and of the χ field is represented by $\frac{\mathbf{w}}{\sqrt{2}}$. Minimizing the fields and ignoring the complex parts we find the restrictions of:

$$\begin{aligned} \mu_\eta^2 &= \frac{\sqrt{2}\alpha \mathbf{uw} - \lambda_4 \mathbf{vu}^2 - \lambda_5 \mathbf{vw}^2 - 2\lambda_1 \mathbf{v}^3}{2\mathbf{v}}; \\ \mu_\rho^2 &= \frac{\sqrt{2}\alpha \mathbf{vw} - \lambda_4 \mathbf{v}^2\mathbf{u} - \lambda_6 \mathbf{uw}^2 - 2\lambda_2 \mathbf{u}^3}{2\mathbf{u}}; \\ \mu_\chi^2 &= \frac{\sqrt{2}\alpha \mathbf{vu} - \lambda_5 \mathbf{u}^2\mathbf{w} - \lambda_6 \mathbf{v}^2\mathbf{w} - 2\lambda_3 \mathbf{w}^3}{2\mathbf{w}}. \end{aligned} \tag{5.19}$$

To keep things simple, only the ρ' and the χ' fields are needed in the lepton sector without neutrinos masses. Knowing that the flavour changing terms that we are interested in will come from the doubly-charged fields, we extract the mass matrix for them, coming from Eq. 5.18, as:

$$M(\rho'^{++},\chi'^{--}) = \frac{1}{2}\begin{pmatrix} \mathbf{w}\left(\frac{\sqrt{2}\alpha\mathbf{v}}{\mathbf{u}}+\lambda_9\mathbf{w}\right) & \sqrt{2}\alpha\mathbf{v}+\lambda_9\mathbf{vw} \\ \sqrt{2}\alpha\mathbf{v}+\lambda_9\mathbf{vw} & \mathbf{u}\left(\frac{\sqrt{2}\alpha\mathbf{v}}{\mathbf{w}}+\lambda_9\mathbf{u}\right)\end{pmatrix}, \tag{5.20}$$

which have the eigenvalues (physical masses) of:

$$M^2_{\rho^{++}} = 0 \quad ; \quad M^2_{\chi^{--}} = \frac{(\mathbf{u}^2+\mathbf{w}^2)(\sqrt{2}\alpha\mathbf{v}+\lambda_9\mathbf{uw})}{2\mathbf{uw}} \quad , \tag{5.21}$$

where it becomes clear that the ρ^{++} field is a Goldstone-boson. Making the usual parameterization of the rotation as:

$$\begin{pmatrix}\rho'^{\pm\pm}\\ \chi'^{\pm\pm}\end{pmatrix} = \begin{pmatrix} cos\theta_{\rho,\chi} & -sin\theta_{\rho,\chi} \\ sin\theta_{\rho,\chi} & cos\theta_{\rho,\chi}\end{pmatrix}\begin{pmatrix}\rho^{\pm\pm}\\ \chi^{\pm\pm}\end{pmatrix}, \tag{5.22}$$

we have the substitution for finding the physical fields.

Next, we write the Yukawa terms:

$$L^{331}_{\mathcal{Y}} = (G^{331}_{\mathcal{Y},e})_{ab}\psi_{a,L}\rho'\psi_{b,eR} + (G^{331}_{\mathcal{Y},E})_{ab}\psi_{a,L}\chi'\psi_{b,ER} + H.c.., \tag{5.23}$$

where $\psi_{b,eR}$ represents the right-handed component of the known fermions and $\psi_{b,ER}$ represents the right-handed component of the new heavy fermions. After expanding these terms we obtain the flavour changing terms that will be important as:

$$\mathcal{L}^{331}_{\mathcal{Y},f.c.} = -\frac{m_b}{\mathbf{u}}K_{ab}\bar{E}_{a,L}e_{b,R}\rho'^{++} - \frac{M_{E_b}}{\mathbf{w}}K^{\dagger}_{ab}\bar{e}_{a,L}E_{b,R}\chi'^{--} + H.c.., \tag{5.24}$$

where K_{ab} is the product of the rotation matrices of the leptons $E_{a,L}$ and $e_{a,L}$ in this order, and M_E is used for the mass of the heavy fermion. This means that the fields E_a and e_a written in Eq. 5.24 are the physical fields. This is the same as found in [75].

We then proceed to make the substitutions from Eq. 5.22:

$$\rho'^{\pm\pm} = -sin\theta_{\rho,\chi}\chi^{\pm\pm} \quad ; \quad \chi'^{\pm\pm} = cos\theta_{\rho,\chi}\chi^{\pm\pm}, \tag{5.25}$$

and ignore the $\rho^{\pm\pm}$ field since it will disappear from the theory with the proper gauge choice. Noting that for this model the gauge invariance will be assumed.

Finally summing the hermitian conjugate terms to find the physical interaction, we find:

$$\begin{aligned}\mathcal{L}_{Y,f.c.,e-E} = \bar{e}_a \Bigg[& \frac{m_{e,a}}{\sqrt{2}\mathbf{u}} K^{\dagger}_{ab} sin\theta_{\rho,\chi} - \frac{M_{E,b}}{\sqrt{2}\mathbf{w}} K^{\dagger}_{ab} cos\theta_{\rho,\chi} \\ & -\gamma^5 \left(\frac{m_{e,a}}{\sqrt{2}\mathbf{u}} K^{\dagger}_{ab} sin\theta_{\rho,\chi} + \frac{M_{E,b}}{\sqrt{2}\mathbf{w}} K^{\dagger}_{ab} cos\theta_{\rho,\chi} \right) \Bigg] E_b \chi^{--} + H.c..\end{aligned} \tag{5.26}$$

To extract the interactions of the doubly-charged scalar with the photon we can use the effective $U(1)_{EM}$ kinetic term of $\chi^{\pm\pm}$ like:

$$\begin{aligned}(D_\mu \chi^{\pm\pm})^\dagger D^\mu \chi^{\pm\pm} &= \left[\left(\partial_\mu - i2eA_\mu \right) \chi^{\pm\pm} \right]^\dagger \left(\partial^\mu - i2eA^\mu \right) \chi^{\pm\pm} \\ &= \partial_\mu \chi^{\mp\mp} \partial^\mu \chi^{\pm\pm} - i2eA^\mu \left[(\partial_\mu \chi^{\mp\mp}) \chi^{\pm\pm} - \chi^{\mp\mp} (\partial_\mu \chi^{\pm\pm}) \right] \\ &+ 4e^2 A^2 \chi^{\mp\mp} \chi^{\pm\pm}.\end{aligned} \tag{5.27}$$

With Eq. 5.26 and Eq. 5.27 the Feynman rules needed to calculate the muon $g-2$ with the heavy lepton running through the loop can be extracted, similarly as in [80], and are shown below:

- Doubly-charged scalar propagator:

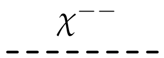

$$= \frac{i}{p^2 - M_\chi^2 + i\varepsilon}; \tag{5.28}$$

- Fermion - doubly-charged scalar vertex:

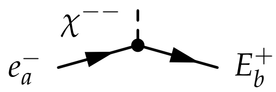

$$\begin{aligned}= \; & iK^{\dagger}_{ab} \left[\frac{m_{e,a}}{\sqrt{2}\mathbf{u}} sin\theta_{\rho,\chi} - \frac{M_{E,b}}{\sqrt{2}\mathbf{w}} cos\theta_{\rho,\chi} \right. \\ & \left. -\gamma^5 \left(\frac{m_{e,a}}{\sqrt{2}\mathbf{u}} sin\theta_{\rho,\chi} + \frac{M_{E,b}}{\sqrt{2}\mathbf{w}} cos\theta_{\rho,\chi} \right) \right];\end{aligned} \tag{5.29}$$

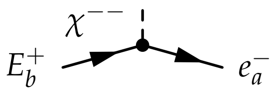

$$\begin{aligned}= \; & iK_{ab} \left[\frac{m_{e,a}}{\sqrt{2}\mathbf{u}} sin\theta_{\rho,\chi} - \frac{M_{E,b}}{\sqrt{2}\mathbf{w}} cos\theta_{\rho,\chi} \right. \\ & \left. +\gamma^5 \left(\frac{m_{e,a}}{\sqrt{2}\mathbf{u}} sin\theta_{\rho,\chi} + \frac{M_{E,b}}{\sqrt{2}\mathbf{w}} cos\theta_{\rho,\chi} \right) \right];\end{aligned} \tag{5.30}$$

· Photon - doubly-charged scalar vertex:

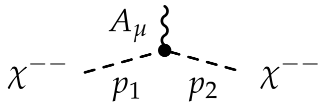

$$= -i2e(p_1 + p_2)_\mu. \tag{5.31}$$

The diagrams containing the flavour violation with the heavy fermion are shown in Figure 5.3. It is important to notice that all three heavy leptons will appear in these diagrams, and there is no particular reason to disregard any of them before the evaluation. For that reason, the b index is maintained and summed over.

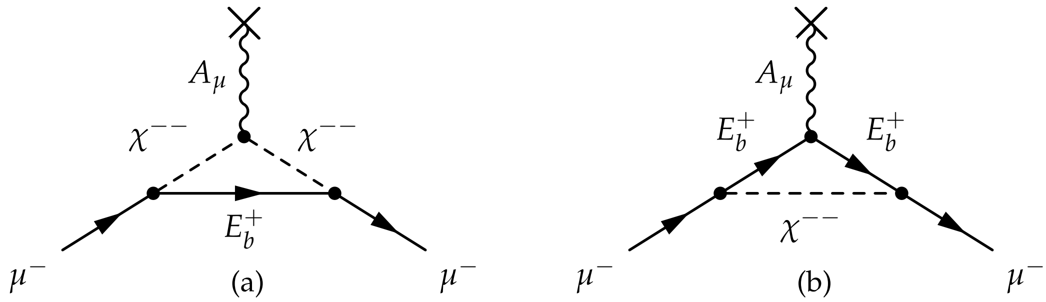

Figure 5.3: Diagram for the doubly-charged scalar contribution: (a) two scalars with a heavy fermion loop and (b) one scalar with two heavy fermions loop

The evaluation of the first diagram (Figure 5.3a) gives:

$$\begin{aligned} i\mathcal{M}^\mu_{\chi,1} &= (-i2e)\, i \sum_{b=1}^{3} \int \frac{d^4k}{(2\pi)^4} \bar{u}(p_2) \\ &\times \frac{(A_\chi + B_\chi \gamma^5)(2k+q)^\mu (\not{k} - \not{p}_1 + M_{E_b})(A^\dagger_\chi - B^\dagger_\chi \gamma^5)}{[(k+q)^2 - M_\chi^2 + i\varepsilon][k^2 - M_\chi^2 + i\varepsilon][(k-p_1)^2 - M_{E_b}^2 + i\varepsilon]} u(p_1) \\ &= (-ie) i \sum_{b=1}^{3} \int \frac{d^4l}{(2\pi)^4} \int_0^1 dx \int_0^{1-x} dy \quad \left(\frac{N_{\chi,1}}{D_{\chi,1}} \right), \end{aligned} \tag{5.32}$$

where:

$$\begin{aligned} A_\chi &= \frac{m}{\sqrt{2}\mathbf{u}} K^\dagger_{\mu b} sin\theta_{\rho,\chi} - \frac{M_{E_b}}{\sqrt{2}\mathbf{w}} K^\dagger_{\mu b} cos\theta_{\rho,\chi}; \\ B_\chi &= -\left(\frac{m}{\sqrt{2}\mathbf{u}} K^\dagger_{\mu b} sin\theta_{\rho,\chi} + \frac{M_{E_b}}{\sqrt{2}\mathbf{w}} K^\dagger_{\mu b} cos\theta_{\rho,\chi} \right). \end{aligned} \tag{5.33}$$

The denominator is written as:

$$\begin{aligned} D_{\chi,1} &= (l^2 - \Delta_{\chi,1} + i\varepsilon)^3; \\ \Delta_{\chi,1} &= (x+y)\left[(x+y-1)m^2 + M_\chi^2\right] - (x+y-1)M_{E_b}^2, \end{aligned} \tag{5.34}$$

and the numerator as:

$$\begin{aligned} N_{\chi,1} &= 2(2!)\bar{u}(p_2)(A_\chi + B_\chi\gamma^5)(2k+q)^\mu(\not{k} - \not{p}_1 + M_{E_b})(A_\chi^\dagger - B_\chi^\dagger\gamma^5)u(p_1) \\ &= -4(x+y-1)\left(|A_\chi|^2\left[(x+y)m - M_{E_b}\right] + |B_\chi|^2\left[(x+y)m + M_{E_b}\right]\right) \\ &\times i[\bar{u}(p_2)\sigma^{\mu\nu}q_\nu u(p_1)] + O\left[\,\bar{u}(p_2)\gamma^\mu u(p_1)\,,\ \bar{u}(p_2)(...)\gamma^5 u(p_1)\,\right]. \end{aligned} \tag{5.35}$$

Then, we are able to calculate the F_2 form factor using:

$$\begin{aligned} \frac{eF_{2,\chi,1}}{2m} &= (-ie)\sum_{b=1}^{3}\int\frac{d^4l}{(2\pi)^4}\int_0^1 dx\int_0^{1-x} dy \\ &\quad \frac{-4(x+y-1)\left(|A_\chi|^2\left[(x+y)m - M_{E_b}\right] + |B_\chi|^2\left[(x+y)m + M_{E_b}\right]\right)}{[l^2 - \Delta_{\chi_1} + i\varepsilon]^3}; \end{aligned} \tag{5.36}$$

$$F_{2,\chi,1} = \sum_{b=1}^{3}\int_0^1 dz\frac{(1-z)zm[M_{E_b}(|B_\chi|^2 - |A_\chi|^2) + (1-z)m(|A_\chi|^2 + |B_\chi|^2)]}{4\pi^2\left[zM_{E_b}^2 - (z-1)(M_\chi^2 - zm^2)\right]}, \tag{5.37}$$

where, again, we used $\delta(1-x-y-z)$ to simplify the notation, and the integral in y simply adds the factor of $(1-z)$.

The integral over the parameter z, however, is not trivial and in order to take conclusions from it, we need to make a simplification, taking the limit of $m \to 0$ in the denominator, as it was done in the previous section. With this approximation, we can compute the integral analytically. As before, we proceed to write the ratio of masses for the heavy particles as $\kappa_{\chi,b} = \frac{M_{E_b}}{M_\chi}$, and obtain:

$$F_{2,\chi,1} = \sum_{b=1}^{3} \frac{1}{24\pi^2} \frac{m}{M_\chi} \left[3(|A_\chi|^2 - |B_\chi|^2) \frac{\kappa_{\chi,b}(1-\kappa_{\chi,b}^2)\left(\kappa_{\chi,b}^4 - \kappa_{\chi,b}^2 ln(\kappa_{\chi,b}^4) - 1\right)}{(\kappa_{\chi,b}^2 - 1)^4} \right.$$
$$\left. + \frac{m}{M_\chi}(|A_\chi|^2 + |B_\chi|^2) \frac{\left(2\kappa_{\chi,b}^6 + 3\kappa_{\chi,b}^4 - 6\kappa_{\chi,b}^2 - 3\kappa_{\chi,b}^4 ln(\kappa_{\chi,b}^4) + 1\right)}{(\kappa_{\chi,b}^2 - 1)^4} \right]. \tag{5.38}$$

The evaluation of the second diagram (Figure 5.3b) gives:

$$i\mathcal{M}_{\chi,2}^{\mu} = (-ie)\,(-i) \sum_{b=1}^{3} \int \frac{d^4k}{(2\pi)^4} \bar{u}(p_2) \tag{5.39}$$
$$\times \frac{(A_\chi + B_\chi\gamma^5)(\not{k} + \not{q} + M_{E_b})\gamma^\mu(\not{k} + M_{E_b})(A_\chi^\dagger - B_\chi^\dagger\gamma^5)}{[(k+q)^2 - M_{E_b}^2 + i\varepsilon][k^2 - M_{E_b}^2 + i\varepsilon][(k-p_1)^2 - M_\chi^2 + i\varepsilon]} u(p_1) \tag{5.40}$$
$$= (-ie)(-i) \sum_{b=1}^{3} \int \frac{d^4l}{(2\pi)^4} \int_0^1 dx \int_0^{1-x} dy \left(\frac{N_{\chi,2}}{D_{\chi,2}}\right). \tag{5.41}$$

The denominator is:

$$\begin{aligned} D_{\chi,2} &= (l^2 - \Delta_{\chi 2} + i\varepsilon)^3; \\ \Delta_{\chi,2} &= (x+y)\left[(x+y-1)m^2 + M_{E_b}^2\right] - (x+y-1)M_\chi^2, \end{aligned} \tag{5.42}$$

simply an interchange of $M_{E_b}^2$ and M_χ^2 in Eq. 5.34. The numerator gives:

$$\begin{aligned} N_{\chi,2} &= (2!)\bar{u}(A_\chi + B_\chi\gamma^5)(\not{k} + \not{q} + M_{E_b})\gamma^\mu(\not{k} + M_{E_b})(A_\chi^\dagger - B_\chi^\dagger\gamma^5)u(p_1) \\ &= 2(x+y)\left(|A_\chi|^2\left[(x+y-1)m - M_{E_b}\right] + |B_\chi|^2\left[(x+y-1)m + M_{E_b}\right]\right) \\ &\times i[\bar{u}(p_2)\sigma^{\mu\nu}q_\nu u(p_1)] + O\left[\,\bar{u}(p_2)\gamma^\mu u(p_1)\,,\ \bar{u}(p_2)(...)\gamma^5 u(p_1)\,\right]. \end{aligned} \tag{5.43}$$

Then the F_2 form factor yields:

$$\frac{eF_{2,\chi,2}}{2m} = (-ie)\sum_{b=1}^{3}\int\frac{d^4l}{(2\pi)^4}\int_0^1 dx\int_0^{1-x} dy$$
$$\frac{2(x+y)\left(|A_\chi|^2\left[(x+y-1)m - M_{E_b}\right] + |B_\chi|^2\left[(x+y-1)m + M_{E_b}\right]\right)}{[l^2-\Delta_{\chi_2}+i\varepsilon]^3}; \tag{5.44}$$

$$F_{2,\chi,2} = \sum_{b=1}^{3}\int_0^1 dz\frac{(1-z)^2 m[-M_{E_b}(|B_\chi|^2-|A_\chi|^2) + zm(|A_\chi|^2+|B_\chi|^2)]}{8\pi^2\left[(1-z)(zm^2-M_{E_b}^2) - zM_\chi^2\right]}. \tag{5.45}$$

Again we take the muon mass to zero in the denominator and perform the integral. Proceeding to use again the ratio $\kappa_{\chi,b}$, we obtain:

$$F_{2,\chi,2} = \sum_{b=1}^{3}\frac{1}{48\pi^2}\frac{m}{M_\chi}\left[3(|A_\chi|^2-|B_\chi|^2)\frac{\kappa_{\chi,b}(1-\kappa_{\chi,b}^2)\left(\kappa_{\chi,b}^4 - 4\kappa_{\chi,b}^2 + ln(\kappa_{\chi,b}^4)+3\right)}{(\kappa_{\chi,b}^2-1)^4}\right.$$
$$\left.-\frac{m}{M_\chi}(|A_\chi|^2+|B_\chi|^2)\frac{\left(\kappa_{\chi,b}^6 - 6\kappa_{\chi,b}^4 + 3\kappa_{\chi,b}^2 + 3\kappa_{\chi,b}^2\, ln(\kappa_{\chi,b}^4)+2\right)}{(\kappa_{\chi,b}^2-1)^4}\right]. \tag{5.46}$$

Now we can sum both diagram contributions. The combination of Eq. 5.37 with this last result yields:

$$F_{2,\chi} = \sum_{b=1}^{3}\frac{1}{16\pi^2}\left[\frac{m}{M_\chi}(|A_\chi|^2-|B_\chi|^2)\frac{\kappa_{\chi,b}(1-\kappa_{\chi,b}^2)\left(3\kappa_{\chi,b}^4-4\kappa_{\chi,b}^2-2\kappa_{\chi,b}^2 ln(\kappa_{\chi,b}^4)+ln(\kappa_{\chi,b}^4)+1\right)}{(\kappa_{\chi,b}^2-1)^4}\right.$$
$$\left.+\frac{m^2}{M_\chi^2}(|A_\chi|^2+|B_\chi|^2)\frac{\left(\kappa_{\chi,b}^4 + 2\kappa_{\chi,b}^2 - 2\kappa_{\chi,b}^2\, ln(\kappa_{\chi,b}^4) - ln(\kappa_{\chi,b}^4) - 5\right)}{(\kappa_{\chi,b}^2-1)^4}\right], \tag{5.47}$$

which is the full result for the graphs in Figure 5.3. By looking at this equation it may seem like we do have a linear term in $\frac{m}{M_\chi}$ like in the hypothetical model discussed, but a more careful analysis is needed. Since:

$$|A_\chi|^2 - |B_\chi|^2 = 2\left|(K)_{\mu,b}\right|^2 sin2\theta_{\rho,\chi}\frac{m\, M_{E,b}}{\mathbf{u\,w}}, \tag{5.48}$$

and using Eq. 5.21 and the fact that $\mathbf{w} >> \mathbf{u} >> \mathbf{v}$, we have:

$$\frac{M_\chi^2}{\mathbf{w}^2} \cong \frac{\lambda_9}{2}, \tag{5.49}$$

being λ_9 a constant of order 1. Now we can rewrite the first term inside the brackets of Eq. 5.47, using also that $\mathbf{u}$ is approximately the Higgs VeV ($v \cong 2M_H$), obtaining:

$$F_{2,\chi} \cong \frac{|(K)_\mu|^2 \, sin2\theta_{\rho,\chi}\sqrt{\lambda_9}}{32\sqrt{2}\pi^2}\left[\frac{m}{M_\chi}\frac{m}{M_H}\frac{\kappa_\chi^2\left(3\kappa_\chi^4 - 4\kappa_\chi^2 - 2\kappa_\chi^2 ln(\kappa_\chi^4) + ln(\kappa_\chi^4) + 1\right)}{(\kappa_\chi^2 - 1)^3}\right], \tag{5.50}$$

where the summation over the new fermions was dropped since we are interested in only the biggest of the contributions. Although this result is not quadratic in $\left(\frac{m}{M_\chi}\right)$ it does have a term that decreases the order of magnitude of this contribution, the additional $\left(\frac{m}{M_H}\right)$, making the idea less viable.

The only difference between the toy model from section 5.1 and this concrete model is the chiral interaction. The fact that the vectorial part ($|A_\chi|^2$) minus the axial part ($|B_\chi|^2$) cancels the quadratic terms from these expressions, remaining only the crossed ones, is something that happens for any charged scalar that has SM interactions.

This implies that, for the mechanism discussed here to work (to realize the prediction from Eq. 5.1), we need either a non-chiral interaction or a mechanism that changes $|A_\chi|^2$ and $|B_\chi|^2$, so that a term without the muon mass remains. The first supposition seems to be more natural, since we have a non-chiral scalar interaction in the SM, although it is not clear how to have non-diagonal interactions in such a case. For the second one, a different mechanism of acquisition of masses would be needed, and this is not trivial.

For completeness, we can comment that a similar thing happens for the vector bosons. The contributions that would be linear in the muon mass gets cancelled by a term of the type ($|A|^2 - |B|^2$), which for left-chirality interactions we have $A_{\chi,V} = 1$ and $B_{\chi,V} = -1$ due to the P_L projector, and the linear part vanishes as well. In the case of the neutral vector bosons that do have $|A_{\chi,V}| \neq |B_{\chi,V}|$, the interactions are diagonal, so this idea does not apply.

5.2.1 Numerical analysis

Although this mechanism to solve the $g-2$ problem using the 3-3-1 model is apparently not viable, we can make a numerical analysis to be sure. To make the numerical analysis, first we check the experimental limits of exclusion for such particles.

For a heavy charged lepton we keep the higher exclusion shown in the last section:

- Stable charged heavy lepton: $M > 102.6\,GeV\ (95\%CL)$

And for the doubly-charged scalar we have the limits from [81]:

- From muon decay: $M > 846\,GeV\ (95\%CL)$
- From electron decay: $M > 768\,GeV\ (95\%CL)$

To find the upper limit for the doubly-charged scalar mass in this 3-3-1 model, we set the restrictions: reminding that κ should not be much bigger than 1, we can set $\kappa < 1$; the constants are also smaller than one, so we have $\left\{\lambda_9, sin2\theta_{\rho,\chi}, \left|K_\mu\right|^2\right\} < 1$. Substituting these values in Eq. 5.50 and setting $F_{2,\chi} = \Delta(a_\mu)$ (from Eq. 4.21) we get:

$$M_\chi < 107\,GeV, \tag{5.51}$$

and then it becomes clear that this mechanism using this particular 3-3-1 model cannot account for the discrepancy in a natural way, since this mass value is experimentally excluded. The value of the constants is probably much more constrained due to experimental data from flavour violation which means that the margin for fine-tuning would be even smaller.

Chapter 6

Conclusion

In this work, it was discussed the possibility of solving the muon $g-2$ issue with an expansion of the scalar sector. A completely hypothetical model and a respected model from the literature were analysed.

We began by describing the muon $g-2$ physics in some depth. It was shown how to obtain the interactions and the physical fields with an overview of the construction of the EWSM. Then a thorough demonstration of how to calculate the $g-2$ and the reason to choose the muon for experiments were laid down. All one-loop computations for this factor are explicit, including the gauge invariance proof in Appendix B.

In Chapter 4 a historical overview and an explanation of the experimental results were shown, exposing the issue to be reviewed: the discrepancy between prediction and experimental value for the muon $g-2$. As explained in the introduction, the goal was to find if it is possible to fix the issue with the addition of new scalar fields in the theory. At first, it was stated that adding only scalars would not solve the problem, so other additions were also needed.

In the last chapter a possible solution was analysed: the inclusion of a new heavy fermion along with the scalar field and non-diagonal interactions. We began by justifying this choice using a toy model, and then evaluating the loop diagrams needed, where it was shown that this combination of new particles, with mass ratios among them ($\kappa = \frac{M_E}{M_{\phi n}}$) around 0.15 to 0.3 could yield values for the $g-2$ factor with the same order of magnitude as the current experiment-theory discrepancy. These ratios are for the new scalars in the *TeV* scale and SM-like Yukawa couplings.

Another observation that is apparent in this hypothetical model is that when the mass of the scalar increases, the ratio of masses also grows. This means that the new fermion mass needs to increase in a proportion higher than the scalar for solving the issue. This can be a technological and economical problem if we want to probe for such particles, but it also gives hints about the maximum value of the mass of the scalar that can solve the issue. Since we want to keep the value of κ

at most of order 1, this can limit the search range and can be important in some models.

Lastly, a solid example was taken from the literature, a particular 3-3-1 model. This model contains 3 scalar triplets and the addition of three new fermions which fits in the description laid before, therefore it was analysed. After computing the contribution to the muon $g-2$ of one particular diagram, it was shown that the order of magnitude did not follow a similar pattern as the hypothetical model discussed. The presence of chiral interactions lowered the contribution by at least $\frac{m}{M_H}$ which turned this mechanism unviable i.e, smaller than the current measured values.

This is a general result for theories with chiral scalar interactions: the interactions will always lower the contribution. And, although not all diagrams for this 3-3-1 model were calculated, the same pattern appears in all of them (the term containing $(|A_\chi|^2 - |B_\chi|^2)$ multiplying the linear part in the expansion of $\frac{m}{M_\chi}$), which means that to find the contribution of the toy model we would need different mechanisms than the SM ones, either of mass acquisition or chiral interactions.

Finally, although the toy model discussed seems to work, the fact that the known non-diagonal interactions are all chiral, and there is no clear explanation for where non-chiral and non-diagonal interactions could appear in a theory, the mechanism discussed here is unlikely to occur. There can be different considerations for the constants and the couplings that could raise the value of the $g-2$ contribution so that it would be possible to fix the discrepancy, but it does not seem like the natural way to deal with them. And again, due to the flavour violation restrictions, this fine-tuning would be very restricted.

Overall, additions of scalar fields with SM-like interactions (same chiral interactions and mass acquisition mechanism) strike as unlikely explanations for the $g-2$ discrepancy. The current experimental restrictions of both the mass scale and flavour violation, combined, make this mechanism look unnatural. In any case, it is worth checking the $g-2$ contributions for models that have different assumptions and also have these three necessary conditions for this mechanism (a new scalar, a new fermion, and a flavour violation vertex).

Appendix A

Dirac Hamiltonian

The objective of this part is to show how to obtain the Hamiltonian of a particle in a magnetic field from the Dirac equation. For this proof specifically, a different convention for the Dirac matrices will be used, due to practicality. The only important difference is for the γ^0 that is written as:

$$\gamma^0 = \begin{pmatrix} \mathbb{1} & 0 \\ 0 & -\mathbb{1} \end{pmatrix}. \tag{A.1}$$

This convention is used by many authors and is called the "Dirac Basis".

The Dirac equation in an external electromagnetic field is written as:

$$\left(i\gamma^\mu \partial_\mu - m - e\gamma^\mu A_\mu\right)\psi = 0. \tag{A.2}$$

Dividing the spacial and time components, remembering that $A_\mu = \left\{\phi, \vec{A}\right\}$, we obtain:

$$\left(i\gamma^0\partial_0 + i\gamma^i\partial_i - m - e\gamma^0\phi - e\gamma^i A_i\right)\psi = 0. \tag{A.3}$$

Now we start by considering the non-relativistic approximation for the Dirac spinor:

$$\psi = e^{-ip\cdot x}\begin{pmatrix} u \\ v \end{pmatrix} = e^{-i(p^0x_0 + p^ix_i)}\begin{pmatrix} u \\ v \end{pmatrix} \overset{\text{N.R}}{\cong} e^{-i(mt)}\begin{pmatrix} u \\ v \end{pmatrix}, \tag{A.4}$$

and then write two expressions in terms of u and v:

$$i\dot{u} + i\vec{\sigma}\vec{\nabla}v - e\phi u + e\vec{\sigma}\vec{A}v = 0; \tag{A.5}$$

$$-i\dot{v} - 2mv - i\vec{\sigma}\vec{\nabla}u + e\phi v - e\vec{\sigma}\vec{A}u = 0. \tag{A.6}$$

For the last equation the mass term in the non-relativistic approximation is dominant, so $2mv >> \{i\dot{v}, e\phi\}$, and we can ignore these terms to write:

$$v = -\left[\frac{i\vec{\sigma}\vec{\nabla} + e\vec{\sigma}\vec{A}}{2m}\right] u. \tag{A.7}$$

Substituting this result in Eq. A.5 and using the identity $(\vec{\sigma}\cdot\vec{a})(\vec{\sigma}\cdot\vec{b}) = (\vec{a}\cdot\vec{b})\mathbb{1} + i(\vec{a}\times\vec{b})\cdot\vec{\sigma}$ (remarking that $\vec{\nabla}\cdot\vec{A} = 0$ and $\vec{\nabla}\times\vec{A} = \vec{B}$), we obtain:

$$i\dot{u} = \left[e\phi + \frac{1}{2m}\left(-\nabla^2 - e\vec{B}\vec{\sigma} + i2e\vec{A}\vec{\nabla} + e^2A^2\right)\right] u. \tag{A.8}$$

The last step is to recognize the Hamiltonian using the Schrodinger equation ($i\dot{u} = \hat{\mathcal{H}}u$), substitute $\vec{\sigma} = 2\vec{S}$, and $\vec{\nabla} = i\vec{p}$, to obtain:

$$\mathcal{H}_{\vec{\mu}} = \left[e\phi + \frac{(\vec{p} - e\vec{A})^2}{2m} - 2\frac{e}{2m}\vec{S}\cdot\vec{B}\right]. \tag{A.9}$$

With the term $2\frac{\vec{S}}{2m} = g_S\frac{\vec{S}}{2m} = g_S\vec{\mu}$, we find $g_S = 2$. An important remark is that the final result is independent of Dirac matrices, therefore is independent of the convention used.

Appendix B

One-loop gauge invariance in the muon $g-2$ computation

To prove the gauge invariance for the graphs in Figures 3.5 and Figure 3.6 we need to use the R_ξ gauge. Using this gauge we can rewrite the propagators to isolate the denominators containing the ξ factor as follows:

$$\begin{aligned}
&-i\frac{1}{k^2-M_i^2+i\varepsilon}\left[g^{\mu\nu}-(1-\xi)\frac{k^\mu k^\nu}{k^2-\xi M_i^2}\right]= \\
&-i\left[\frac{g^{\mu\nu}}{k^2-M_i^2+i\varepsilon}-\frac{\frac{k^\mu k^\nu}{M_i^2}}{k^2-M_i^2+i\varepsilon}+\frac{\frac{k^\mu k^\nu}{M_i^2}}{k^2-\xi M_i^2+i\varepsilon}\right],
\end{aligned} \tag{B.1}$$

where i can represent Z or W.

Using this propagator we will analyse the gauge invariance separately for both cases.

B.1 Z diagram

For the Z diagram gauge invariance proof we need to reevaluate Figure 3.5 in the R_ξ gauge. We can immediately identify the ξ dependent denominator for the Z computation, realizing that the only difference will lay in the extra ξ multiplying the mass term for the Z, as follows:

$$\begin{aligned}
D_{z,\xi} &= [l^2-\Delta_{Z,\xi}+i\varepsilon]^3; \\
\Delta_{Z,\xi} &= (y^2+xy-y)q^2+(1-x)^2m^2+x\xi M_Z^2.
\end{aligned} \tag{B.2}$$

The same denominator appears for the diagram of the neutral Goldstone boson

(Using Eq. 2.13). The term for the Z diagram that is ξ dependent is:

$$
\begin{aligned}
i\mathcal{M}^{\mu}_{Z,\xi} = (-ie) - i\left(\frac{g}{4cos\theta_w}\right)^2 \int \frac{d^4k}{(2\pi)^4}\bar{u}(p_2) \\
\frac{(\not{k}-\not{p}_1)(A+\gamma^5)(\not{k}+\not{q}+m)\gamma^{\mu}(\not{k}+m)(\not{k}-\not{p}_1)(A+\gamma^5)}{M_Z^2\, D_{z,\xi}}u(p_1).
\end{aligned}
\tag{B.3}
$$

Using the same techniques as in the main text to separate the F_2 form factor, and letting aside the constants, we obtain:

$$
\int_0^1 dx \int_0^{1-x} dy \int \frac{d^4l}{(2\pi)^4}\left[\frac{l^2(1-3x)-2m^2(x-1)^3}{M_Z^2\, D_{z,\xi}}\right] \times [\bar{u}(p_2)(p_1+p_2)^{\mu}u(p_1)]\,. \tag{B.4}
$$

For the diagram of the Neutral Goldstone boson, we can simply take the result obtained from Eq. 3.52 since the nominator does not change using the R_ξ gauge, rewritten below:

$$
\int_0^1 dx \int_0^{1-x} dy \int \frac{d^4l}{(2\pi)^4}\left[-4\frac{m^2}{M_Z^2\, D_{z,\xi}}(1-x)^2\right] \times [\bar{u}(p_2)(p_1+p_2)^{\mu}u(p_1)]\,. \tag{B.5}
$$

The combination of the two last equations, letting aside $[\bar{u}(p_2)(p_1+p_2)^{\mu}u(p_1)]$, and the constants, gives:

$$
F_{2,Z,\xi} \propto \int_0^1 dx \int_0^{1-x} dy \int \frac{d^4l}{(2\pi)^4}\frac{l^2(1-3x)-2m^2(x-1)^2(x+1)}{M_Z^2\, D_{z,\xi}}. \tag{B.6}
$$

We can then perform the integration in the momentum by taking the limit of $q \to 0$ and using Eq. 3.40 and the dimensional regularization for $d = 4-\epsilon$:

$$
\int \frac{d^4l}{(2\pi)^4}\frac{l^2}{(l^2-\Delta+i\varepsilon)^3} \to \frac{-i}{16\pi^2}ln\left(\frac{\Delta}{\lambda^2}\right), \tag{B.7}
$$

where λ is the scale for dimensional regularization. Then we obtain:

$$
F_{2,Z,\xi} \propto \int_0^1 dx \int_0^{1-x} dy \left[\frac{2m^2(x-1)^2(x+1)}{(4\pi)^2 M_Z^2 \Delta_{Z,\xi}} + \frac{3x-1}{(4\pi)^2 M_Z^2}ln\left(\frac{\Delta_{Z,\xi}}{\lambda^2}\right)\right]. \tag{B.8}
$$

If this result is gauge invariant, then if we derive the result in terms of ξ we should obtain zero. The result of this derivative, after performing the integral in the y parameter, and ignoring the constants is:

$$\frac{dF_{2,Z,\xi}}{d\xi} \propto \int_0^1 dx \left[\frac{(x-1)x(3x-1)}{m^2(x-1)^2+\xi x M_Z^2} - \frac{m^2(x^2-1)(x-1)^2 x}{(m^2(x-1)^2+\xi x M_Z^2)^2} \right] \tag{B.9}$$

This integral can be solved analytically by realizing that the first and second terms are partial derivatives of the numerator and denominator, respectively. Being:

$$\mathcal{P} = \frac{1}{m^2\frac{(x-1)^2}{x}+\xi M_Z^2} \quad ; \quad \frac{\partial \mathcal{P}}{\partial x} = -\frac{m^2(x^2-1)}{(m^2(x-1)^2+\xi x M_Z^2)^2}; \tag{B.10}$$

$$\mathcal{Q} = (x-1)^2 x \quad ; \quad \frac{\partial \mathcal{Q}}{\partial x} = (3x-1)(x-1), \tag{B.11}$$

we see that

$$\frac{dF_{2,Z,\xi}}{d\xi} \propto \int_0^1 dx \left[\mathcal{P}\frac{\partial \mathcal{Q}}{\partial x} + \mathcal{Q}\frac{\partial \mathcal{P}}{\partial x} \right] \propto \left[\frac{(x-1)^2 x^2}{m^2(x-1)^2+\xi x M_Z^2} \right] \Bigg|_{x=0}^{x=1}, \tag{B.12}$$

We can see that this term vanishes for both $x=1$ and $x=0$, making the overall result:

$$\frac{dF_{2,Z,\xi}}{d\xi} = 0. \tag{B.13}$$

This proves that the result does not depend on ξ, or more precisely, that it is gauge invariant.

B.2 W diagram

For the W diagram gauge invariance proof we need to reevaluate Figure 3.6 in the R_ξ gauge. The computations will be summarized for brevity.

Substituting the propagator from Eq. B.1 instead of the simple metric tensor in Eq. 3.55 we readily see that 4 denominators will appear. The first is equal to the one obtained before (Eq. 3.57) and the others have differences in the Δ component.

below is shown the denominator with the limit of $q^2 \to 0$ already taken:

$$\begin{aligned} D_{W,2} &= [l^2 - \Delta_{W,2} + i\varepsilon]^3; \\ \Delta_{W,2} &= m^2(x^2 - x) + M_W^2[1 - x + (\xi - 1)y]; \end{aligned} \tag{B.14}$$

$$\begin{aligned} D_{W,3} &= [l^2 - \Delta_{W,3} + i\varepsilon]^3; \\ \Delta_{W,3} &= m^2(x^2 - x) + M_W^2[\xi(1 - x - y) + y]; \end{aligned} \tag{B.15}$$

$$\begin{aligned} D_{W,4} &= [l^2 - \Delta_{W,4} + i\varepsilon]^3; \\ \Delta_{W,4} &= m^2(x^2 - x) + M_W^2\xi(1 - x). \end{aligned} \tag{B.16}$$

These terms have the full dependence on ξ of the expression. We now evaluate Figure 3.6a in the R_ξ gauge as:

$$\begin{aligned} &\int_0^1 \int_0^{1-x} dxdy \int \frac{d^4l}{(4\pi)^4}(-ie)\left(i\frac{g^2}{2}\right)\gamma^\nu Int_W^{\lambda\sigma\mu}(\not{k} - \not{p}_1)\gamma^\rho P_L \\ &\left[\frac{g^{\nu\lambda}g^{\sigma\rho} - \frac{g^{\nu\lambda}k^\sigma k^\rho}{M_W^2} - \frac{(k+q)^\nu(k+q)^\lambda g^{\sigma\rho}}{M_W^2} + \frac{(k+q)^\nu(k+q)^\lambda k^\sigma k^\rho}{M_W^4}}{D_W} + \right. \\ &\qquad \frac{\frac{(k+q)^\nu(k+q)^\lambda g^{\sigma\rho}}{M_W^2} - \frac{(k+q)^\nu(k+q)^\lambda k^\sigma k^\rho}{M_W^4}}{D_{W,2}} + \\ &\qquad \left. \frac{\frac{g^{\nu\lambda}k^\sigma k^\rho}{M_W^2} - \frac{(k+q)^\nu(k+q)^\lambda k^\sigma k^\rho}{M_W^4}}{D_{W,3}} + \frac{\frac{(k+q)^\nu(k+q)^\lambda k^\sigma k^\rho}{M_W^4}}{D_{W,4}}\right], \end{aligned} \tag{B.17}$$

remembering that $Int_W^{\lambda\sigma\mu}$ is defined by Eq. 3.56

Doing the same with Figure 3.6b and 3.6c, respectively:

$$\begin{aligned} &\int_0^1 \int_0^{1-x} dxdy \int \frac{d^4l}{(4\pi)^4}(-ie)\left(i\frac{mg^2}{2}\right)\gamma^\nu g^{\mu\lambda}(\not{k} - \not{p}_1)P_L \\ &\qquad \left[\frac{g^{\nu\lambda} - \frac{(k+q)^\nu(k+q)^\lambda}{M_W^2}}{D_{W,3}} + \frac{\frac{(k+q)^\nu(k+q)^\lambda}{M_W^2}}{D_{W,4}}\right]. \end{aligned} \tag{B.18}$$

$$\int_0^1 \int_0^{1-x} dxdy \int \frac{d^4 l}{(4\pi)^4}(-ie)\left(i\frac{mg^2}{2}\right) g^{\mu\sigma}(\not{k}-\not{p}_1)\gamma^\rho P_L \left[\frac{g^{\sigma\rho}-\frac{(k)^\sigma (k)^\rho}{M_W^2}}{D_{W,2}}+\frac{\frac{(k)^\sigma (k)^\rho}{M_W^2}}{D_{W,4}}\right]. \tag{B.19}$$

Finally for the diagram in Figure 3.6d:

$$\int_0^1 \int_0^{1-x} dxdy \int \frac{d^4 l}{(4\pi)^4}(-ie)\left(i\frac{g^2}{2}\right)\left(\frac{m}{M_W}\right)^2 (\not{k}-\not{p}_1)\left[\frac{(-2k-q)^\mu}{D_{W,4}}\right] P_R \tag{B.20}$$

The calculations are straight-forward, following the same techniques from the main text and give the following result in terms of the Feynman parameters:

$$\begin{aligned} F_{2,W,\xi} = \int_0^1 \int_0^{1-x} dxdy \int \frac{d^4 l}{(4\pi)^4}\left(\frac{g^2}{16}\right)\left(\frac{m}{M_W}\right)^2 \\ \left[\frac{4l^2(-x)(2x+1)+4m^2(-x^2)(x-1)^2+4M_W^2(1-x)(2x-3))}{D_W}+\right. \\ \frac{l^2\left[4(x-1)^2-6y\right]+2m^2x^2(x^2-4x-2y+3)+4M_W^2(x+y-1)}{D_{W,2}}+ \\ \frac{l^2(4x^2-2x+6y-2)+2m^2x^2\left[(x-1)^2+2y\right]-4M_W^2 y}{D_{W,3}}+ \\ \left.\frac{l^2(6x-2)+4m^2x(x-1)^2}{D_{W,4}}\right]+ \\ \frac{l^4}{2M_W^2}(13x^2+2x+y-2)\left[-\frac{1}{D_W}+\frac{1}{D_{W,2}}+\frac{1}{D_{W,3}}-\frac{1}{D_{W,4}}\right]. \end{aligned} \tag{B.21}$$

The first thing to notice is that the terms with l^4 will vanish after regularization. This can be seen by using:

$$\int \frac{d^4 l}{(2\pi)^4}\frac{l^4}{(l^2-\Delta+i\varepsilon)^3} \to i\frac{3}{16\pi^2}\frac{\Delta}{\epsilon}. \tag{B.22}$$

Even though the denominator is divergent, with $\epsilon \to 0$, the sum $(\Delta_W - \Delta_{W,2} - \Delta_{W,3} + \Delta_{W,4})$ is exactly zero and this term vanishes. For the remaining terms, we use Eq. B.7 and Eq. 3.40 and expand in terms of $\frac{m^2}{m_W^2}$. For brevity, it will not be shown here. After performing the integral in the Feynman parameters we end up with the surprising:

$$F_{2,W,\xi} = \left(\frac{g}{8\pi}\right)^2 \left(\frac{m}{M_W}\right)^2 \left[\frac{10}{3} + \frac{2}{3}\left(\frac{m}{M_W}\right)^2 + \frac{3}{10}\left(\frac{m}{M_W}\right)^4 + O\left(\frac{m^6}{M_W^6}\right)\right]. \tag{B.23}$$

This result is the same as the one obtained with the Feynman gauge (Eq. 3.64) and also agrees with K. Fujikawa [82]. It shows that not only the value of F_2 does not depend on the gauge in general, as it is also gauge-independent for each factor in the perturbation expansion, since there is no relation between the masses and the ξ value.

Appendix C

Computation of the F1 form factor up to one loop

Considering the QED renormalized Lagrangian:

$$\mathcal{L} = i(1 - \delta Z_2)\bar{\psi}\partial\psi + (1 - \delta Z_1)e\bar{\psi}\gamma^\mu\psi A_\mu + (...), \tag{C.1}$$

where δZ_1 and δZ_2 are the counter terms for the interaction and the wave function, respectively.

Looking for the sum of the contributions to the F_1 form factor up to one loop, we have:

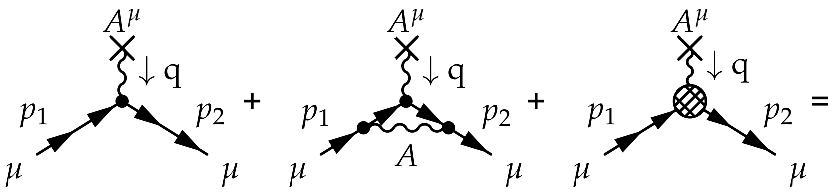

$$(-ie)F_1\left[\bar{u}(p_2)\gamma^\mu u(p_1)\right] = (-ie)\left[1 + \Gamma(p_1, p_2) + \delta Z_1\right]\left[\bar{u}(p_2)\gamma^\mu u(p_1)\right], \tag{C.2}$$

where the diagrams are respectively, the tree level, the one loop with the photon, and the counter term diagram, $\Gamma(p_1, p_2)$ is the part of the loop evaluation that multiplies $(-ie)\gamma^\mu$ and δZ_1 is the counter term for the renormalization of the vertex.

There is a simple way to see that the term F_1 is 1 for the contribution shown in Eq. C.2. For that we use the diagram for the fermion self-energy and the diagrams of the loop vertex, shown in Figure C.1.

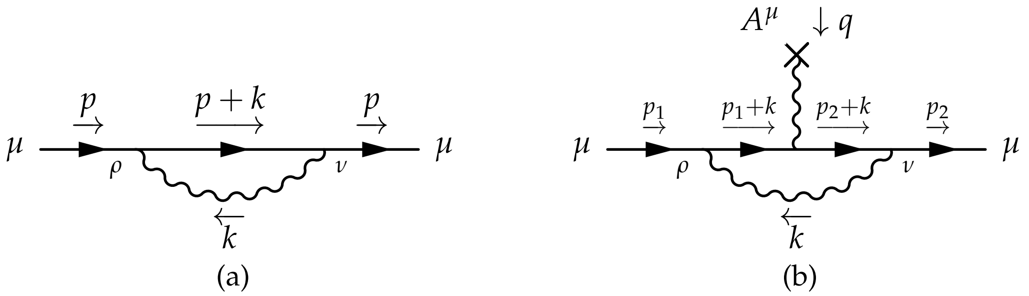

Figure C.1: Feynman diagram for the (a) fermion self-energy and (b) one loop correction of the vertex

Evaluating the first diagram (Figure C.1a) we get:

$$\begin{aligned} i\mathcal{M}_{C1a} &= (-ie)^2 \int \frac{d^4k}{(2\pi)^4} \frac{-ig_{\nu\rho}}{[k^2+i\varepsilon]} \bar{u}(p) \\ &\times \gamma^\nu \left[\frac{i}{\not{p}+\not{k}-m+i\varepsilon} \right] \gamma^\rho u(p) = \bar{u}(p)\Sigma(p)u(p), \end{aligned} \tag{C.3}$$

with $\Sigma(p)$ evaluated as:

$$\begin{aligned} \Sigma(p) &= (-ie)^2 \int \frac{d^4k}{(2\pi)^4} \frac{-ig_{\nu\rho}}{[k^2+i\varepsilon]} \gamma^\nu \left[\frac{i}{\not{p}+\not{k}-m+i\varepsilon} \right] \gamma^\rho \\ &= (-ie)^2 \int \frac{d^4k}{(2\pi)^4} \frac{-2(\not{p}+\not{k})+4m}{k^2+2xpk+xp^2-m^2+i\varepsilon} \\ &= (-ie)^2 \int \frac{d^4k'}{(2\pi)^4} \frac{-2(1-x)\not{p}+4m}{(k'^2-x^2m^2+i\varepsilon)}, \end{aligned} \tag{C.4}$$

where in the last line it was used $k' = k + xp$, $dk' = dk$, and all odd powers of k' were ignored. Now we can realize that this term has the form of:

$$\Sigma(p) = A(p) + B(p)\not{p}, \tag{C.5}$$

and that this will be a counter term added to the Lagrangian to have a finite propagator. The important counter term for this computation is:

$$\mathcal{L}_{C.T.} = -(\delta Z_2)\bar{\psi}\not{\partial}\psi \quad ; \quad -\delta Z_2 = \left.\frac{\partial\Sigma(p)}{\partial\not{p}}\right|_{\not{p}=m} = B(p). \tag{C.6}$$

Evaluating the second diagram (Figure C.1b) we get the same as Eq. 3.26, but for this proof, we are using a different convention for the momentum in the loop, since it will be more appropriate. For this new convention we have:

$$
\begin{aligned}
i\mathcal{M}^{\mu}_{C1b} = (-ie)^3 \int \frac{d^4k}{(2\pi)^4} \frac{-ig_{\nu\rho}}{[k^2 + i\varepsilon]} \bar{u}(p_2) \\
\times \gamma^{\nu} \frac{i(\not{p}_1 + \not{k} + m)}{[(p_1 + k)^2 - m^2 + i\varepsilon]} \gamma^{\mu} \frac{i(\not{p}_2 + \not{k} + m)}{[(p_2 + k)^2 - m^2 + i\varepsilon]} \gamma^{\rho} u(p_1),
\end{aligned}
\tag{C.7}
$$

but instead of doing the computation, the following trick can be applied:

$$
\begin{aligned}
\frac{i(\not{p}_1 + \not{k} + m)}{[(p_1 + k)^2 - m^2 + i\varepsilon]} \gamma^{\mu} \frac{i(\not{p}_2 + \not{k} + m)}{[(p_2 + k)^2 - m^2 + i\varepsilon]} \xrightarrow[p_1 = p_2 = p]{q \to 0} \\
\left[\frac{i}{\not{p} + \not{k} - m + i\varepsilon}\right]^2 \gamma^{\mu} = -\frac{\partial}{\partial p_{\mu}} \left[\frac{i}{\not{p} + \not{k} - m + i\varepsilon}\right].
\end{aligned}
\tag{C.8}
$$

Then, Eq. C.7 can be rewritten as:

$$
\begin{aligned}
i\mathcal{M}^{\mu}_{C1b} = (-ie) \left(-\frac{\partial}{\partial p_{\mu}}\right) (-ie)^2 \int \frac{d^4k}{(2\pi)^4} \frac{-ig_{\nu\rho}}{[k^2 + i\varepsilon]} \bar{u}(p) \\
\times \gamma^{\nu} \left[\frac{i}{\not{p} + \not{k} - m + i\varepsilon}\right] \gamma^{\rho} u(p) = (-ie)\, \bar{u}(p) \left(-\frac{\partial \Sigma(p)}{\partial p_{\mu}}\right) u(p)
\end{aligned}
\tag{C.9}
$$

and since:

$$
-\frac{\partial \Sigma(p)}{\partial p_{\mu}}\bigg|_{\not{p}=m} = -\gamma^{\mu} \frac{\partial \Sigma(p)}{\partial \not{p}}\bigg|_{\not{p}=m} = \delta Z_2 \gamma^{\mu}, \tag{C.10}
$$

from Eq. C.6, we get:

$$
\Gamma(p) = \delta Z_2 \tag{C.11}
$$

Substituting in Eq. C.2 we have:

$$
F_1 = 1 + \delta Z_2 - \delta Z_1. \tag{C.12}
$$

The two diagrams from Figure C.1 clearly should be equal as $q \to 0$ (apart from the factor of $-ie\gamma^{\mu}$), therefore we must have:

$$
\delta Z_1 = \delta Z_2, \tag{C.13}
$$

meaning that $F_1 = 1$. This proves that the contribution of the loop diagrams for F_1 is simply a counter term for the Lagrangian, and not a physical value. This procedure can be repeated for any order of loops and with any other particle in the loop. It is interesting that the exact form of the renormalization factors δZ_1 and

δZ_2 are not even needed to see that they will cancel each other in the contribution for F_1.

Bibliography

[1] Horatiu Năstase. *Classical field theory*. Cambridge University Press, 2019.

[2] G. Aad and et al. (ATLAS Collaboration). Observation of a new particle in the search for the standard model higgs boson with the atlas detector at the lhc. *Physics Letters B*, 716:1–29, 09 2012.

[3] Riccardo Penco. An introduction to effective field theories. *arXiv preprint arXiv:2006.16285*, 2020.

[4] Fred Jegerlehner. *The anomalous magnetic moment of the muon*. Springer, 2008.

[5] G. W. Bennett and et al. (Brookhaven Muon $g-2$ collaboration). Final report of the e821 muon anomalous magnetic moment measurement at bnl. *Physical Review D*, 73(7), Apr 2006.

[6] B. Abi and et al. (Fermilab Muon $g-2$ Collaboration). Measurement of the positive muon anomalous magnetic moment to 0.46 ppm.

[7] Yutaro Sato. J-PARC Muon $\mathrm{g}-2$/EDM experiment. *JPS Conf. Proc.*, 33:011110, 2021.

[8] Marco Antonio Moreira. The standard model of particle physics. *Revista Brasileira de Ensino de Física*, 31:1306.1–1306.11, 04 2009.

[9] Chris Quigg. *Gauge Theories of the Strong, Weak, and Electromagnetic Interactions: Second Edition*. Princeton University Press, USA, 9 2013.

[10] Matthew D. Schwartz. *Quantum Field Theory and the Standard Model*. Cambridge University Press, 2013.

[11] Jorge Romao and Joao Silva. A resource for signs and feynman diagrams of the standard model. *International Journal of Modern Physics A*, 27, 09 2012.

[12] Tara Shears. The standard model. *Philosophical transactions. Series A, Mathematical, physical, and engineering sciences*, 370:805–17, 02 2012.

[13] P.A. Zyla et al. Review of Particle Physics. *PTEP*, 2020(8):083C01, 2020.

[14] Tadao Nakano and Kazuhiko Nishijima. Charge Independence for V-particles*. *Progress of Theoretical Physics*, 10(5):581–582, 11 1953.

[15] Michael Edward Peskin and Daniel V. Schroeder. *An Introduction to Quantum Field Theory*. Westview Press, 1995. Reading, USA: Addison-Wesley (1995) 842 p.

[16] Makoto Kobayashi and Toshihide Maskawa. CP-Violation in the Renormalizable Theory of Weak Interaction. *Progress of Theoretical Physics*, 49(2):652–657, 02 1973.

[17] Adel Bilal. Lectures on anomalies, 2008.

[18] M. Thomson. *Modern Particle Physics*. Cambridge University Press, 2013.

[19] N. Heard. *An Introduction to Bayesian Inference, Methods and Computation*. Springer International Publishing, 2021.

[20] Uwe-Jens Wiese. *The Standard Model of Particle Physics*. Institute for Theoretical Physics, University of Bern, 2021.

[21] Ilaria Brivio and Michael Trott. The standard model as an effective field theory. *Physics Reports*, 793:1–98, 2019. The standard model as an effective field theory.

[22] Y. Fukuda and et al. (Super-Kamiokande Collaboration). Evidence for oscillation of atmospheric neutrinos. *Phys. Rev. Lett.*, 81:1562–1567, Aug 1998.

[23] Alain Bellerive, JR Klein, AB McDonald, AJ Noble, AWP Poon, SNO Collaboration, et al. The sudbury neutrino observatory. *Nuclear Physics B*, 908:30–51, 2016.

[24] E Kh Akhmedov. Neutrino physics. *arXiv preprint hep-ph/0001264*, 2000.

[25] Edward W. Kolb and Michael S. Turner. *The Early Universe*, volume 69. 1990.

[26] A. D. Sakharov. Violation of CP Invariance, C asymmetry, and baryon asymmetry of the universe. *Pisma Zh. Eksp. Teor. Fiz.*, 5:32–35, 1967.

[27] Antonio Riotto and Mark Trodden. Recent progress in baryogenesis. *Annual Review of Nuclear and Particle Science*, 49(1):35–75, Dec 1999.

[28] A. M. Baldini et al. Search for the lepton flavour violating decay $\mu^+ \to \mathrm{e}^+\gamma$ with the full dataset of the MEG experiment. *Eur. Phys. J. C*, 76(8):434, 2016.

[29] Ernany Rossi Schmitz. Complex scalar dark matter in a b-l model, 2014. Masters dissertation.

[30] B. L. Sánchez-Vega, J. C. Montero, and E. R. Schmitz. Complex scalar dark matter in a *b-l* model. *Phys. Rev. D*, 90:055022, Sep 2014.

[31] David J. E. Marsh. Axions and alps: a very short introduction, 2017.

[32] Daniel Baumann. Tasi lectures on primordial cosmology, 2018.

[33] Paul Langacker. *The standard model and beyond*. Taylor & Francis, 2017.

[34] CDF Collaboration†‡, T Aaltonen, S Amerio, D Amidei, A Anastassov, A Annovi, J Antos, G Apollinari, JA Appel, T Arisawa, et al. High-precision measurement of the w boson mass with the cdf ii detector. *Science*, 376(6589):170–176, 2022.

[35] James P Miller, Eduardo de Rafael, and B Lee Roberts. Muon (g 2): experiment and theory. *Reports on Progress in Physics*, 70(5):R03, May 2007.

[36] Julian Schwinger. On quantum-electrodynamics and the magnetic moment of the electron. *Phys. Rev.*, 73:416–417, Feb 1948.

[37] Roman Jackiw and Steven Weinberg. Weak-interaction corrections to the muon magnetic moment and to muonic-atom energy levels. *Phys. Rev. D*, 5:2396–2398, May 1972.

[38] T. Aoyama and et al. The anomalous magnetic moment of the muon in the standard model. *Physics Reports*, 887:1–166, Dec 2020.

[39] Richard H Parker, Chenghui Yu, Weicheng Zhong, Brian Estey, and Holger Müller. Measurement of the fine-structure constant as a test of the standard model. *Science*, 360(6385):191–195, 2018.

[40] Tatsumi Aoyama, Toichiro Kinoshita, and Makiko Nio. Theory of the anomalous magnetic moment of the electron. *Atoms*, 7(1):28, 2019.

[41] Michel Davier, Andreas Hoecker, Bogdan Malaescu, and Zhiqing Zhang. Reevaluation of the hadronic vacuum polarisation contributions to the standard model predictions of the muon $g-2$ and $\alpha(m_z^2)$ using newest hadronic cross-section data. *The European Physical Journal C*, 77(12):1–12, 2017.

[42] Alexander Kurz, Tao Liu, Peter Marquard, and Matthias Steinhauser. Hadronic contribution to the muon anomalous magnetic moment to next-to-next-to-leading order. *Physics Letters B*, 734:144–147, 2014.

[43] Gilberto Colangelo, Martin Hoferichter, and Peter Stoffer. Two-pion contribution to hadronic vacuum polarization. *Journal of High Energy Physics*, 2019(2):1–49, 2019.

[44] Martin Hoferichter, Bai-Long Hoid, and Bastian Kubis. Three-pion contribution to hadronic vacuum polarization. *Journal of High Energy Physics*, 2019(8):1–26, 2019.

[45] M Davier, A Hoecker, B Malaescu, and Z Zhang. A new evaluation of the hadronic vacuum polarisation contributions to the muon anomalous magnetic moment and to $\alpha(m_z^2)$. *The European Physical Journal C*, 80(3):1–13, 2020.

[46] Alexander Keshavarzi, Daisuke Nomura, and Thomas Teubner. g- 2 of charged leptons, $\alpha(m_z^2)$, and the hyperfine splitting of muonium. *Physical Review D*, 101(1):014029, 2020.

[47] Alexander Kurz, Tao Liu, Peter Marquard, and Matthias Steinhauser. Hadronic contribution to the muon anomalous magnetic moment to next-to-next-to-leading order. *Physics Letters B*, 734:144–147, 2014.

[48] Kirill Melnikov and Arkady Vainshtein. Hadronic light-by-light scattering contribution to the muon anomalous magnetic moment reexamined. *Physical Review D*, 70(11):113006, 2004.

[49] Pere Masjuan and Pablo Sanchez-Puertas. Pseudoscalar-pole contribution to the $(g_\mu - 2)$: a rational approach. *Physical Review D*, 95(5):054026, 2017.

[50] Gilberto Colangelo, Martin Hoferichter, Massimiliano Procura, and Peter Stoffer. Dispersion relation for hadronic light-by-light scattering: two-pion contributions. *Journal of High Energy Physics*, 2017(4):1–82, 2017.

[51] Martin Hoferichter, Bai-Long Hoid, Bastian Kubis, Stefan Leupold, and Sebastian P Schneider. Dispersion relation for hadronic light-by-light scattering: pion pole. *Journal of High Energy Physics*, 2018(10):1–57, 2018.

[52] Antoine Gérardin, Harvey B Meyer, and Andreas Nyffeler. Lattice calculation of the pion transition form factor with n f= 2+ 1 wilson quarks. *Physical Review D*, 100(3):034520, 2019.

[53] Johan Bijnens, Nils Hermansson-Truedsson, and Antonio Rodríguez-Sánchez. Short-distance constraints for the hlbl contribution to the muon anomalous magnetic moment. *Physics Letters B*, 798:134994, 2019.

[54] Gilberto Colangelo, Franziska Hagelstein, Martin Hoferichter, Laetitia Laub, and Peter Stoffer. Longitudinal short-distance constraints for the hadronic light-by-light contribution to (g- 2) μ with large-nc regge models. *Journal of High Energy Physics*, 2020(3):1–89, 2020.

[55] Gilberto Colangelo, Martin Hoferichter, Andreas Nyffeler, Massimo Passera, and Peter Stoffer. Remarks on higher-order hadronic corrections to the muon g- 2. *Physics Letters B*, 735:90–91, 2014.

[56] Thomas Blum, Norman Christ, Masashi Hayakawa, Taku Izubuchi, Luchang Jin, Chulwoo Jung, and Christoph Lehner. Hadronic light-by-light scattering contribution to the muon anomalous magnetic moment from lattice qcd. *Physical Review Letters*, 124(13):132002, 2020.

[57] Tatsumi Aoyama, Masashi Hayakawa, Toichiro Kinoshita, and Makiko Nio. Complete tenth-order qed contribution to the muong2. *Physical Review Letters*, 109(11), Sep 2012.

[58] Andrzej Czarnecki, William J Marciano, and Arkady Vainshtein. Refinements in electroweak contributions to the muon anomalous magnetic moment. *Physical Review D*, 67(7):073006, 2003.

[59] C Gnendiger, D Stöckinger, and H Stöckinger-Kim. The electroweak contributions to (g- 2) μ after the higgs-boson mass measurement. *Physical Review D*, 88(5):053005, 2013.

[60] S. Borsanyi and et al. (BMW collaboration). Leading hadronic contribution to the muon magnetic moment from lattice qcd. *Nature*, 593(7857):51–55, 2021.

[61] Antonio Pich. The standard model of electroweak interactions. *arXiv preprint arXiv:1201.0537*, 2012.

[62] B. Lee Roberts. The history of the muon (g-2) experiments, 2018.

[63] Paul Kunze. Untersuchung der ultrastrahlung in der wilsonkammer. *Zeitschrift für Physik*, 83(1):1–18, 1933.

[64] Carl D Anderson and Seth H Neddermeyer. Cloud chamber observations of cosmic rays at 4300 meters elevation and near sea-level. *Physical Review*, 50(4):263, 1936.

[65] Richard L. Garwin, Leon M. Lederman, and Marcel Weinrich. Observations of the failure of conservation of parity and charge conjugation in meson decays: the magnetic moment of the free muon. *Phys. Rev.*, 105:1415–1417, Feb 1957.

[66] A Yamamoto, Y Makida, K Tanaka, F Krienen, BL Roberts, HN Brown, G Bunce, GT Danby, M G-Perdekamp, H Hseuh, et al. The superconducting inflector for the bnl g-2 experiment. *Nuclear Instruments and Methods in Physics Research Section A: Accelerators, Spectrometers, Detectors and Associated Equipment*, 491(1-2):23–40, 2002.

[67] AP Schreckenberger, D Allspach, D Barak, J Bohn, C Bradford, D Cauz, Seung Pyo Chang, A Chapelain, S Chappa, S Charity, et al. The fast non-ferric kicker system for the muon g- 2 experiment at fermilab. *Nuclear Instruments and Methods in Physics Research Section A: Accelerators, Spectrometers, Detectors and Associated Equipment*, 1011:165597, 2021.

[68] T. Albahri and et al. (Fermilab Muon $g-2$ collaboration). Measurement of the anomalous recession frequency of the muon in the fermilab muon $g-2$ experiment. *Physical Review D*, 103(7), Apr 2021.

[69] Walter Greiner et al. *Relativistic quantum mechanics*, volume 2. Springer, 2000.

[70] David Bailin and Alexander Love. *Introduction to Gauge Field Theory Revised Edition*. Taylor & Francis, 1993.

[71] Stanley Mandelstam. Determination of the pion-nucleon scattering amplitude from dispersion relations and unitarity. general theory. In *Memorial Volume for Stanley Mandelstam*, pages 151–167. World Scientific, 1958.

[72] Song Li, Yang Xiao, and Jin Min Yang. A pedagogical review on muon $g - 2$. *arXiv preprint arXiv:2110.04673*, 2021.

[73] David JE Marsh. Axions and alps: a very short introduction. *arXiv preprint arXiv:1712.03018*, 2017.

[74] Csaba Csaki. The minimal supersymmetric standard model. *Modern Physics Letters A*, 11(08):599–613, 1996.

[75] Vicente Pleitez and MD Tonasse. Heavy charged leptons in an su (3) l u (1) n model. *Physical Review D*, 48(5):2353, 1993.

[76] Georges Aad, Brad Abbott, Dale Charles Abbott, A Abed Abud, Kira Abeling, Deshan Kavishka Abhayasinghe, Syed Haider Abidi, OS AbouZeid, Nadine L Abraham, Halina Abramowicz, et al. Search for heavy higgs bosons decaying into two tau leptons with the atlas detector using p p collisions at s= 13 tev. *Physical review letters*, 125(5):051801, 2020.

[77] Pablo Achard, O Adriani, M Aguilar-Benitez, J Alcaraz, G Alemanni, J Allaby, A Aloisio, MG Alviggi, H Anderhub, VP Andreev, et al. Search for heavy neutral and charged leptons in e+ e- annihilation at lep. *Physics Letters B*, 517(1-2):75–85, 2001.

[78] Juan Carlos Montero Garcia. Física nova, modelos 3-3-1 e a massa dos neutrinos, 2001. associate professor thesis.

[79] JC Montero, Vicente Pleitez, and O Ravinez. Soft superweak cp violation in a 3-3-1 model. *Physical Review D*, 60(7):076003, 1999.

[80] George De Conto Santos. Electron and muon anomalous magnetic dipole moment in the 3-3-1 model with heavy leptons, 2018. Doctoral Thesis.

[81] Morad Aaboud, Georges Aad, Brad Abbott, B Abeloos, SH Abidi, OS AbouZeid, NL Abraham, H Abramowicz, H Abreu, R Abreu, et al. Search for doubly charged higgs boson production in multi-lepton final states with the atlas detector using proton–proton collisions at $\sqrt{s} = 13\,tev$. *The European Physical Journal C*, 78(3):1–34, 2018.

[82] Kazuo Fujikawa, Benjamin W Lee, and AI Sanda. Generalized renormalizable gauge formulation of spontaneously broken gauge theories. *Physical Review D*, 6(10):2923, 1972.